

STUDY OF THE SEISMIC BEHAVIOR OF STEEL BUILDINGS WITH A 1/6 SCALE MODEL AND SHAKING TABLE TESTS

by

Paul Hernán Kohan

A thesis submitted in partial fulfillment of the requirements for the degree of

MASTER OF SCIENCE
in
CIVIL ENGINEERING

UNIVERSITY OF PUERTO RICO
MAYAGÜEZ CAMPUS
2007

Approved by:

Felipe J. Acosta, PhD
Member, Graduate Committee

Date

Luis E. Suarez, PhD
Member, Graduate Committee

Date

Daniel Wendichansky, PhD
President, Graduate Committee

Date

Megh Raj Goyal, PhD
Representative of Graduate Studies

Date

Ismael Pagán Trinidad, M.S.C.E
Chairperson of the Department

Date

ABSTRACT

This thesis summarizes the design, construction and instrumentation of a 1/6 scale model of a steel structure typically used in commercial buildings in Puerto Rico, and the evaluation of methods to upgrade its performance when subjected to earthquake motions, based on the use of different combinations of a pulley device that dissipates energy through friction, and two auxiliary masses, allowed to impact with the ground. In order to evaluate the effectiveness of the proposed alternatives, Snap-Back Tests and Simulated Earthquake Tests were conducted on a SDOF system and on the scale model with and without the devices. Significant reductions in the accelerations and displacements of critical nodes of the scale model, and on the bending moments at the bottom of the central columns were produced when friction effects were fully developed, without collision of the auxiliary masses.

RESUMEN

Esta tesis presenta el diseño, construcción e instrumentación de un modelo a escala 1/6 de una estructura de acero típicamente utilizada en edificios comerciales en Puerto Rico, y la evaluación de métodos para mejorar su respuesta a terremotos, basados en la utilización de una combinación de un sistema de poleas, que disipa energía a través de fricción, y de dos masas auxiliares, que pueden impactar con el suelo. Para evaluar la efectividad de las alternativas propuestas se ejecutaron ensayos del tipo Liberación-Rápida y de Simulación de Terremotos en una mesa vibradora, sobre un sistema de un grado de libertad y sobre el modelo a escala. Se observó que las mayores reducciones en las aceleraciones y desplazamientos de los nodos más críticos, y en los momentos flectores en la parte inferior de las columnas centrales se produjeron cuando los efectos de fricción en las poleas se desarrollaron completamente, independientemente del comportamiento de las masas auxiliares.

A mis padres, Luís y Emi

AGRADECIMIENTOS

Quiero agradecer a la Oficina del Comisionado de Seguros de Puerto Rico por haber financiado esta investigación.

Al Dr. Daniel Wendichansky por darme la oportunidad de realizar estos estudios y por su guía a lo largo del proyecto. A los miembros del comité Dr. Felipe J. Acosta y en especial al Dr. Luís Suarez, quien siempre estuvo dispuesto a responder mis dudas.

A toda mi familia, en especial a mis padres Luís y Emi, por apoyarme y alentarme todo este tiempo, y por ser una constante fuente de inspiración.

A mi novia Ana Gabriela, por haber estado conmigo todos los días, por aguantarme en los momentos difíciles, y por compartir con alegría mis logros.

A quienes en poco tiempo se convirtieron en grandes amigos, por compartir conmigo esta experiencia, por ayudarme sin pretensiones y por darme ánimo en los momentos necesarios.

A mis compañeros de laboratorio por su amistad y por estar siempre dispuestos a darme una mano.

Por ultimo, a los técnicos de laboratorio por las veces que me prestaron su ayuda y al personal del departamento por su colaboración.

TABLE OF CONTENTS

ABSTRACT	II
RESUMEN	III
AGRADECIMIENTOS	V
TABLE OF CONTENTS	VI
LIST OF FIGURES	IX
LIST OF TABLES	XI
CHAPTER I	1
INTRODUCTION	1
1.1 INTRODUCTION	1
1.2 RESEARCH OBJECTIVES	3
1.3 ORGANIZATION OF THE THESIS	4
CHAPTER II	5
LITERATURE REVIEW	5
2.1 OBSERVED PERFORMANCE OF STEEL BUILDING STRUCTURES IN EARTHQUAKES	5
2.2 SHAKING TABLE TEST	7
2.3 PASSIVE ENERGY DISSIPATION SYSTEMS	12
2.4 INTERNAL FORCE TRANSDUCER	17
CHAPTER III	18
SCALE MODEL DEFINITION AND CONSTRUCTION	18
3.1 INTRODUCTION	18
3.2 SHAKING TABLE FACILITY	18
3.3 PROTOTYPE DEFINITION	21
3.4 SIMILITUDE REQUIREMENTS	22
3.5 MODEL DEFINITION	26
CHAPTER IV:	32
INSTRUMENTATION	32
4.1 INTRODUCTION	32
4.2 ACCELEROMETERS	33
4.3 SPECIAL FORCE TRANSDUCERS (LOAD CELLS)	34
4.4 DISPLACEMENT TRANSDUCERS	40

4.5	DATA ACQUISITION SYSTEM.....	40
4.6	DATA REDUCTION	41
CHAPTER V		42
	EVALUATION OF RETROFITTING ALTERNATIVES.....	42
5.1	INTRODUCTION	42
5.2	SINGLE DEGREE OF FREEDOM SYSTEM DESCRIPTION	43
5.3	DESCRIPTION OF THE RETROFITTING ALTERNATIVES	44
5.3.1	GENERAL SET UP.....	44
5.3.2	ALTERNATIVE 1: FREE PULLEY WITH HANGING MASS SYSTEM (FP).....	47
5.3.3	ALTERNATIVE 2: RESTRAINED PULLEY WITH HANGING MASS SYSTEM (RP)	48
5.3.4	ALTERNATIVE 3: FREE PULLEY WITH SUPPORTED MASS (FPSM).....	50
5.3.5	ALTERNATIVE 4: RESTRAINED PULLEY WITH SUPPORTED MASS (RPSM)	50
5.3.6	ALTERNATIVE 5: FLEXIBLE CABLE SYSTEM (FC)	51
5.4	TEST PROGRAM	51
5.4.1	SELECTION OF THE EARTHQUAKE RECORDS	53
5.5	RESULTS FROM SNAP-BACK TESTS	56
5.5.1	SNAP-BACK TESTS FOR SDOF	56
5.5.2	SNAP-BACK TESTS FOR FP.....	56
5.5.3	SNAP-BACK TESTS FOR RP	57
5.5.4	SNAP-BACK TESTS FOR FPSM.....	58
5.5.5	SNAP-BACK TESTS FOR RPSM.....	59
5.5.6	SNAP-BACK TESTS FOR FC	59
5.6	CONCLUSIONS FROM SNAP-BACK TESTS	61
5.7	RESULTS FROM SIMULATED EARTHQUAKES TESTS	72
5.8	CONCLUSIONS FROM SIMULATED EARTHQUAKES TESTS	75
CHAPTER VI:		77
	SCALE MODEL TESTS	77
6.1	INTRODUCTION	77
6.2	TESTING PROGRAM.....	77
6.3	IDENTIFICATION OF STRUCTURAL DYNAMIC PROPERTIES.....	82
6.4	RESULTS FROM SIMULATED EARTHQUAKES TESTS	84
6.5	CONCLUSIONS.....	86
CHAPTER VII:.....		97
	CONCLUSIONS	97
7.1	PROJECT SUMMARY	97
7.2	CONCLUSIONS.....	98
7.3	RECOMMENDATIONS FOR FUTURE RESEARCH	100
REFERENCES.....		102

APENDIX A.....	106
APENDIX B.....	108
APENDIX C.....	113
APENDIX D.....	118

LIST OF FIGURES

FIGURE 3-1: GENERAL LAYOUT OF THE PROTOTYPE.....	22
FIGURE 3-2: GENERAL LAYOUT OF THE MODEL STRUCTURE.....	29
FIGURE 3-3: WEST SIDE VIEW OF THE MODEL.....	30
FIGURE 3-4: EAST SIDE VIEW OF THE MODEL.....	30
FIGURE 3-5: VIEW OF THE STEEL PLATES.....	30
FIGURE 3-6: BASE – COLUMN CONNECTION.....	31
FIGURE 3-7: BEAM – TO – COLUMN CONNECTION.....	31
FIGURE 4-1: GENERAL LAYOUT OF THE INSTRUMENTATION.....	32
FIGURE 4-2: ACCELEROMETERS LAYOUT.....	33
FIGURE 4-3: VIEW OF THE LOAD CELLS IN COLUMN.....	34
FIGURE 4-4: LAYOUT OF LOAD CELLS IN A COLUMNS.....	34
FIGURE 4-5: AXIAL LOAD CELL.....	36
FIGURE 4-6: BENDING MOMENT LOAD CELL.....	36
FIGURE 4-7: VIEW OF THE STRAIN GAGES ARRANGEMENTS.....	36
FIGURE 4-8: SET-UP FOR LOAD CELL CALIBRATION.....	39
FIGURE 4-9: VIEW OF SET-UP FOR LOAD CELL CALIBRATION.....	39
FIGURE 4-10 VIEW OF THE LVDTs.....	40
FIGURE 5-1: SINGLE DEGREE OF FREEDOM SYSTEM.....	44
FIGURE 5-2: LAYOUT OF THE GENERAL SET UP.....	45
FIGURE 5-3: VIEW OF THE GENERAL SET-UP.....	45
FIGURE 5-4: LAYOUT OF THE PULLEY SYSTEM.....	46
FIGURE 5-5: VIEW OF THE PULLEY SYSTEM.....	46
FIGURE 5-6: ANALYTICAL MODEL OF THE GENERAL SET UP.....	46
FIGURE 5-7: PULLEY SCHEME.....	47
FIGURE 5-8: SET UP FOR MEASURING THE FRICTION BETWEEN CABLE AND PULLEY.....	49
FIGURE 5-9: CABLE TENSION VS. WEIGHT DISPLACEMENT.....	49
FIGURE 5-10: LAYOUT OF ALTERNATIVE 3.....	50
FIGURE 5-11: EARTHQUAKES RECORDS USED IN SIMULATED EARTHQUAKES TESTS.....	54
FIGURE 5-12: ELASTIC RESPONSE SPECTRA WITH $Z= 1\%$	55
FIGURE 5-13: ELASTIC RESPONSE SPECTRA WITH $Z= 10\%$	55
FIGURE 5-14: MASS M ACCELERATION RESPONSE FROM SNAP-BACK TESTS FOR SDOF SYSTEM.....	63
FIGURE 5-15 FOURIER TRANSFORM OF MASS M ACCELERATION FOR SDOF SYSTEM.....	63
FIGURE 5-16: MASS M ACCELERATION RESPONSE FROM SNAP-BACK TESTS FOR FP.....	64
FIGURE 5-17: FOURIER TRANSFORMS OF MASS M ACCELERATION TESTS FOR FP.....	64
FIGURE 5-18: MASS M ACCELERATION RESPONSE FROM SNAP-BACK TESTS FOR RP.....	65
FIGURE 5-19: FOURIER TRANSFORMS OF MASS M ACCELERATION TESTS FOR RP.....	65
FIGURE 5-20: MASS M ACCELERATION RESPONSE FROM SNAP-BACK TESTS FOR FPSM.....	66
FIGURE 5-21: FOURIER TRANSFORMS OF MASS M ACCELERATION TESTS FOR FPSM.....	66
FIGURE 5-22: MASS M ACCELERATION RESPONSE FROM SNAP-BACK TESTS FOR RPSM.....	67
FIGURE 5-23: FOURIER TRANSFORMS OF MASS M ACCELERATION TESTS FOR RPSM.....	67

FIGURE 5-24: MASS M ACCELERATION RESPONSE FROM SNAP-BACK TESTS FOR FC CASES	68
FIGURE 5-25: FOURIER TRANSFORM OF MASS M ACCELERATION FOR FC CASES	69
FIGURE 5-26: FORCE VS. DEFORMATION FOR RUBBER BANDS AND SPRING.....	70
FIGURE 5-27: SET-UP FOR THE COMPARISON OF THE SYSTEM USING RUBBER BANDS AND SPRING.....	70
FIGURE 5-28: VIEW OF THE SET-UP FOR THE COMPARISON OF THE SYSTEM USING RUBBER BANDS AND SPRING	70
FIGURE 5-29: ACCELERATIONS FOR FC SYSTEM WITH SPRING AND RUBBER BANDS	71
FIGURE 5-30: FOURIER TRANSFORM OF MASS M ACCELERATION FOR FC.....	71
FIGURE 5-31: COMPARISON OF MASS M ACCELERATION RESPONSE FOR EL CENTRO TEST.....	73
FIGURE 5-32: COMPARISON OF MASS M RELATIVE DISPLACEMENTS FOR EL CENTRO TEST	74
FIGURE 5-33: PEAK ACCELERATIONS ON % OF THE SDOF PEAK ACCELERATION FROM SIMULATED EARTHQUAKE TESTS	76
FIGURE 5-34: MAXIMUM DRIFTS ON % OF THE SDOF MAXIMUM DRIFT FROM SIMULATED EARTHQUAKE TESTS	76
FIGURE 6-1: SHAKING TABLE ACCELERATION RECORD FROM WHITE NOISE TEST.....	79
FIGURE 6-2: FOURIER TRANSFORM OF THE TABLE ACCELERATION FROM WHITE NOISE TEST	79
FIGURE 6-3: GENERAL SET UP	80
FIGURE 6-4: WEST AND EAST SIDE VIEW OF THE MODEL WITH SECONDARY STRUCTURES	80
FIGURE 6-5: VIEW OF THE LOAD CELLS	81
FIGURE 6-6: SIGN CONVENTION FOR CABLE FORCES	81
FIGURE 6-7: VIEW OF THE RUBBER BANDS	81
FIGURE 6-8: TRANSFER FUNCTIONS OF THE NODES ACCELERATIONS FROM WHITE NOISE TEST	83
FIGURE 6-9: NATURAL MODES OF VIBRATION	84
FIGURE 6-10: COMPARISON OF EL CENTRO TESTS ACCELERATIONS FROM ACCELEROMETER A_{22}	91
FIGURE 6-11: COMPARISON OF EL CENTRO RELATIVE DISPLACEMENT FROM LVDT 2	92
FIGURE 6-12: COMPARISON OF EL CENTRO BENDING MOMENTS AT BOTTOM OF COLUMN 4	93
FIGURE 6-13: COMPARISON OF CABLE TENSION AND FRAME 2 SECOND LEVEL VELOCITY	94
FIGURE 6-14: COMPARISON OF RP AND RP* RESPONSES FROM THE SAN SALVADOR TEST	94
FIGURE 6-15: RESULTS FROM SIMULATED EARTHQUAKE TESTS AS A PERCENTAGE OF BARE MODEL RESPONSE.	95
FIGURE 6-16: COMPARISON BETWEEN RF AND RF* RESPONSE.....	96

LIST OF TABLES

TABLE 3-1: SHAKING TABLE CHARACTERISTICS.....	20
TABLE 3-2: PROTOTYPE WEIGHT	21
TABLE 3-3: SIMILITUDE RELATIONSHIPS FOR ARTIFICIAL MASS SIMULATION METHOD (MONCARZ AND KRAWINKLER 1981)	24
TABLE 3-4: SUMMARY OF THE PROTOTYPE AND MODEL SECTIONS PROPERTIES	28
TABLE 3-5: SUMMARY OF THE PROVIDED MODEL WEIGHT	28
TABLE 3-6: SUMMARY OF THE ADDITIONAL WEIGHT REQUIREMENT	29
TABLE 4-1: CALIBRATION CONSTANTS FOR LOAD CELLS	38
TABLE 5-1: DYNAMIC PROPERTIES OF THE SINGLE DEGREE OF FREEDOM SYSTEM	44
TABLE 5-2: SUMMARY OF THE PERFORMED TESTS ON THE RETROFITTING ALTERNATIVES	52
TABLE 5-2: DESCRIPTIONS OF THE EARTHQUAKES.....	53
TABLE 5-4: DAMPING RATIO FROM SNAP-BACK TESTS	62
TABLE 5-5: PEAK ACCELERATIONS FROM SIMULATED EARTHQUAKE TESTS	72
TABLE 5-6: MAXIMUM DRIFT (IN) FROM SIMULATED EARTHQUAKE TESTS.....	72
TABLE 6-1: SUMMARY OF THE TESTING PROGRAM	79
TABLE 6-2: PEAK ACCELERATION.....	88
TABLE 6-3: PEAK RELATIVE DISPLACEMENT	89
TABLE 6-4: MAXIMUM INTERNAL FORCES	90

CHAPTER I

INTRODUCTION

1.1 INTRODUCTION

Through history, earthquakes have been a natural event feared by men because of its catastrophic consequences, resulting in hundreds of casualties and economical lost. For instance, on the average, 10,000 people die each year from earthquakes and estimated losses due to earthquakes from 1926 to 1950 amount to \$10,000,000,000 (Naeim 2001).

Only through the understanding of this phenomenon and how structures respond to it, consequences can be diminished. Each earthquake presents an opportunity to observe and study the performance of real buildings. The lessons learned during these extreme events accelerate research work on structural performance and motivate advances in seismic design.

However, the development of our knowledge can not depend only on the actual occurrence of these natural events. Damage observed in the 1994 Northridge and 1995 Kobe earthquakes highlighted the importance of accumulating real data by experimentation regarding the earthquake response, damage level, and collapse of structures (FEMA-355E; Youssef et al. 1995). Alternative sources to acquired information must be used.

Earthquake simulators provide a versatile resource to generate earthquake-like motions making possible measurements of input and output parameters needed to analyze the behavior of models of structural systems.

Due to size constraints it is difficult to study the dynamic response of full scale buildings in a laboratory. Testing of complete structures is then limited to small-scale models. One adequate modeling method, which is applicable to a great number of buildings, is the artificial mass simulation.

Many investigations based on previous earthquakes have led to the development of new retrofit strategies. A number of devices have been developed not only as solution to damaged structures, but as tools to provide significant performance advantages for the earthquake resistance design of new buildings. Although lots of methodologies have been developed, the need of reaching to a simple and economic solution is still a goal to accomplish.

This investigation has two principal objectives. First, to study the behavior and performance of a steel structure, typically used in commercial buildings in Puerto Rico, through scale modeling techniques. And second, to propose and evaluate the effectiveness of retrofitting methods to improve the response of this structure when subjected to ground motion.

1.2 RESEARCH OBJECTIVES

The goal of this research is to study the behavior of steel structures typically used in commercial buildings in Puerto Rico, subjected to earthquake ground motion using scale models, and to develop and study retrofitting alternatives. To achieve these goals, the following objectives were proposed:

- Develop a scale replica model of a prototype steel structure, which simulate all aspects that may contribute to the earthquake response of the full scale prototype.
- Propose an instrumentation system that provides an adequate evaluation of the model response behavior.
- Identify the dynamic characteristics of the proposed model.
- Study the behavior of the proposed model subjected to different earthquakes excitations.
- Investigate several alternatives to retrofit the structure to improve its structural performance.
- Study the seismic performance of the retrofitted model structure and compare the measured response with the response of the original (unretrofitted) model for the same excitations.

1.3 ORGANIZATION OF THE THESIS

A brief description of the contents of the following chapters is provided next.

Chapter II summarizes the literature consulted during this investigation. Four subjects were of particular interest: observed performance of steel buildings structures in earthquakes, shaking table test, passive energy dissipator systems, and internal force transducer.

Chapter III presents the consideration on which the definition of the prototype and the scale model were based, and the details of the model design and construction. The UPRM shaking table facility is described, and basic concepts of similitude theory are reviewed.

Chapter IV describes the instrumentation system implemented to measure the scale model response. The design, construction and calibration of the internal force transducer to measure column internal forces is presented.

Chapter V describes the concepts on which the proposed alternatives of retrofitting are based. Results from Snap-Back Tests and Simulated Earthquake Tests conducted on a single degree of freedom system, used to evaluate the effectiveness of the alternatives, are presented and discussed.

Chapter VI presents results of Simulated Earthquake Tests conducted on the scale model retrofitted with the different alternatives. Also, results form White Noise Tests used to determine dynamic properties of the model, are presented.

Finally, Chapter VII summarized the conclusions that were drawn from the performed tests, and present recommendations for future works.

CHAPTER II

LITERATURE REVIEW

2.1 OBSERVED PERFORMANCE OF STEEL BUILDING STRUCTURES IN EARTHQUAKES

Taking into consideration the severity of the ground shaking and large number of steel structures existing in the affected area, the Northridge earthquake can be regarded as the first severe seismic field test of modern steel structures in the U. S. (Krawinkler 1995). From inspections made to affected buildings it was noticed that although significant structural problems were identified, almost no structural collapses occurred.

Perhaps the most alarming pattern of structural damage involved brittle failures at beam-to-column connections in steel moment resisting frames (SMRFs), observed in many buildings from 1 to 26 stories high (Krawinkler 1995; Youssef et al. 1995). The most common failure was fracture at weldments connecting the beam flange to the column flange (Krawinkler et al. 1996). These types of local failure significantly decrease both the energy absorption capacity of the structure (elastic strain energy) and particularly the energy dissipation capacity (plastic deformation energy) (Bertero et al. 1994).

Most braced frames performed as projected. The typical local failures observed in this

buildings were: overall buckling or local buckling (or both) of frame braces; failures of connections of braces, and the fracture of column base plates (Bertero et al. 1994).

Other sources of information regarding steel building performance during earthquakes are provided by surveys performed in Japan after the Kobe earthquake. Some notable similarities in damage pattern produced by the Northridge and Kobe earthquakes are summarized next (FEMA-355E):

- a. Steel buildings in Japan and the U.S. had not experienced much damage in previous earthquakes. These two earthquakes exposed for the first time in each country the potential damage in welded steel moment resisting frame buildings.
- b. Many modern building structures designed and constructed with the current practices were damaged. Thus, damage was not exclusively associated with old technology and design practices.
- c. Although much damage was observed, no building constructed using the most recent design and construction practices collapsed.
- d. Many welded beam-to-column connections failed by fracturing, indicating that welded connections were one of the weakest links in steel moment frames.

Although the damage was similar, sources of damage were found to differ significantly between Japan and the U.S. in various aspects, including materials, design, fabrication, and inspection. As a result of these differences, practical solutions adopted to overcome the problems are also different (Nakashima and Chusilp 2002).

2.2 SHAKING TABLE TEST

Many articles on scale model tests on shaking tables can be found in the literature. The most relevant ones are summarized hereafter.

Moncarz and Krawinkler (1981) summarized part of a four year study on the feasibility and limitations of small-scale model studies in earthquake engineering. The basics of similitude theory and its application to the modeling of dynamically excited structures are reviewed in this work and similitude laws for various types of models are developed. Recommendations are made for the fabrication and joining of model elements for steel structures. The research has demonstrated that model analysis can be used in many cases to obtain quantitative information on the seismic behavior of complex structures which cannot be confidently analyzed by conventional techniques. Methodologies for model testing and response evaluation were developed in the project and applications of model analysis in seismic response studies on various types of civil engineering structures were evaluated.

Mills (1979) used a three story single bay steel frame structure, previously tested on the shaking table at the University of California at Berkeley, as a prototype for a 1:6 scale model study. The dynamic properties of the prototype were well defined allowing the correlation of the model response. Using the artificial mass simulation method, an accurate simulation of the prototype structure in terms of global and local response parameters was achieved. The nature of the prototype elastic and inelastic response was duplicated by the small scale model. Observed minor discrepancies in model-prototype correlation can be explained by the larger weld sizes of the model and by the influence of earthquake simulation reproduction capabilities on the response of the test structure.

Krawinkler (1988) presented a summary of information on scale effects in commonly used experimental procedures in earthquake engineering research. An evaluation of the effects of scaling of length and time, material and fabrication effects are discussed. It is concluded that the global elastic and inelastic response characteristics of complex structures can be simulated at model scales, even at rather small scales. Thus testing to failure of complex structural configuration in a controlled laboratory environment and at an affordable cost are possible. The author also concludes that the detailed localized response, particularly at connections and joints, can often not be reproduced adequately at reduced scales.

Nader and Astaneh-Asl (1989) examined experimental results on the dynamic behavior of one story steel structure tested with fixed, semi fixed, and flexible connections. Local responses such as columns internal forces and connections deformation time histories, floor acceleration, global responses such as drift, and dynamic characteristics such as natural frequencies were used to compare the behavior of the structure with each type of connector. The instrumentation and data reduction procedures to obtain these quantities are detailed in the report.

Bracci et al. (1992) evaluated a typical gravity load designed low-rise reinforced concrete frame building (lightly reinforced concrete structures) for seismic adequacy. A 1:3 scale three story model was built. The procedure to determine the additional mass needed when applying the artificial mass simulation method is well described. Four tests for the identification of the dynamic characteristic are presented (Impact Hammer Test, Pull-Back Test, Snap-Back Test and Compensated White Noise). These characteristics include natural frequencies, modal shapes, equivalent viscous damping ratios, stiffness matrix and modal

participation factors. The experimental test results are compared to analytical predictions from the program STAADTM (1989). The comparisons and discrepancies among the various tests and analytical predictions are also discussed. It was shown that the white noise shaking table test provided a justifiable correlation with the other identification tests, and thus it was chosen to be used throughout the testing of the model building.

Uang and Bertero (1986) summarized the research conducted on the behavior of a 0.3-scale model of a six story steel structure with different alternatives of concentric braces. The artificial mass simulation method was used. The tested structure was a scale model of a steel structure at larger scale previously constructed and tested, then correlation between their behavior was made. It was concluded that earthquake simulator tests of a reduced scale model can provide a better understanding of the dynamic response of the structure to earthquake ground motion. Good correlation can be expected between the test results of the full-scale and the reduced scale models if the difference in local behavior due to different detailing is recognized and taken into account. Also the analysis of the structure through energy method is presented along with the theoretical concepts presented.

Rodriguez et al. (2006) discuss an analytical model developed to study the linear and nonlinear dynamic response of a four-story steel scaled building subjected to low-level and high-level shake table tests inducing nominally elastic and inelastic responses, respectively. The analytical model was calibrated and validated against the results of the experimental program. A comparison of measured and calculated responses is presented in the paper. Absolute floor accelerations were found to be more sensitive to high-frequency content than other response parameters such as base shear force and overturning base moment. The model

is also used to observe differences in dynamic response of buildings when subjected to shake table tests with low fidelity in the reproduction of earthquake records. A methodology to obtain viscous damping ratio for each of the modes of vibration is developed. The results indicated that damping, in this case, is not constant during the dynamic response, and that the variability of this parameter increases for higher modes of vibration.

Chang et al. (1991) compare the dynamic characteristic of a full-size five-story steel prototype structure and a 2/5 scale laboratory model. The basic structural properties of both structures were identified through different procedures, and it was shown that the model structure obtained through the artificial mass simulation method can suitably simulate the dynamic behavior of the model. Three different bracing systems were tested in the scaled model, and their strengthening effect was shown by the measured frequency increase.

Wallace et al. (1985) studied a correlation between a steel braced frame scale model and a full size prototype structure. The scaled models were found to reproduce the global elastic and inelastic response characteristics of their prototype counterpart very well. It was concluded that brace buckling causes severe deterioration in story shear resistance, but the presence of a ductile moment frame surrounding the bracing system provides ductility and vertical load carrying capacity after brace buckling.

In El-Attar et al. (1991) a 1/6 scale 2-story lightly reinforced concrete building was tested. Several aspects and details to be considered when testing reduced scale models are discussed. Difference between the input and output acceleration was observed, then an effort to reduce these distortions was made. Methods to compare input and output signals are presented. The off-line compensation technique was used to reduce these differences with

acceptable results.

In Barreras (1999) two methods for the empirical determination of the natural vibration periods of buildings are studied by using a steel scale model of four floors. The methods studied consisted of an analysis by impulses (Impact Hammer Test) and an analysis by environmental vibration. In order to analyze the reliability and applicability of these methods, a criterion based on the analysis of the coherence between the input and output signals measured in the base and top of the building, was used. In the analysis by impulses, the frequencies of the first two modes of vibration were identified in the Fourier spectrum of the output signal and in the transfer function. The coherence function at these frequencies has values near one, indicating a good reliability in the results obtained. In the analysis with environmental vibration, the fundamental frequency was not detected when the input signal had small amplitude. In this case, the coherence function evaluated at frequencies near the fundamental has values near zero. Using one signal with larger amplitude the natural modes were identified in the transfer function and in the Fourier spectrum of the output signal.

The UPRM's earthquake simulator is described in Cortés Delgado (2005). The design, construction and calibration of the shake table are summarized. The dynamic characteristics of the reaction frame, simulator platform, and oil column are examined along with the possible interaction effects with a test structure. An initial determination of the quality of shake table reproduction has been obtained by carrying out preliminary experimental tests and analyzing the data. It was concluded that the earthquake simulator is capable of producing periodic motion and has been found operational at a range of 0.0 - 20.0 Hz. A small rotation of the simulator platform was detected. This rotation can be due to a mass

eccentricity, actuator or linear bearings misalignment. Table limitations discussed in this work are summarized in section 3.2.

2.3 PASSIVE ENERGY DISSIPATION SYSTEMS

Conventional design recognized that it is not economical to design ordinary structures to remain free of damage during a major earthquake. Modern building codes permits a reduction of the forces for design below the elastic level on the premise that, in a properly designed structure, inelastic action will provide that structure with significant energy dissipation capacity, and enable it to survive a severe earthquake without collapse. This inelastic action is typically intended to occur in specially detailed critical regions of the structure. Inelastic behavior in these regions, while able to dissipate substantial energy, also often results in significant damage to the structural member, and although the regions may be well detailed, their hysteretic behavior will degrade with repeated inelastic cycling (Aiken et al. 1993).

Several innovative approaches have been developed to provide significant performance advantages for the earthquake resistance design of new buildings, and also for the retrofit upgrading of the seismic performance of existing buildings. One of these approaches involves adding energy absorbers to a structure. The aim of including energy absorbers in a structure for earthquake resistance is to concentrate hysteretic behavior in specially designed and detailed regions of the structure and to avoid inelastic behavior in primary gravity load-resisting structural (Aiken et al. 1993). These energy absorbers are called passive energy dissipators.

The basic energy relationship of the structure is represented in the following equation (Bertero 1998; Uang and Bertero 1986; Uang and Bertero 1988):

$$E_I = E_K + E_S + E_\zeta + E_H \quad (2.1)$$

where:

E_I = earthquake input energy ; E_K = kinetic energy in structure

E_S = strain energy in structure ; E_ζ = viscous damping energy

E_H = hysteretic damping energy

The role of a passive energy dissipator is to increase E_H so that, for a given E_I , the elastic strain energy in the structure is minimized. This means that the structure will undergo smaller deformations for a given level of input energy than if it did not include energy dissipators.

Soong and Spencer (2002) summarized and described the more common energy dissipator devices used at the present time, and classify them in the following groups: Metallic yield dampers, Friction dampers, Viscoelastic dampers, Viscous fluid dampers, Tuned mass dampers, Tuned liquid dampers.

A review of the evolution of energy dissipation devices of hysteretic type is presented in Martinez-Rueda (2002). It is concluded that, in general, the desirable characteristics for energy dissipation devices of hysteretic type may be summarized as:

- optimum hysteretic behavior (i.e., virtually elastoplastic)
- economic (avoidance of exotic or sophisticated materials is advantageous)

- easy to install
- easy to repair, replace or recalibrate
- adequate long term behavior
- existence of calibration and design procedures/guidelines

It is also noticed that in some cases the current techniques may become so structurally invasive that they can lead to undesired side effects such as significant amount of construction work, large increments in building weight and base shear, critical alterations to building layout, and severe disturbance to building occupants.

In this research special interest was placed on friction dampers. These systems utilize the mechanism of solid friction that develops between two solid bodies sliding relative to one another to provide the desired energy dissipation. The use of these systems also changes the natural frequency of the structure and allows it to alter its fundamental dynamic characteristics during a severe earthquake.

The mechanical energy dissipation in a Friction Damped Braced Frame (FDBF) is equal to the product of slip load by the total slip travel summed over all devices. For very high slip loads the energy dissipation in friction will be zero, as there will be no slippage. If the slip loads are very low, large slip travels will occur but the amount of energy dissipation again will be negligible. Between these extremes, there is an intermediate slip load distribution which results in optimum energy dissipation. This intermediate distribution is defined as the “Optimum Slip Load Distribution”. The optimum slip load distribution can be evaluated by a series of nonlinear step dynamic analysis using a general purpose computer

program. In Cherry and Filiatrault (1993) an alternative method using the time history of the elastic strain energy stored in the structure is proposed, considering that the best response of the structure is obtained when the strain energy is a minimum at every instant of time.

Several articles on passive energy dissipators devices were consulted, specially of hysteretic type. Those where shaking table tests were used to analyze the devices resulted of special interest. Along with the device details, attention was placed on the instrumentation, the program tests and the parameters used to evaluate the device effectiveness. Some of these articles are summarize hereafter.

Filiatrault and Cherry (1987) presents the results obtained from tests conducted on Pall friction damper. The system consists if a mechanism containing brake lining pads introduced at the intersection of frame cross-braces. Seismic tests of a three story Friction Damped Braced Frame model were performed on an earthquake simulator table. The effectiveness of the friction devices in improving the seismic response is shown through diminution of lateral deflections, bending moments in beams, and floor horizontal accelerations. It was shown that the measure deflection at the top of the retrofitted structure was only 31% of the equivalent deflection of the frame without devices, and the acceleration at the same level was reduced by 53%.

Aiken et al. (1993) summarized the research conducted on seven types of passives energy dissipators tested under earthquake shaking condition in four different model structures. Four of the systems studied are friction systems, and of these, three (Sumitomo, Pall, and Friction-Slip) are based in Coulomb friction. The fourth is the Flour-Daniel Energy Dissipating Restraint, which is a device capable of providing self-centering friction resistance

that is proportional to displacement. The three other systems all have different energy dissipation mechanism: ADAS elements, which utilize the yielding of mild-steel X-plates; viscoelastic shear dampers using a 3M acrylic copolymer as the dissipative element; and Nickel-Titanium alloy shape-memory devices that take advantage of reversible, stress-induced phase changes in the alloy to dissipate energy. The seven systems and the tests performed are well described. The effectiveness of the various systems is evaluated by comparing the response of the test structures without and with the energy dissipator systems. The principal parameters considered were base shear, story drifts and story acceleration. It was concluded that all of the systems investigated exhibited characteristics beneficial to improved structural response to earthquake loading. As an example, the drifts were reduced by 10 to 60 percent, while story accelerations were reduced by 25 and 60 percent when using the friction dampers and the viscoelastic damper respectively.

A device based on a self-centering friction mechanism is investigated in Filiatrault et al. (2000). This device uses ring springs, also known as friction springs, as the key components to dissipate seismic-induced energy. Results of characterization tests performed on a 200-kN capacity damper prototype and shake table tests on a half-scale moment-resisting steel frame equipped with the same damper prototype are presented. The results of the characterization tests showed that the force-displacement hysteresis loops of the damper were self centering, repeatable, stable, identical in tension-compression, and nearly identical for all frequencies considered. In different shaking table tests (using El Centro time history record, scaling the PGA at different values) the peak relative displacement was reduced between a 38-50%, and the peak acceleration was reduced by 30% when the seismic damper is introduced.

2.4 INTERNAL FORCE TRANSDUCER

Internal force transducers (ITF) can be defined as devices capable of directly measuring the internal forces of a structural element (Sause and Bertero 1983). A simple IFT is a device which can be inserted in the structural member to measure internal forces. The advantages of this type of ITF are: (a) can be constructed from materials which have reliable force-deformation relations, (b) can be reliably instrumented, and (c) can be properly calibrated so that it is possible to directly measure the internal forces. A disadvantage is the potential for interference of the measuring device with the continuity of the structural elements in which the internal forces are measured.

The development and design criteria, fabrication consideration, and the calibration and installation of internal force transducer is presented in Sause and Bertero (1983). It is concluded that for the purpose of studying the dynamic response of structures to earthquake motions, and for short term static loading tests, the performance of this kind of transducer is acceptable.

Special force transducers to measure internal force of a scale model were fabricated by Bracci et al. (1992). Considerations on the design and calibration of the transducers are presented in this report.

The principles of the operation and fabrication of strain gage based transducers are described in Harris and Sabnis (1999), and in several Vishay Measurement Group technical articles (Vishay Measurements Group 2001a; Vishay Measurements Group 2001b; Vishay Measurements Group 2001c; Vishay Measurements Group 2001d).

CHAPTER III

SCALE MODEL DEFINITION AND CONSTRUCTION

3.1 INTRODUCTION

In this chapter the definition and construction of the scale model of the steel structure prototype used in this research is described. The prototype definition was based on the UPRM shaking table limitations and the general characteristics of steel structures typically used in commercial buildings in Puerto Rico (Appendix A). The facility limitations and the considerations applied on the prototype definition are discussed.

Using the artificial mass simulation (AMS) method a one-sixth scale model was defined. The characteristics and construction details of the scale model are presented. In addition, basic concepts of similitude theory which leads to the AMS method are reviewed.

3.2 SHAKING TABLE FACILITY

The UPRM Structural Laboratory is equipped with a uni-directional electro-hydraulic shaking table. The table facility is described in detail by Cortés Delgado (2005). Some important characteristics are summarized in Table 3-1 and discussed herein.

The plan dimensions of the platform are 7.5 ft by 4.5 ft with the longer dimension in the translating direction. The simulator platform weighs approximately 2,200 lb.

The simulator platform is supported by four-high accuracy, high-load capacity, preloaded and low-friction Crossed Roller Slide Tables. The load capacity of each roller is 2,640 lb. Therefore, considering the platform weight, the remaining load capacity of the table is 8,360 lb.

The displacement of the platform is produced by a MTS Model 244.21 hydraulic actuator. The span or stroke of the actuator, that is the maximum displacement capacity, is 6.0 in, or ± 3.0 in from the center position. For harmonic movements, span and frequency are inversely proportional. Therefore the maximum span decreases for increasing frequency.

The maximum mean velocity generated by the actuator is 29.62 in/sec. This value depends on the ability of the servo-hydraulic system to provide full flow rate to the actuator and diminishes beyond motions with frequencies of about 30 Hz.

The maximum acceleration of the seismic simulator is limited by the properties of the servo-hydraulic system and the mass that the system is driving. The maximum force that the actuator can produce is 11 kip. For a given table mass and using Newton's Second Law, the maximum table acceleration is:

$$a_{\max}^{bare} = \frac{F_{\max}}{W_{table}} = \frac{F_{\max}}{W_{table}} g \quad (2.2)$$

where a_{\max}^{bare} is the maximum bare table acceleration, F_{\max} represents the maximum actuator force, and W_{table} represents the weight of the bare table, and g is the gravitational acceleration

constant. Therefore, the maximum bare table acceleration is:

$$a_{\max}^{\text{bare}} = \frac{48,930 \text{ N}}{9,786 \text{ N}} g = \frac{11,000 \text{ lb}}{2,200 \text{ lb}} g = 5.0 g \quad (2.3)$$

However, when the table is loaded with a test structure, the maximum acceleration diminishes.

The maximum theoretical operating frequency of the oil column is 32 Hz. Nevertheless, it was concluded, by conducting several calibration tests, that the earthquake simulator is operational at a range of 0.0 – 20.0 Hz.

The simulator platform can be considered rigid because its natural frequency is almost three times (2.92) the theoretical maximum operating frequency of the table. Therefore, it was not expected any interaction effects between the simulator platform and a test structure at that operating frequency.

The controller used is the TestStar IIs AP System, composed of the Model 493.01 Servo-Controller and the Control computer (PC) with the software to control the Servo-Controller called MultiPurpose TestWare.

Table 3-1: Shaking Table Characteristics

Characteristics	Limit Value
Plan Dimensions	7.5 ft by 4.5 ft
Platform Weight	2,200 lb
Rollers load capacity	2,640 lb each
Span of the actuator	6.0 in, or ± 3.0 in from the center position
Maximum velocity	29.62 in/sec
Maximum bare table acceleration	5.0 g
Frequency range	0.00 – 20.0 Hz

3.3 PROTOTYPE DEFINITION

Two issues were considered in the selection of the prototype. First, the prototype's structural characteristics were selected to be representative of industrial or commercial buildings constructed in Puerto Rico. To accomplish this, the dimensions adopted for the prototype frame were based on two sources: a survey of typical constructions in the Mayagüez area, and from the data presented in López-Rojas (2005). Second, the prototype was selected such that a scale model of this structure could fit within the geometric constraints and load capacity of the UPRM Structural Laboratory shaking table. These limitations were discussed in section 3.2 and summarized in Table 3-1.

Taking into consideration these factors, the proposed prototype structure is a two story, two-by-one bays steel structure whose layout is shown in Figure 3-1. The story height is 15 ft and the bay length is 22.5 ft. The prototype beams and columns were selected from commercial shapes. Standard sections W12x96 were proposed for the columns and W21x40 for the beams. The structure is assumed to be built on stiff rock conditions such that no soil interaction or differential settlements need to be considered. The prototype weight is shown in Table 3-2, which is the combination of the columns and beams weight and the floor system.

Table 3-2: Prototype Weight

	First level (kip)	Second level (kip)
Beams	9.9	9.9
Columns	8.6	4.3
Floor system	45.6	45.6
Total	64.1	59.8

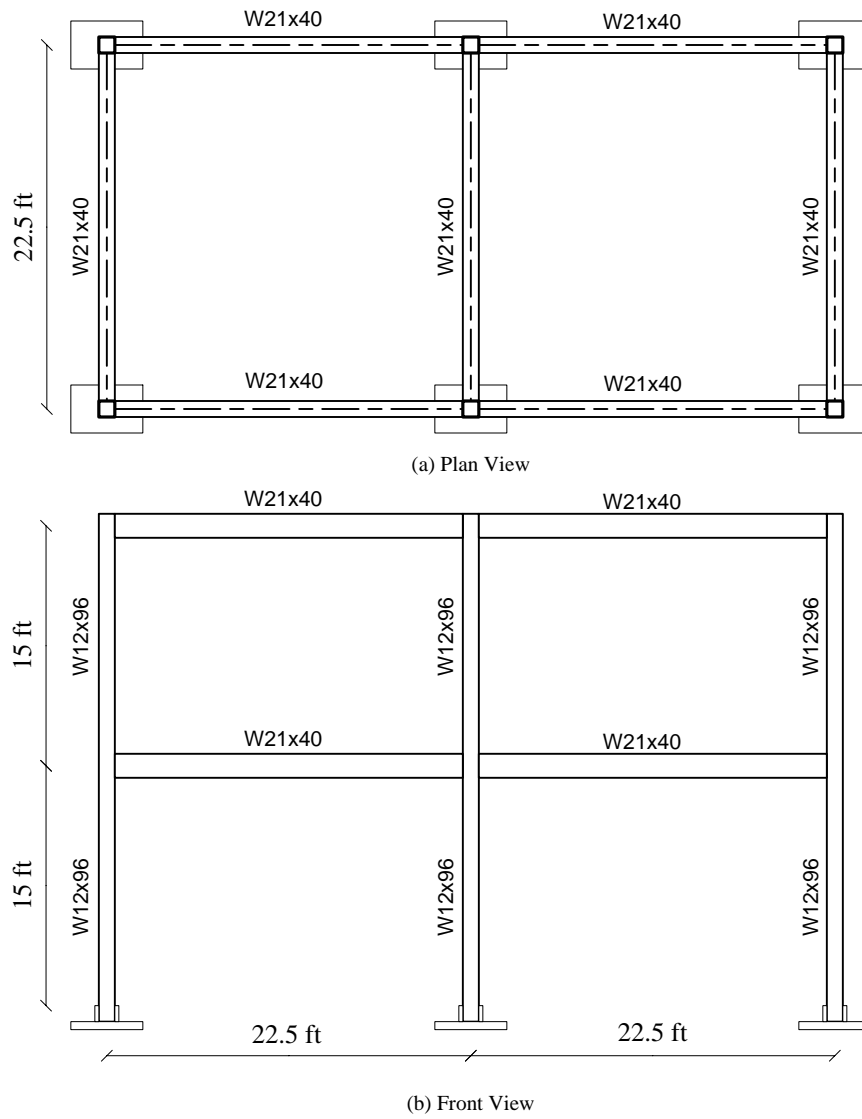


Figure 3-1: General Layout of the Prototype

3.4 SIMILITUDE REQUIREMENTS

The objective of this section is to introduce briefly the concepts which leads to the scaling laws used in this work and the basis of the artificial mass simulation method.

Modeling theory establishes the rules (similitude requirements) according to which the model and the prototype have to be related so that the behavior of one can be expressed as a function of the other. This theory establishes that all physical quantities can be expressed in terms of a group of basic or fundamental quantities (mass, time and length; or force, time and length). Since these basic quantities are independent on each other, as many scales can be selected arbitrarily as there are basic quantities needed to describe the problem (Moncarz and Krawinkler 1981). In a dynamic problem which may be described by mass, length and time, three scales can be selected arbitrarily. In order to fit in the shaking table platform, the model size needs to be reduced, therefore the length scale needs to be set ($\lambda_l = l_p / l_m$). The gravitational effect on the model stresses must be accounted, therefore an acceleration scale equal to one was chosen ($\lambda_a = 1$). The third independent scale law set in this case is related to the materials used in the construction of the model and prototype, and will be the relation between its modulus of elasticity ($\lambda_E = E_p / E_m$). If the same material is used in both prototype and model, then this relation is also equal to one ($\lambda_E = 1$). Through dimensional analysis, all the remaining similitude relationship can be derived as function of this three. Several important relationships are summarized in Table 3-3.

The mass, m , is defined as the product of the material density, ρ , and material volume, V . Therefore, in order to accomplish mass similitude, both volume and density should be scaled. But generally the material used in the construction of the model are selected arbitrarily and do not satisfy this condition. If no correction is applied in the model structure, then the mass, gravitational force, frequency and acceleration would not be scaled in the proper fashion, since the required and provided material densities are different.

Therefore an adjustment of the material density must be provided by adding masses to the model structure (artificial mass simulation).

Table 3-3: Similitude Relationships for Artificial Mass Simulation Method (Moncarz and Krawinkler 1981)

Parameter	Units	Any Material	Same Material and Acceleration	Same Material and Acceleration (1/6)
Geometric Length, L	L	λ_L	λ_L	6
Modulus of Elasticity, E	$\frac{F}{L^2}$	λ_E	1	1
Acceleration, a	$\frac{T}{L^2}$	1	1	1
Density, ρ	$\frac{F \cdot T^2}{L^4}$	$\frac{\lambda_E}{\lambda_L \cdot \lambda_a}$	$\frac{1}{\lambda_L}$	0.17
Time, t	T	$\lambda_L^{1/2}$	$\lambda_L^{1/2}$	$\sqrt{6} = 2.45$
Frequency, ω	$\frac{1}{T}$	$\lambda_L^{-1/2}$	$\lambda_L^{-1/2}$	$\frac{1}{\sqrt{6}} = 0.41$
Force, F	F	$\lambda_E \cdot \lambda_L^2$	λ_L^2	36
Mass, m	$\frac{F \cdot T^2}{L}$	$\lambda_E \cdot \lambda_L^2$	λ_L^2	36
Strain	$\frac{L}{L}$	1	1	1
Stress	$\frac{F}{L^2}$	λ_E	1	1
Energy	$F \cdot L$	$\lambda_E \cdot \lambda_L^3$	λ_L^3	216

This problem is well described in Bracci et al (1992) as follows. If the same material is to be used in the prototype and model, the required scaling factor for material density, λ_ρ^{req} , is:

$$\lambda_\rho^{req} = \frac{\lambda_E}{\lambda_L \cdot \lambda_a} = \frac{1}{\lambda_L \cdot 1} = \frac{1}{\lambda_L} \quad (2.4)$$

The provided model material density is the same as in the prototype, such that:

$$\lambda_\rho^{prov} = 1 \quad (2.5)$$

Since the scaling factor for material volume is λ_L^3 (see

Table 3-3) the required and provided masses of the model are defined below:

$$m_m^{req} = m_p \cdot \frac{1}{\lambda_\rho^{req}} \cdot \frac{1}{\lambda_v} = m_p \cdot \frac{1}{\lambda_L} \cdot \frac{1}{\lambda_L^3} \rightarrow m_m^{req} = m_p \cdot \frac{1}{\lambda_L^2} \quad (2.6)$$

$$m_m^{prov} = m_p \cdot \frac{1}{\lambda_\rho^{prov}} \cdot \frac{1}{\lambda_v} = m_p \cdot 1 \cdot \frac{1}{\lambda_L^3} \rightarrow m_m^{prov} = m_p \cdot \frac{1}{\lambda_L^3} \quad (2.7)$$

where m_m^{req} is the required mass of the model, m_m^{prov} is the provided mass of the model and m_p is the mass of the prototype. Therefore from the differences in material density properties, the provided mass is less than required for similitude. To correct this difference, the additional mass, Δm , that must be added to the model is:

$$\Delta m = m_p \cdot \left(\frac{1}{\lambda_L^2} - \frac{1}{\lambda_L^3} \right) \quad (2.8)$$

When using a one-sixth scale this variation is 5/216 of the prototype total mass. Since the scaling factor for required gravitation acceleration is 1.00, the additional weight required in the model is:

$$\Delta W_m = \frac{5}{216} W_p = \frac{5}{216} \lambda_L^3 W_m^{prov} = 5 W_m^{prov} \quad (2.9)$$

A more convenient determination of the required mass for the model to satisfy similitude is through the gravitational force, also described by Bracci et al. (1992). The required gravitational force (weight) of the model, W_m^{req} , is defined in terms of the gravitational force of the prototype and the appropriate scale factor from Table 3-3 as follows:

$$W_m^{req} = W_p \cdot \frac{1}{\lambda_L^2} = \frac{1}{36} W_p \quad (2.10)$$

where W_p is the gravitational force of the prototype structure and λ_L is the geometric length scale factor. Therefore the weight to be added is the difference of the required and provided weight of the model:

$$\Delta W = W_m^{req} - W_m^{prov} \quad (2.11)$$

3.5 MODEL DEFINITION

It was intended to construct and test the largest possible steel model that could be accommodated on the earthquake simulator. Taking into consideration the previously discussed geometric constraints and load capacity of the UPRM shaking table, a one-sixth

(1/6) scale was used. Table 3-3 shows the scale factors used to model the structure.

The general layout of the 1/6 scale model structure is shown in Figure 3-2. Figure 3-3, Figure 3-4, and Figure 3-5 shows photographs of the constructed model taken from different angles.. The columns were numbered from 1 to 6. The story model height is 30 in, for both levels, and the bays length is 45.5 in. The columns are fixed to the base as shown in Figure 3-6. All the beam-to-column connections are flexible as it is seen in Figure 3-7, and therefore no moment is transferred.

It was intended to study the behavior of the model subjected to a simulated earthquake acting along its weak direction, hence special supports were added to the platform to overcome the geometrical table limitations. Each support weight was 191.1 lb. This additional weight was considered to establish the load capacity of the table.

The properties of the shapes used in the construction of the scale model are summarized in Table 3-4. The same table also summarizes the required and provided properties of the shapes needed to satisfy moment of inertia and cross sectional area similitudes. Since the response of this model was more influenced by the moment of inertia of the columns than by its geometry and area, then some variation in these parameters could be made (Mills et al. 1979). Therefore HSS2x2x3/16 shapes were used for columns, instead of W-shapes. It was also considered that since the beam-to-column connections were flexible, neither the area nor the moment of inertia of the beams would affect significantly the general behavior of the model, then S3x5.7 were used for the beams.

As discussed in Section 3.4, to satisfied mass similitude, extra weight must be added, other than the self weight of the model structure. The weight of the prototype is shown in

Table 3-2. The provided weight of the model is summarized in Table 3-5. The required weight was determined through similitude requirement for gravitational forces, as defined in equation (2.10). The weight to be added to each level of the model is displayed in Table 3-6.

In order to solve the weight deficiency, steel plates were added, as shown in Figure 3-5. Each plate was 46 in long, 6 in wide and 5/8 in thick, and weighted 50 lb; therefore 28 plates were placed at each level. There was no connection between the plates and they were simply supported by the beams, thus no rigid diaphragm was defined.

Table 3-4: Summary of the Prototype and Model Sections Properties

	Prototype		Model			
			Required		Provided	
	Column	Beam	Column	Beam	Column	Beam
Shape	W12x96	W21x44	-	-	HSS2x2x3/16	S3x5.7
Inertia (in ⁴)	833.0	843.0	0.64	0.65	0.641	2.52
Area (in ²)	28.2	12.0	0.78	0.36	1.190	1.67

Table 3-5: Summary of the Provided Model Weight

	First level (kip)	Second level (kip)
Beams	0.181	0.181
Columns	0.094	0.054
Total	0.275	0.235

Table 3-6: Summary of the Additional Weight Requirement

	Required Weight W_m^{req} (kip)	Provided Weight W_m^{prov} (kip)	Weight to be added $\Delta W = W_m^{req} - W_m^{prov}$ (kip)
Firs level	1.781	0.275	1.506
Second level	1.661	0.235	1.426

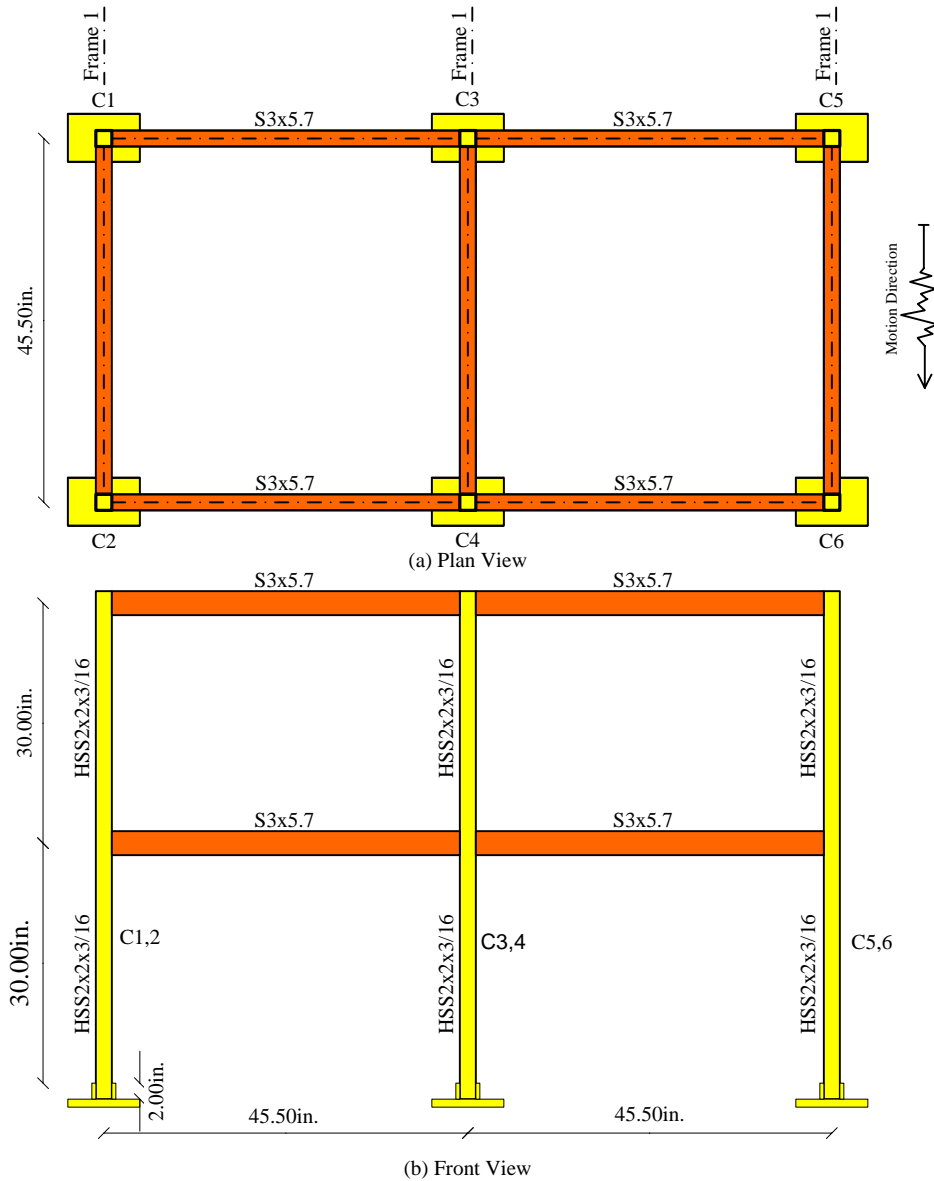


Figure 3-2: General Layout of the Model Structure



Figure 3-3: West Side View of the Model



Figure 3-4: East Side View of the Model



Figure 3-5: View of the Steel Plates

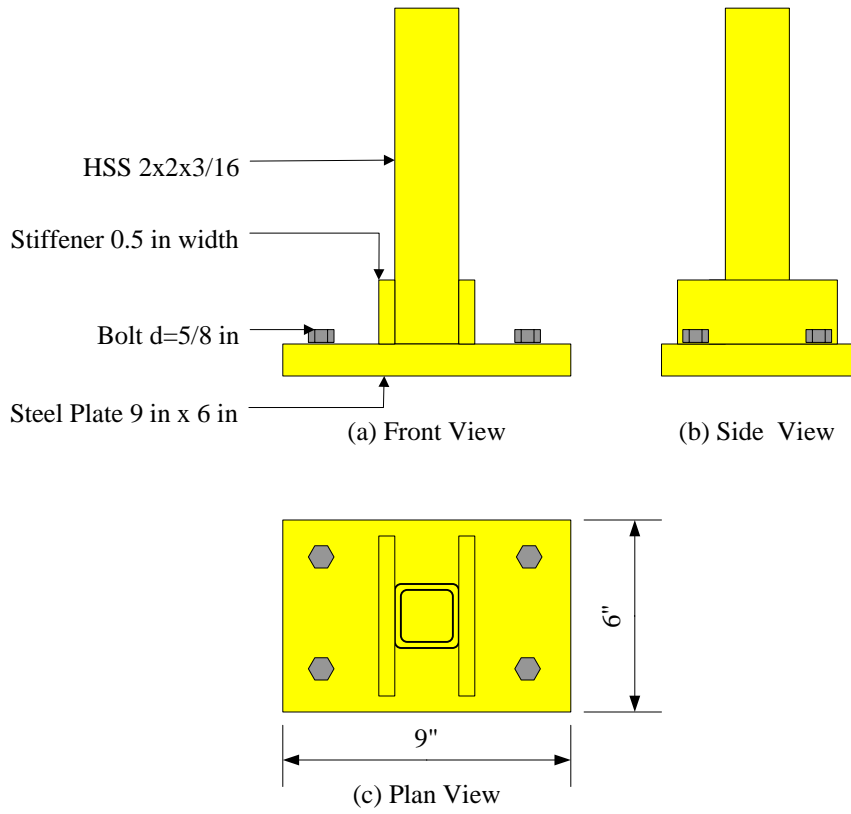


Figure 3-6: Base – Column Connection

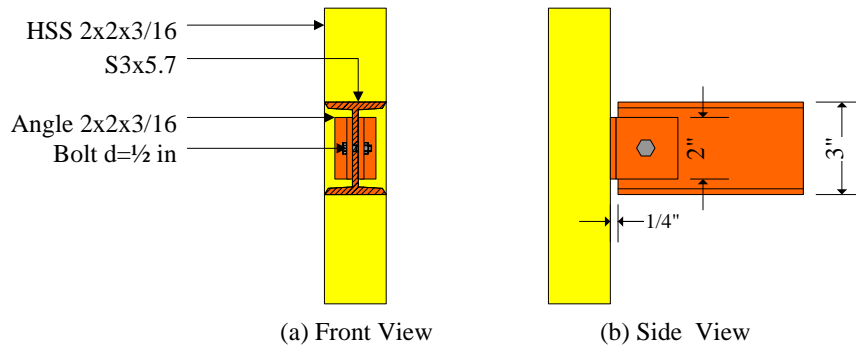


Figure 3-7: Beam – to – Column Connection

CHAPTER IV:

INSTRUMENTATION

4.1 INTRODUCTION

The following sections describe the instrumentation implemented to measure the structural response of the model. The principal variables used to analyze the response of the model were nodes acceleration and displacement, and column internal forces. Linear variable differential transformers (LVDT), piezoresistive accelerometers and special force transducers (load cells) were installed. The general layout of the instrumentation is shown in Figure 4-1.

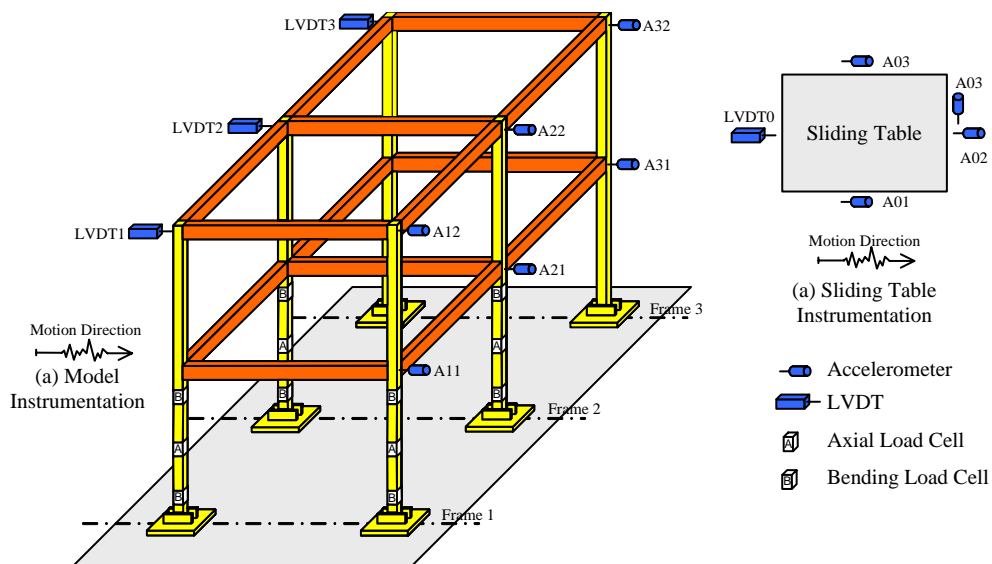


Figure 4-1: General layout of the Instrumentation

4.2 ACCELEROMETERS

Piezoresistive accelerometers model JTFA made by Sensotec were used to measure absolute accelerations in different points. The range of the accelerometer used is $\pm 5g$ with a $\pm 1\%$ nonlinearity error. The accelerometers were firmly attached to their locations with screws.

Six accelerometers were used to measure nodes acceleration located in columns 2, 4, and 6, one at first level node and one at second level node, as shown in Figure 4-2. The channel denomination used was A_{ij} , where i is the frame number and j is the level.

Base acceleration was measured with 4 accelerometers, three located parallel to the direction of motion, two at the sides ($A01$ and $A03$), the third ($A02$) at the front of the sliding table, and a fourth one ($A04$) was located perpendicular to the direction of motion to detect torsional effects.



Figure 4-2: Accelerometers layout

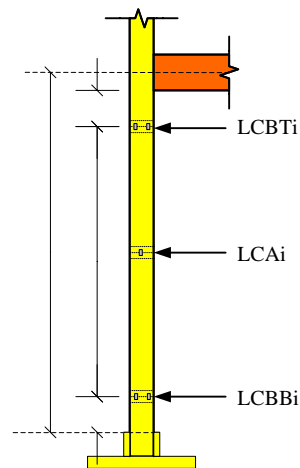
4.3 SPECIAL FORCE TRANSDUCERS (LOAD CELLS)

Special force transducers (load cells) to measure the internal force response of the model have been installed in four of the first story columns (column 1 and 2 at frame 1, and column 3 and 4 at frame 2) , as shown in Figure 4-1 and Figure 4-3. On each column two load cells are used to measure bending in the direction of the motion, at the top and bottom of the column, and one in the middle of it to measure the axial force. The location of the load cells in a column is presented in Figure 4-4.

Axial and bending moment load cells are based on different arrangements of Wheatstone bridge circuits. In both cases full bridges were chosen to improve the output signal.



Figure 4-3: View of the Load Cells in Column



LCBTi : Load Cell for measure bending in the top of column i
 LCAi : Load Cell for measure axial force in i column i
 LCBBi : Load Cell for measure bending in the bottom of column i

Figure 4-4: Layout of Load Cells in a Columns

The strain gages used are type CEA-06-125UN-350 fabricated by Vishay Micro Measurements. The resistance (R) in ohms at 24°C is 350.0±0.3%, and the gage factor (GF) at 24°C is 2.100±0.5%. In both types of load cells an input voltage of 10V was used.

- ***Axial load cell calibration constant***

The location of the strain gages and the wiring used for the axial load cells is presented in Figure 4-5. With this arrangement the relationship between the input voltage V_{in} and the output voltage V_{out} is:

$$\frac{V_{out}}{V_{in}} = 2(1 + \nu) \frac{GF}{4} \varepsilon_A \quad (2.12)$$

where ν is the Poisson's ratio of the column steel, and ε_A is the strain at the gage location.

The axial strain ε_A produced by axial load P is:

$$\varepsilon_A = \frac{P}{E A} \quad (2.13)$$

where E is the elastic modulus, and A is the cross-sectional area of the column.

The relationship between the axial load and the output voltage is obtained by replacing ε_A from (2.12) in equation(2.13):

$$P = E A \frac{I}{2(1 + \nu) \frac{GF}{4} \frac{V_{out}}{V_{in}}} = K_{axial} V_{out} \quad (2.14)$$

where K_{axial} is the theoretical calibration constant of the axial load cell.

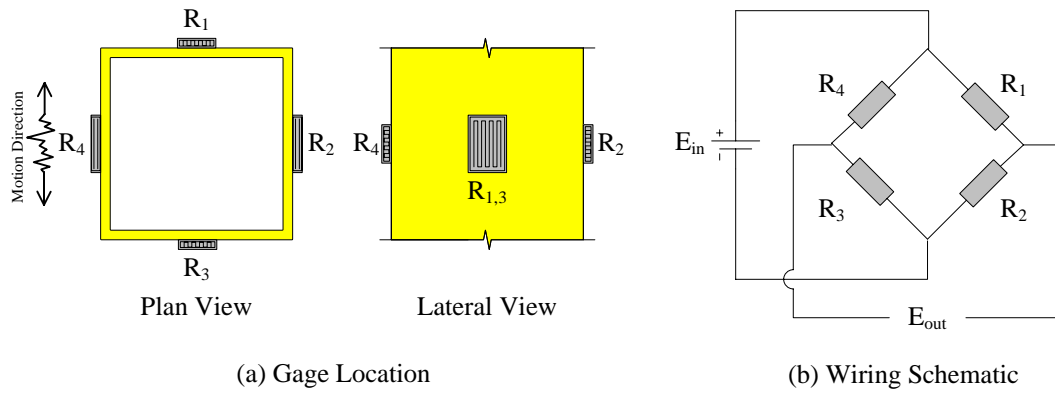


Figure 4-5: Axial Load Cell

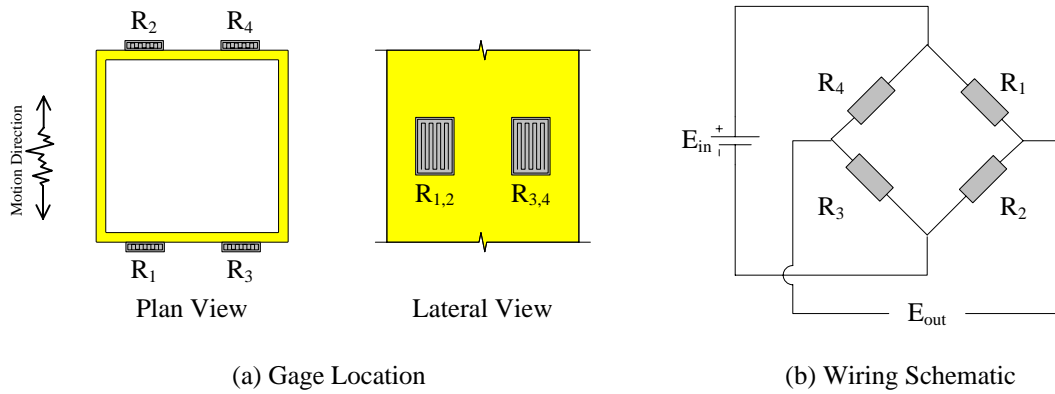


Figure 4-6: Bending Moment Load Cell

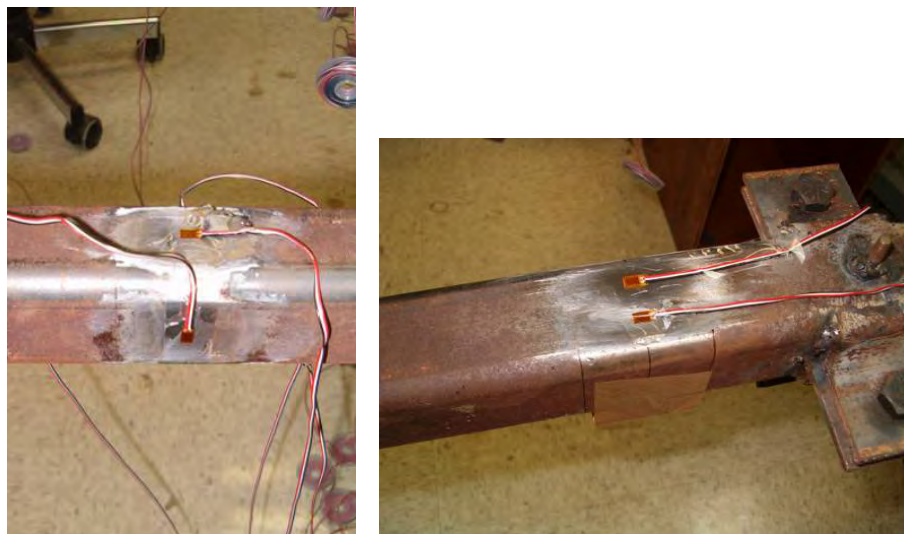


Figure 4-7: View of the Strain Gages Arrangements

Substituting the values for each variable, the theoretical constant for the axial load cell is:

$$P = 29,000 \frac{\text{kip}}{\text{in}^2} \times 1.19 \text{in}^2 \times \frac{I}{2(1+0.3) \frac{2.1}{4}} \times \frac{E_{out}}{10V} \times \frac{V}{1000 \text{mV}} = 2.528 \frac{\text{kip}}{\text{mV}} \times V_{out}$$

$$K_{axial} = 2.528 \frac{\text{kip}}{\text{mV}} \quad (2.15)$$

- **Bending moment load cell calibration constant**

The location of the strain gages and the wiring used for the bending moment load cells are presented in Figure 4-6. With this arrangement the relationship between the input voltage V_{in} and the output voltage V_{out} is:

$$\frac{V_{out}}{V_{in}} = GF \varepsilon_B \quad (2.16)$$

The strain ε_B produced by a bending moment M is:

$$\varepsilon_B = \frac{M}{ES} \quad (2.17)$$

where S is the sectional modulus of the shape.

The relationship between the bending moment and the output voltage is obtained by replacing ε_B from (2.16) in equation (2.17):

$$M = ES \frac{I}{GF} \frac{V_{out}}{V_{in}} = K_{bending} V_{out} \quad (2.18)$$

where $K_{bending}$ is the theoretical calibration constant of the bending moment load cell.

Replacing the values for each variable, the theoretical constant for the bending moment load cell is:

$$M = 29,000 \frac{\text{kip}}{\text{in}^2} \times 0.641 \text{in}^3 \times \frac{1}{2.1} \times \frac{E_{out}}{10V} \times \frac{V}{1000 \text{mV}} \times \frac{\text{ft}}{12 \text{in}} = 0.0738 \frac{\text{kip} - \text{ft}}{\text{mV}} \times V_{out}$$

$$K_{bending} = 0.0738 \frac{\text{kip} - \text{ft}}{\text{mV}} \quad (2.19)$$

Due to the differences in the actual strain from the assumed distribution and the lack of precision in the shapes properties values due to fabrication processes, the load cells were calibrated against known internal forces. Figure 4-8 presents the general layout of the set-up used. The loading was provided manually using a 5 ton jack. Several cycles of loading were performed. For each load cell the calibration constant was obtained from the plot of the load versus voltage variation. The values of the calibration constants for each load cell are summarized in Table 4-1, and the respective plots are presented in Appendix B.

Table 4-1: Calibration Constants for Load Cells

Load Cell Identification	Column 1	Column 2	Column 3	Column 4
LCBTi $\left(\frac{\text{kip} - \text{ft}}{\text{mV}} \right)$	0.0774	0.0755	0.0764	0.0761
LCAi $\left(\frac{\text{kip}}{\text{mV}} \right)$	2.6015	2.6527	2.6447	2.561
LCBBi $\left(\frac{\text{kip} - \text{ft}}{\text{mV}} \right)$	0.0765	0.0749	0.0749	0.0748

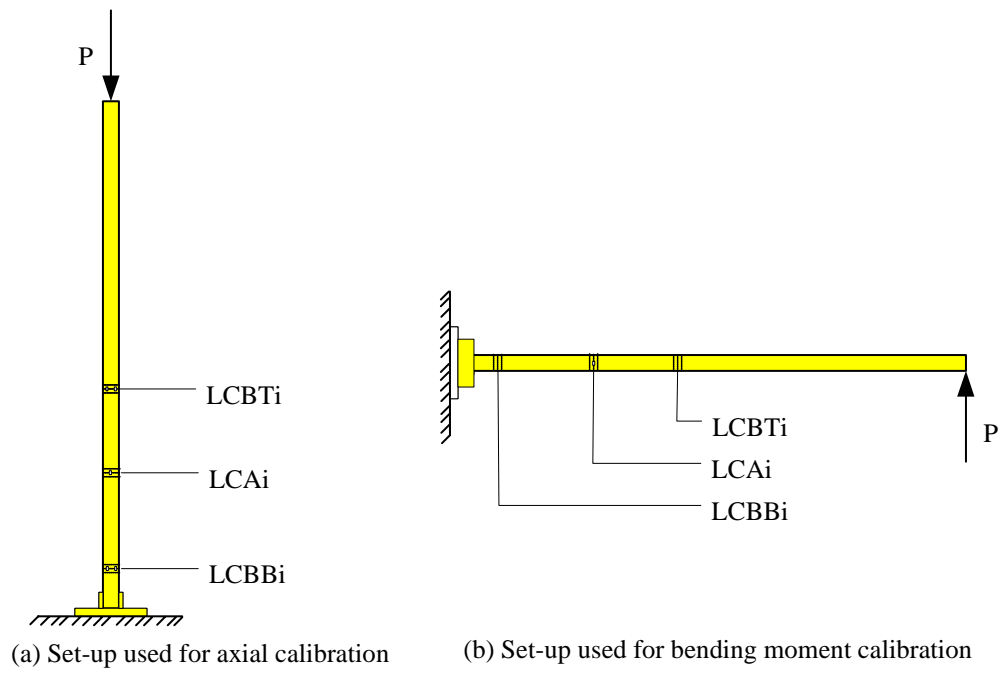


Figure 4-8: Set-Up for Load Cell Calibration

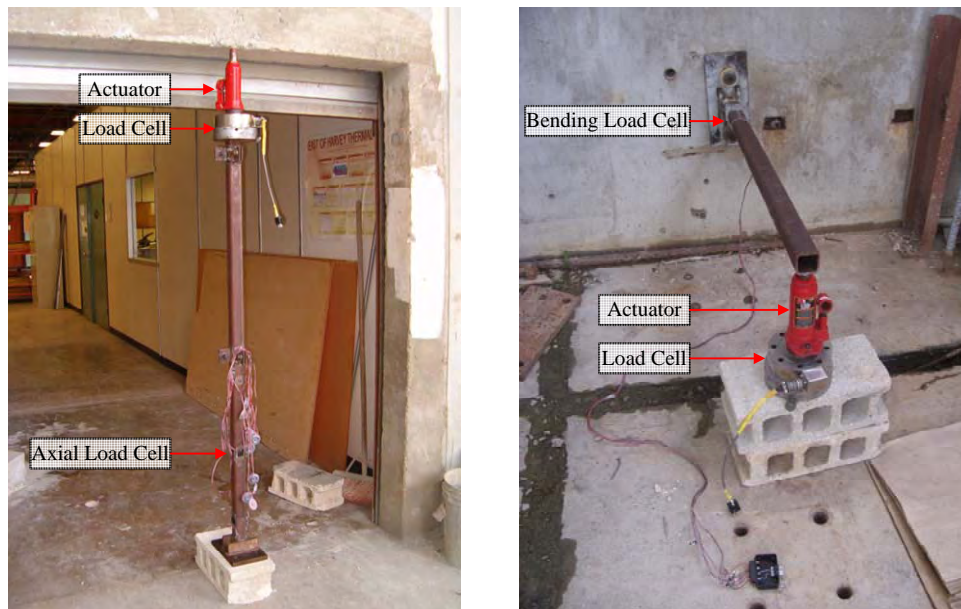


Figure 4-9: View of Set-Up for Load Cell Calibration

4.4 DISPLACEMENT TRANSDUCERS

Three Linear Variable Differential Transformers (LVDT), made by Sensotec, were used to measure the relative displacements of the top level nodes and the absolute displacements in the longitudinal direction of the table, as shown in Figure 4-1 and Figure 4-10 View of the LVDT. The LVDTs used have a global displacement range of ± 3 in.

The identification used for these transducers was *LVDT_i*, where *i* is the frame number.



Figure 4-10 View of the LVDTs

4.5 DATA ACQUISITION SYSTEM

The output signals from the transducers were passed through two signal conditioner devices: a Dewetron's Model DAQ-PV was used for the accelerometers and LVDTs, and a Dewetron's Model DAQ-P Bridge for the load cells. This device also provided the excitation voltage.

The information processed by the signal conditioners was stored in the Data Acquisition Computer. This computer is equipped with an Iotech signal processing board and DasyLab 5.0 software. The signal processing board model installed at the Data

Acquisition PC (DAQ) is an Iotech model 16-bit board called DAQ BOARD-200A. It has a 100 kHz A/D converter and eight differential or sixteen single-ended analog input channels.

As the fundamental frequency of the model found in preliminary tests was under 10 Hz, it was decided to perform data block scans at 0.01 sec intervals to produce at least 10 points per fundamental cycle.

4.6 DATA REDUCTION

Recorded data containing noise is an inevitable phenomenon whenever an electronic data acquisition system is used. A single pole analog low pass filter, provided in the DADISP 2002 software was used to remove this noise. A cut-off frequency equal to 20 Hz was selected for the following reasons: (a) the first and second mode of vibration of the scale model were found to be within this range; (b) this is the highest frequency at which the shaking table is operational.

Additionally, to smooth the resulting processed signal a three points moving average was used.

CHAPTER V

EVALUATION OF RETROFITTING ALTERNATIVES

5.1 INTRODUCTION

One of the goals of this investigation was to explore different retrofitting schemes to improve the response of the steel structure studied to earthquakes motions. These alternatives should satisfy three main conditions: (i) the method used could not block the internal circulation of the building (not invasive), and therefore should be applied externally, (ii) the retrofitting system should have a simple mechanism so no further calibration or special materials must be needed, and (iii) the system should not be expensive.

In the following sections the alternatives of retrofitting are described and analyzed. A single degree of freedom system (SDOF) was used to represent the basic structure where the different alternatives were applied using variations of a general set up. The SDOF system and the general set up are described in section 5.2.

Snap-back tests were performed to analyze each alternative individually. These tests allowed us to understand the operation of the retrofitting system and to determine which variables influence the results. Then, tests using simulated earthquakes were performed to

compare the different alternatives. In these tests the response of the systems subjected to the same input motion was measured, thus allowing for a direct comparison of the benefits of each scheme.

Different parameters were considered to evaluate the effectiveness of the alternatives: the damping ratio was used in the snap-back tests, whereas peak acceleration and peak relative displacement were employed in the simulated earthquake tests.

Two methods were used to determine the damping ratio: the logarithmic decrement method and the half-power bandwidth method. The logarithmic decrement method can be used on the response signals from single and multiple degree of freedom systems which are primarily governed by a single mode of vibration. The half-power bandwidth method can be used for systems with small damping and well separated modes. In these cases the peaks in the Transfer Function occur precisely at the natural frequencies of the model, just as in the Fourier Transform. Therefore, due to the characteristics of the SDOF used, both methods could be applied.

5.2 SINGLE DEGREE OF FREEDOM SYSTEM DESCRIPTION

It was intended to use a simple structure to understand the retrofitting effects of the alternatives proposed. Then, the single degree of freedom system (SDOF) shown in Figure 5-1 was used. The dynamic characteristics of the system are summarized in Table 5-1. The stiffness coefficient K was determined as the slope of a force vs. deformation curve. The theoretical fundamental frequency of the system was determined as:

$$\omega = \sqrt{\frac{K}{M}} = \sqrt{\frac{K \cdot g}{W}} = \sqrt{\frac{68.3 \times 386.4}{55}} = 21.9 \frac{\text{rad}}{\text{sec}} \rightarrow f = 3.49 \text{ Hz} \quad (2.20)$$

Table 5-1: Dynamic Properties of the Single Degree of Freedom System

Weight W (lb)	55.0
Stiffness K (lb/in)	68.3
Frequency ω (rad/sec)	21.9
Frequency f (Hz)	3.49
Period T (sec)	0.287

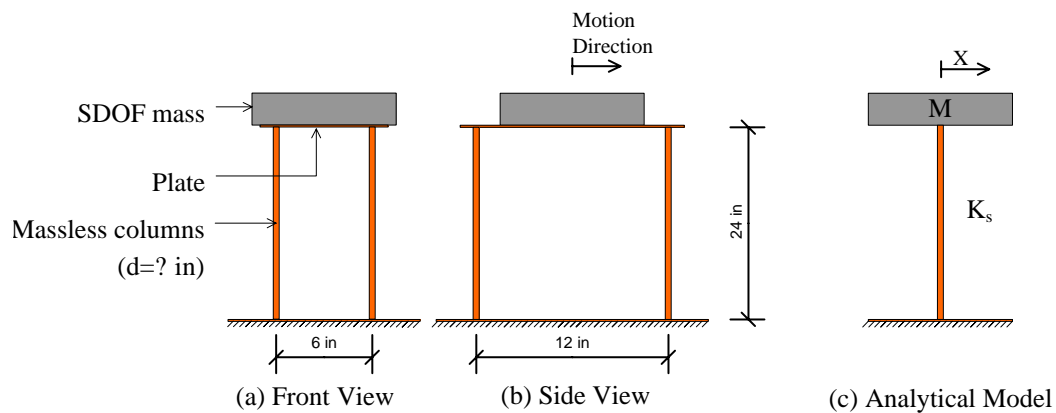


Figure 5-1: Single Degree of Freedom System

5.3 DESCRIPTION OF THE RETROFITTING ALTERNATIVES

5.3.1 GENERAL SET UP

The retrofitting schemes were evaluated using variations of the same general set up. A layout of the general set up is presented in Figure 5-2 and a photograph of the constructed model is shown in Figure 5-3. It consists of two secondary masses connected to the SDOF with a cable through a pulley system.

The pulleys were attached to a rod supported by a ball bearing pillow block unit as

shown in Figure 5-4 and Figure 5-5. In different tests the pulleys were changed but the mechanism that permits the rotation (the ball bearing units) remained the same.

An analytical model of the general set up is presented in Figure 5-6. In all the tests performed m_2 and m_3 had the same value, thus for simplicity in this report these masses were called m , while m_1 was called M . The secondary masses m were defined as a percentage of M . Values of 2, 10 and 20 % were used, and they were identified as $m_{2\%}$, $m_{10\%}$ and $m_{20\%}$ respectively. Likewise, sets of pulleys with diameters of 2, 6 and 12 inches were used and were called d_2 , d_6 and d_{12} . The stiffness coefficient of the SDOF was referred to as K_s and the stiffness of the cables was denoted k_c .

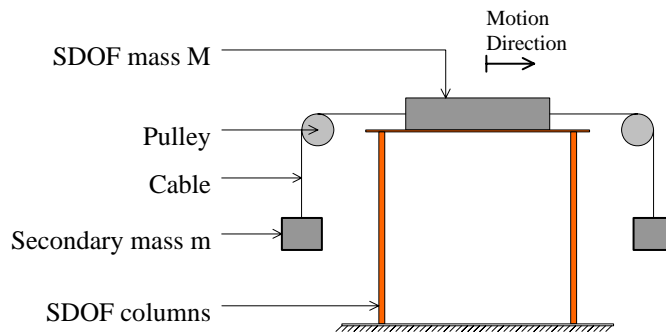


Figure 5-2: Layout of the General Set Up

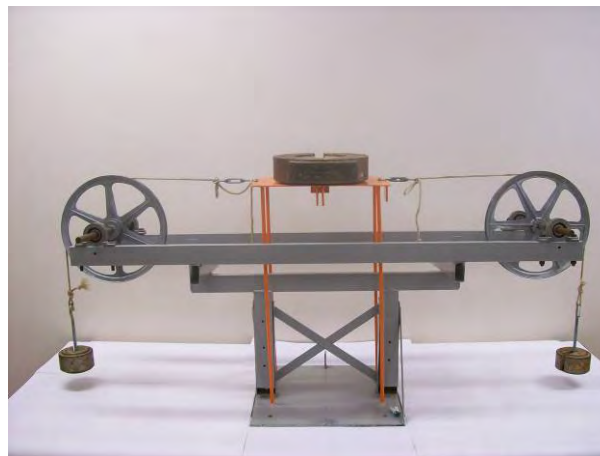


Figure 5-3: View of the General Set-Up

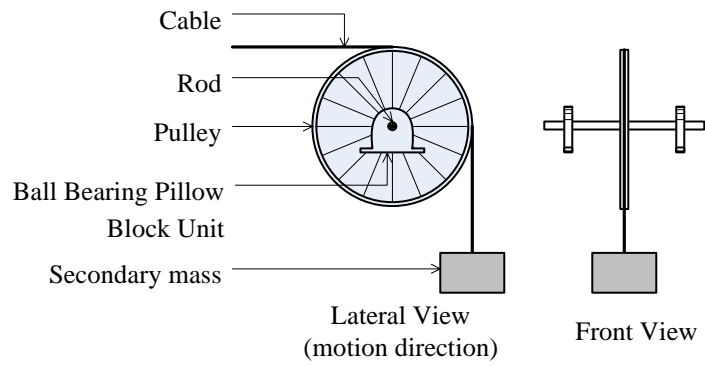


Figure 5-4: Layout of the Pulley System



Figure 5-5: View of the Pulley System

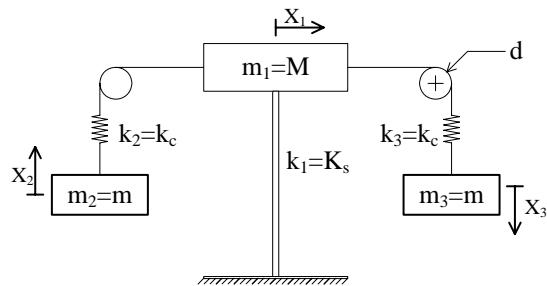


Figure 5-6: Analytical Model of the General Set Up

5.3.2 ALTERNATIVE 1: FREE PULLEY WITH HANGING MASS SYSTEM (FP)

An analytical model of the first alternative of retrofitting is presented in Figure 5-6. The secondary masses m were hanging from the cables and the pulleys were allowed to rotate. The cable used was considered inextensible, and thus when the system was excited the three masses experienced the same displacements through time.

As shown in the scheme presented in Figure 5-7, the internal friction of the pillow block produces a resisting moment M_r opposed to the movement, while the tension ΔT on the cable produced a moment $M_T = \Delta T \cdot d$ in the direction of the motion. The moment M_r is the same for a given mass m and different pulley diameters, because it depends on the internal friction effects of the pillow block, but M_T is proportional to the pulley diameter. Then, the bigger d , the smaller is the tension ΔT needed to overcome the resisting moment.

This alternative was based on the use of the resisting moment of the pillow M_r , as a mechanism to dissipate energy. It was expected that the bigger the pulley, the smaller the energy dissipation effects.

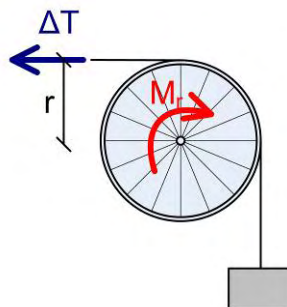


Figure 5-7: Pulley Scheme

5.3.3 ALTERNATIVE 2: RESTRAINED PULLEY WITH HANGING MASS SYSTEM (RP)

This alternative had the same layout than the FP system, but the pulleys were fixed, so no rotation was allowed. Therefore, friction forces were generated between the cable and the pulleys. The rationale for proposing alternative is to use the friction forces as a mechanism to dissipate energy.

An attempt to measure the friction between the cable and the pulley was made. The set up used is shown in Figure 5-8. Two weights w were connected with one cable through two pulleys. The weights used correspond to the masses $m_{10\%}$ and $m_{20\%}$, and the pulley diameters were d_2 , d_6 and d_{12} . At the beginning of the test the weights were hanging in equilibrium, then an additional weight Δw was added until a displacement was ensued. The incipient displacement was measured with a LVDT. Figure 5-9 displays plots of the tension variation ΔT in two points of the cable produced by Δw , measured with the two load cell (Figure 5-8), as a function of the weight displacement, measure with an LVDT.

It was observed that for a given weight w , the friction forces for pulleys d_2 and d_{12} exhibit similar values. This was expected, since the forces due to dry friction should be proportional to the normal forces. However, the friction forces measured using pulley d_6 were larger. It was consider that this difference was due to grooves exhibit only on the d_6 pulley's surface.

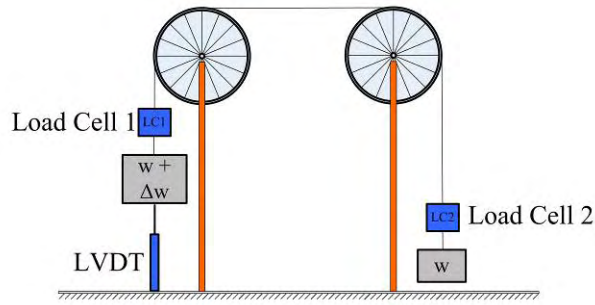


Figure 5-8: Set up for measuring the friction between cable and pulley

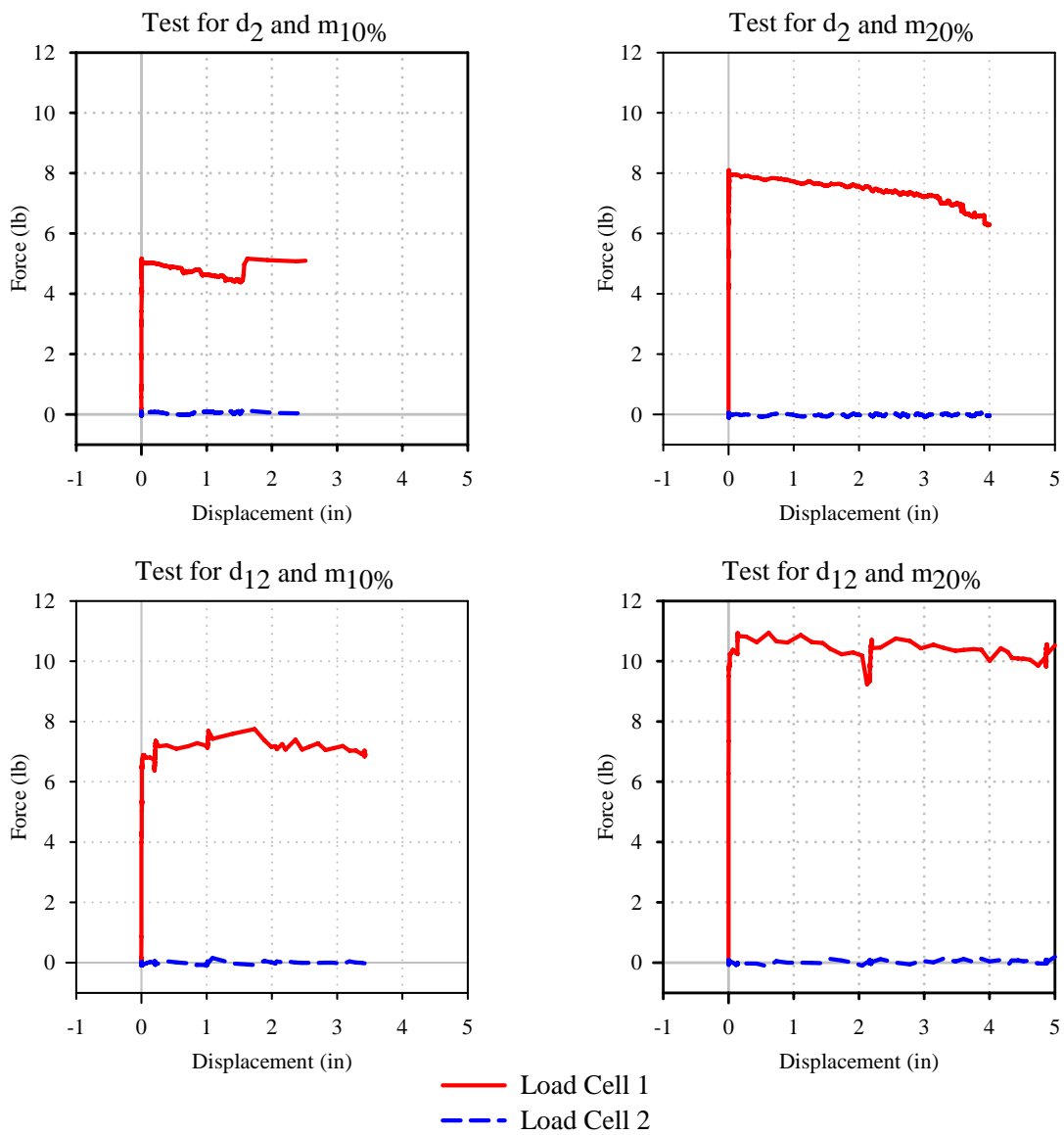


Figure 5-9: Cable Tension vs. Weight Displacement

5.3.4 ALTERNATIVE 3: FREE PULLEY WITH SUPPORTED MASS (FPSM)

In this alternative the secondary masses m were initially resting at the ground level, as shown in Figure 5-10. The pulley shafts were allowed to rotate, and pulleys with a diameter d_{12} were used, so the torque to overcome the internal friction effects of the pillow block was minimized. When the system was excited the masses m was raised and then hit the floor in an alternate fashion. An amount of energy is lost in each collision. This alternative makes use of these collisions as a mechanism to dissipate energy from the system.

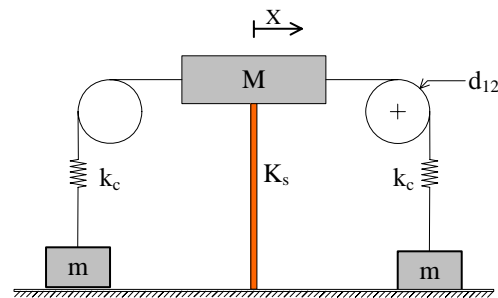


Figure 5-10: Layout of Alternative 3

5.3.5 ALTERNATIVE 4: RESTRAINED PULLEY WITH SUPPORTED MASS (RPSM)

This alternative is based on the previously described FPSM system but the shafts were fixed. Therefore, the energy provided to the structure by the external excitation will be dissipated through the collisions of the secondary masses m , and through the friction forces between the cable and the pulley.

5.3.6 ALTERNATIVE 5: FLEXIBLE CABLE SYSTEM (FC)

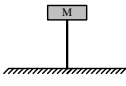
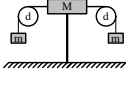
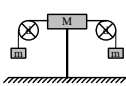
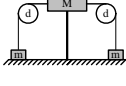
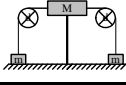
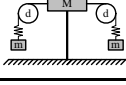
This alternative is based on the original FP system but the cable that connects the secondary masses with the SDOF system was replaced for a number of rubber bands acting in parallel. The coefficient k_c was a function of the stiffness of the group of rubber bands. Pulleys with diameter d_{12} were used, and were allowed to rotate. This was done to minimize the moment required to overcome the internal friction on the pillow blocks. This alternative scheme was proposed to study the influence of the cable stiffness k_c in the response of the system.

5.4 TEST PROGRAM

Table 5-2 presents a summary of the tests performed to analyze the proposed alternatives of retrofitting. Two types of tests were conducted:

- Snap-Back Tests. The objective of this series of tests was to evaluate each alternative individually, and to identify which variables affect the results obtained and how. The excitation was achieved by a pull-and-release procedure. In all cases the initial offset was 0.5 in.
- Simulated Earthquake Tests. These tests were used to compare the response of the system retrofitted with different alternatives, when subjected to the same input motion. For that reason, useful conclusions can be drawn from the direct comparison of the responses.

Table 5-2: Summary of the Performed Tests on the Retrofitting Alternatives

Alternative	M (lb/g)	m (%M)	d (in)	Performed Tests				
				Snap -Back	El Centro	Taft	North_ ridge	San Salvador
SDOF 	10	-	-					
	20	-	-	✓				
	50	-	-	✓	✓	✓	✓	✓
FP 	50	2	2	✓				
	50	10	2	✓	✓	✓		
	50	20	2	✓	✓	✓		
	50	2	6	✓				
	50	10	6	✓	✓	✓		
	50	20	6	✓	✓	✓		
	50	2	12	✓				
	50	10	12	✓	✓	✓	✓	✓
	50	20	12	✓	✓	✓		
RP 	50	10	2	✓	✓	✓	✓	✓
	50	20	2	✓				
	50	10	6	✓				
	50	20	6	✓				
	50	10	12	✓	✓	✓	✓	✓
	50	20	12	✓				
FPSM 	10	10	12	✓				
	10	20	12	✓				
	20	10	12	✓				
	20	20	12	✓				
	50	10	12	✓	✓	✓	✓	✓
	50	20	12	✓				
RPSM 	50	10	2	✓	✓	✓	✓	✓
	50	10	12	✓	✓	✓	✓	✓
	50	20	12	✓				
FC 	50	10	12	✓	✓	✓	✓	✓
	50			✓				
	50			✓				

5.4.1 SELECTION OF THE EARTHQUAKE RECORDS

The selection of the earthquakes used was based on three principal considerations. First, the natural frequencies of the SDOF and the scale model should be within the range of the dominant the frequency content of the earthquakes records. Second, the earthquakes should reflect a probable type of seismic motion that could occur in Puerto Rico. And third, the maximum displacement, velocity and acceleration of the records should be within the shaking table limitations.

Four earthquakes acceleration records were selected to perform this tests. Table 5-3 displays some characteristics of these ground motions. The El Centro and Taft Earthquakes records have been typically used in Puerto Rico in structural design for many years. The Northridge and San Salvador Earthquakes records were chosen among a selection made by Martínez Cruzado et al. (2001) to produce design spectra for Puerto Rico.

Table 5-3: Descriptions of the Earthquakes

Earthquake and Location	Station	Mag.	PGA (g)
Imperial Valley, 18/5/1940	El Centro	7.0	0.313
KERN County, 21/7/1920	Taft Lincoln School	7.4	0.156
Northridge, 17/01/1994	Castaic	6.6	0.568
San Salvador, 10/10/1986	Hotel Camino Real	5.5	0.345

To satisfy time similitude requirements a scale factor of $\lambda_t = \lambda_L^{1/2}$ was used to compress the time history of the accelerogram. The earthquake records were applied at different amplitudes to evaluate the model structure performance under seismic excitation. Measured accelerogram records, used in the evaluation of the retrofitting alternatives, are presented in Figure 5-11, along with the original input signal. Difference between these

signals might be due to accidental eccentricities and table limitations.

Figure 5-12 and Figure 5-13 show the elastic response spectra of the four earthquakes with a peak ground acceleration of 1g and considering 1% and 10% damping ratios respectively. The theoretical natural period of the SDOF is indicated in each graph. It can be noticed that for periods close to the natural period, and for damping ratios below 10%, amplification of the acceleration will occur. But if the damping ratio is higher than 10% no amplification would be produced by any of the earthquakes selected.

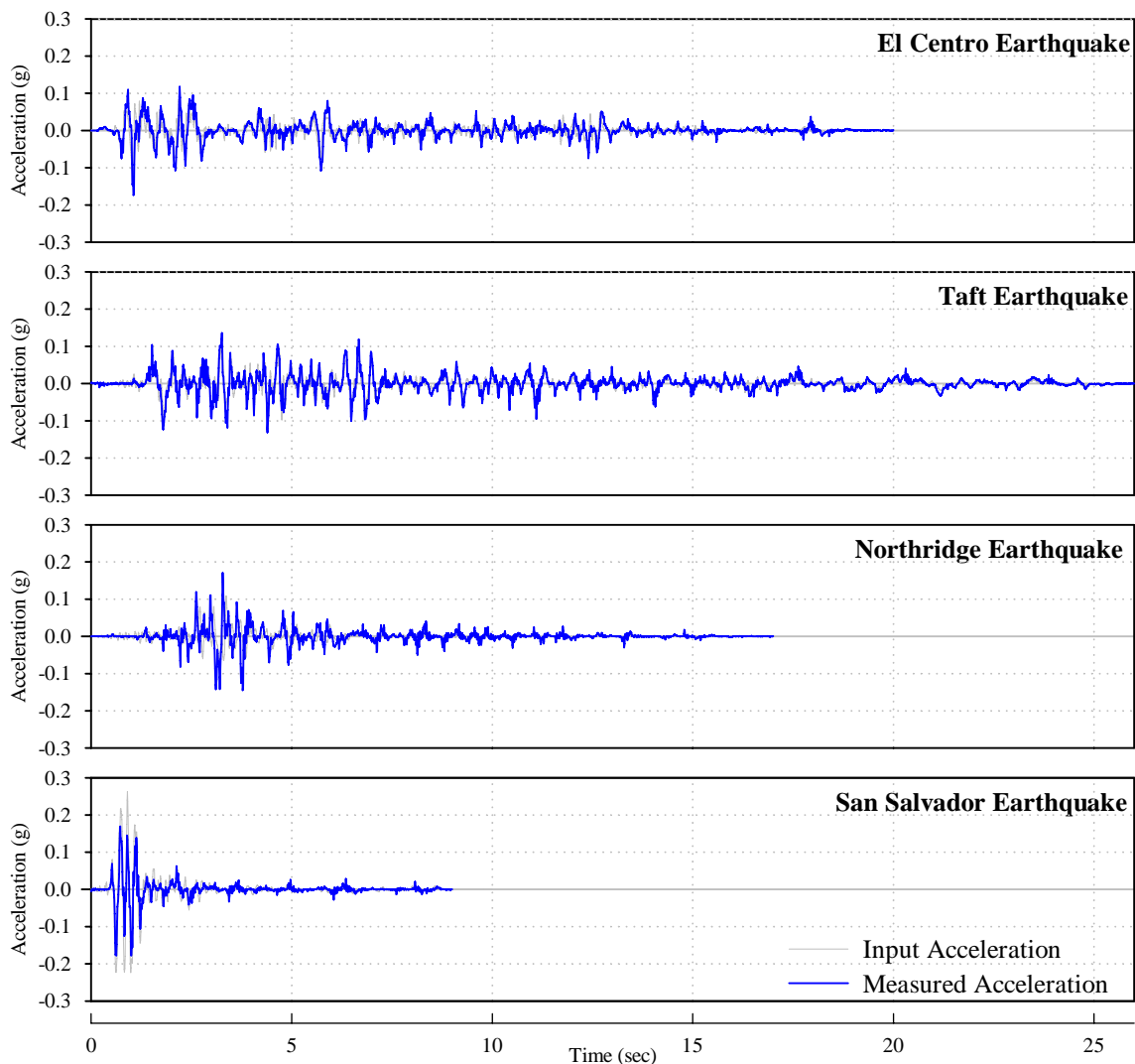


Figure 5-11: Earthquakes Records used in Simulated Earthquakes Tests

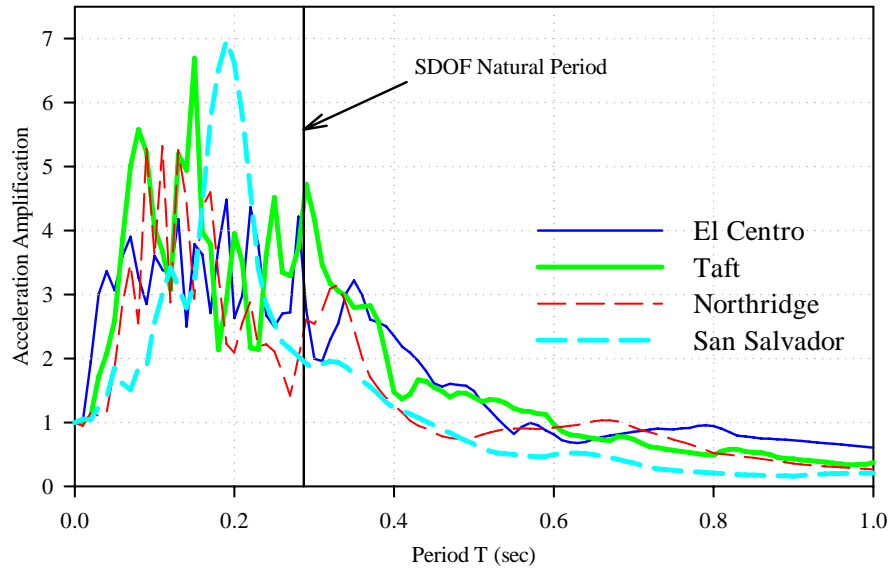


Figure 5-12: Elastic Response Spectra with $\zeta=1\%$

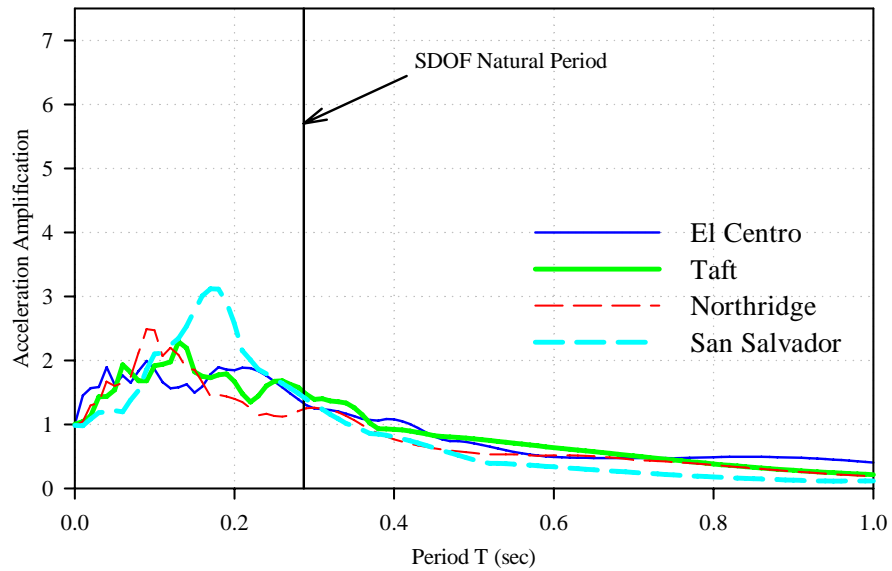


Figure 5-13: Elastic Response Spectra with $\zeta=10\%$

5.5 RESULTS FROM SNAP-BACK TESTS

5.5.1 SNAP-BACK TESTS FOR SDOF

Several free vibration tests were conducted to verify the value of the theoretical natural frequency ω , and to determine the value of the damping ratio ζ . Figure 5-14 presents the mass M acceleration records of two of these tests conducted for $M = 50$ lb /g. In the first case no LVDT was used and in the second a LVDT was placed to record the displacements of the mass M . The Fourier Transform of both records is presented in Figure 5-15.

The transfer function peak for the first case was found at a frequency of 3.39 Hz, and for the second case at 3.41 Hz. Both values are similar and very close to the theoretical natural frequency calculated in section 5.2.

The damping ratios determined by means of the half-power method for both cases, without and with LVDT, were 0.22% and 1.11% respectively. Therefore the use of an LVDT introduces certain amount of damping to the system. This effect was ignored in the following tests since the LVDT was used in all the tests and the damping produced has a small value.

5.5.2 SNAP-BACK TESTS FOR FP

Snap-back tests using secondary masses $m_{2\%}$, $m_{10\%}$ and $m_{20\%}$, and the pulleys with diameters d_2 , d_6 and d_{12} , were performed. The acceleration response time history of the mass M obtained with masses $m_{10\%}$ and pulleys with different diameters are presented in Figure 5-16. The respective Fourier Transforms are presented in Figure 5-17. The damping ratio was calculated in each case using the half-power bandwidth method. The results are summarized in Table 5-4.

Relative displacement between the cable and the pulley was observed in tests in which the 2 inches pulley was used, and therefore the damping calculated was a result of internal friction on the pillow block, plus the friction between the cable and the pulley. In this alternative it was intended to analyze only the pillow block internal friction effects on the response, thus tests with pulley d_2 were not considered representative.

It was observed that when using secondary masses $m_{2\%}$ the cable was not in contact with the pulleys all the time. Thus it was decided to discard this option in the following tests.

From the remaining results it was observed that the damping ratio diminishes as the pulley diameter increase and it was minimum when pulley d_{12} was used. Then to minimize the effect of the pillow block the pulley d_{12} was used in further tests. It was also concluded that the use of secondary masses $m_{20\%}$ did not produced an important improvement in the response with respect to the tests where secondary masses $m_{10\%}$ was used.

5.5.3 SNAP-BACK TESTS FOR RP

The mass M acceleration time history of the tests corresponding to masses $m_{10\%}$ and pulleys with different diameters are presented in Figure 5-18, and the respective Fourier Transform are shown in Figure 5-19. The damping ratios, calculated in each case using the half-power bandwidth method, are summarized in Table 5-4.

In all cases the damping ratios were increased in comparison with the SDOF. As a consequence of the high values of damping obtained, the Fourier Transform does not presents sharp peaks.

The damping ratios calculated for a given secondary mass and pulleys d_2 and d_{12} presented similar values. This was expected since the friction force in these cases depends primarily on the normal force (the weight of the secondary masses in these cases), as discussed in section 5.3.3.

Pulley d_6 produced higher damping, since the friction forces between the cable and the pulley were larger because of the presence of grooves in the pulley surface.

For the same pulley diameter, the damping ratio for a secondary masses $m_{20\%}$ was almost double than that for masses $m_{10\%}$.

The results obtained implied that in this configuration the damping is a function of the friction produced between the cable and the pulley. Then the effectiveness of the alternative depends on the value of the friction coefficient between those elements. It was also concluded that the diameter of the pulley does not significantly affect the response.

5.5.4 SNAP-BACK TESTS FOR FPSM

Snap-back tests performed on the FPSM alternative using secondary masses $m_{10\%}$ and $m_{20\%}$ are presented in this section. Since it was only intended to observe the effect on the system response of the secondary masses collisions, the effect of the pillow block had to be minimized. Therefore, only pulley d_{12} was used. The acceleration responses of the mass M for these cases are presented in Figure 5-20 and the respective Fourier Transforms are displayed in Figure 5-21. The damping ratios, calculated in each case using the half-power bandwidth method, are shown in Table 5-4.

It is noticed that in both cases a considerable increase in the damping ratio was achieved. It was also concluded that even though better results were achieved using $m_{20\%}$, the augment in the damping ratio was not important. Thus, no significant advantage is obtained with the use of larger secondary masses

5.5.5 SNAP-BACK TESTS FOR RPSM

This section presents the results of the snap-back tests performed on the RPSM alternative using secondary masses $m_{10\%}$ and $m_{20\%}$. The mass M acceleration records for these cases are presented in Figure 5-22 and the respective Fourier Transforms are shown in Figure 5-23. The damping ratio was calculated in each case using the half-power bandwidth method. The results are summarized in Table 5-4.

In both cases an augment in the damping ratio was achieved. As discussed in the previous section, no advantage was observed by increasing the secondary mass.

5.5.6 SNAP-BACK TESTS FOR FC

Eight free snap-back tests were performed to determine the number of rubber bands that produced the best improvement on the system response. The acceleration time histories and the respective Fourier Transforms are presented in Figure 5-24 and Figure 5-25. In all cases secondary masses $m_{10\%}$ and pulley d_{12} were used. In *case 1* a minimum number of rubber bands were used. This minimum number is a function of the minimum strength needed to resist the forces when the system was excited. In the following tests rubber bands

were added until the behavior of the system was similar to the cases where an inextensible cable was used. This was achieved in *case 8*.

The area below a Fourier Transform peak can be related with the damping ratio. By observing the transfer functions of the different cases it was concluded that *case 5* provided more damping.

Additional free vibration tests were performed to compare the results obtained by using rubber bands and a spring with the same stiffness. For these tests only one secondary mass was connected to the system, as shown in Figure 5-27 and Figure 5-28. Plots of force vs. deformation for the rubber band and for the spring used are presented in Figure 5-26. The stiffness of each element, calculated as the slope of the trend line, was 3.65 lb/in for the spring and 3.54 lb/in for the rubber band.

The results of three tests are presented, namely: (a) SDFS with an inextensible cable, (b) the system with the spring, and (c) the system with rubber bands. The acceleration records for the mass M and for the secondary mass m are presented in Figure 5-29. Additionally, the Fourier Transforms for the acceleration records of the mass M are presented in Figure 5-30.

When using the inextensible cable, only one peak in the transfer function was found in the frequency range from 0 to 10 Hz. This implies that the system still behaves as a single degree of freedom oscillator. When using the spring two peaks are found. Therefore the system behaves as a two degree of freedom system, as expected. In this case no augment on damping with respect to the use of the inextensible cable was observed. When rubber bands were used, also two peaks were found in the Fourier Transform but a significant decrease on

the area below the peak was observed, indicating an increase in the damping. Examining these results it was concluded that the augment in the damping was due to the properties of the rubber.

5.6 CONCLUSIONS FROM SNAP-BACK TESTS

The most important conclusions obtained from the results of the snap-back tests are summarized next.

- All the alternatives proposed produced an increase in the damping of the system.
- The results obtained from FP depend on the internal properties of the pillow block unit: the more resistance to rotate, the more damping is produced. Since the larger the pulley, diameter the smaller the tension in the cable required to overcome the resistance to rotate of the pillow block, the damping ratio obtained is smaller. In other words: the damping ratio diminishes as the pulley diameter increases. In this work the minimum damping was obtained when pulley was used. Therefore pulley d_{12} was used in tests where the pillow block friction was intended to be minimized.
- The results obtained from RP tests implied that the damping in this alternative is a function of the friction produced between the cable and the pulley. Then the effectiveness of this alternative depends on the value of the friction coefficient between those elements and on the weight on the secondary masses. It was also

observed that the effectiveness in the increase of the damping was independent of the diameter of the pulley used.

- The use of secondary masses $m_{20\%}$, on the FPSM and RPSM systems did not produce significant improvement on the results, in comparison with masses $m_{10\%}$. As the use of larger masses implied constructive inconveniences on a full scale structure, only secondary masses $m_{10\%}$ are proposed to be used.
- Among all the cases studied, the best results were obtained for the alternatives where friction between the cable and the pulley occurred.
- The use of rubber bands to connect secondary masses with the principal system produced an increase on the damping ratio. It was concluded that these results depend on the damping properties of the rubber band used rather than on its stiffness.

Table 5-4: Damping Ratio from Snap-Back Tests

Alternative	d (in)	Mass m (on % of M)		
		2%	10%	20%
FP	12	2.3	2.4	2.4
	6	5.8	4.3	4.3
	2	14.7	32.4	41.9
RP	12	-	26.7	48.7
	6	-	33.1	51.2
	2	-	26.1	45.9
FPSM	12	-	12.72	16.63
RPSM	12	-	29.60	22.70

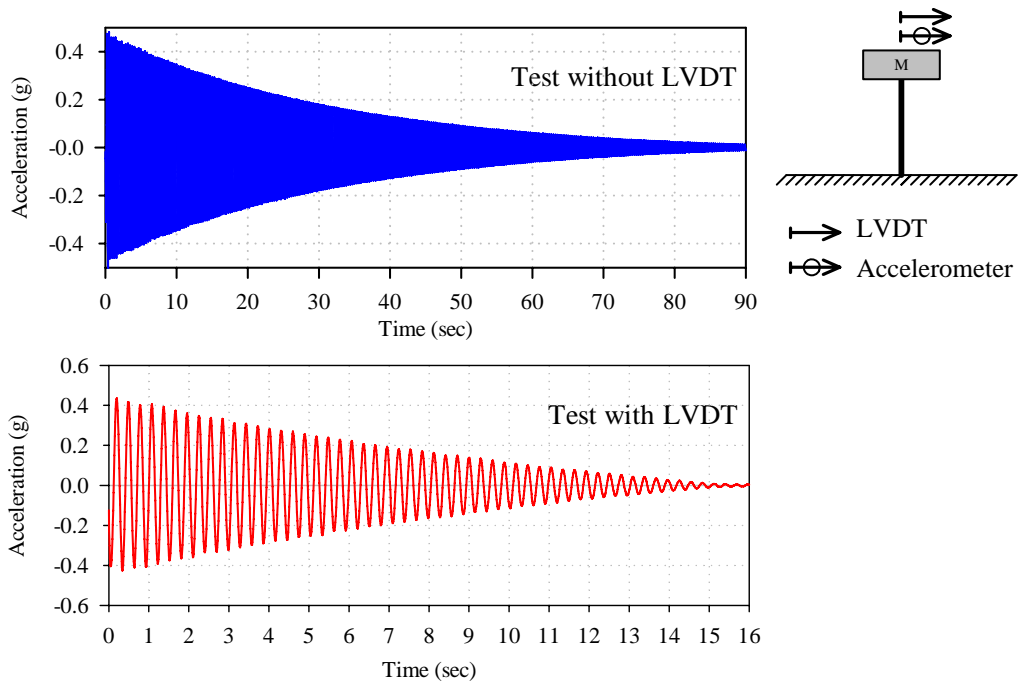


Figure 5-14: Mass M Acceleration Response from Snap-Back Tests for SDOF System

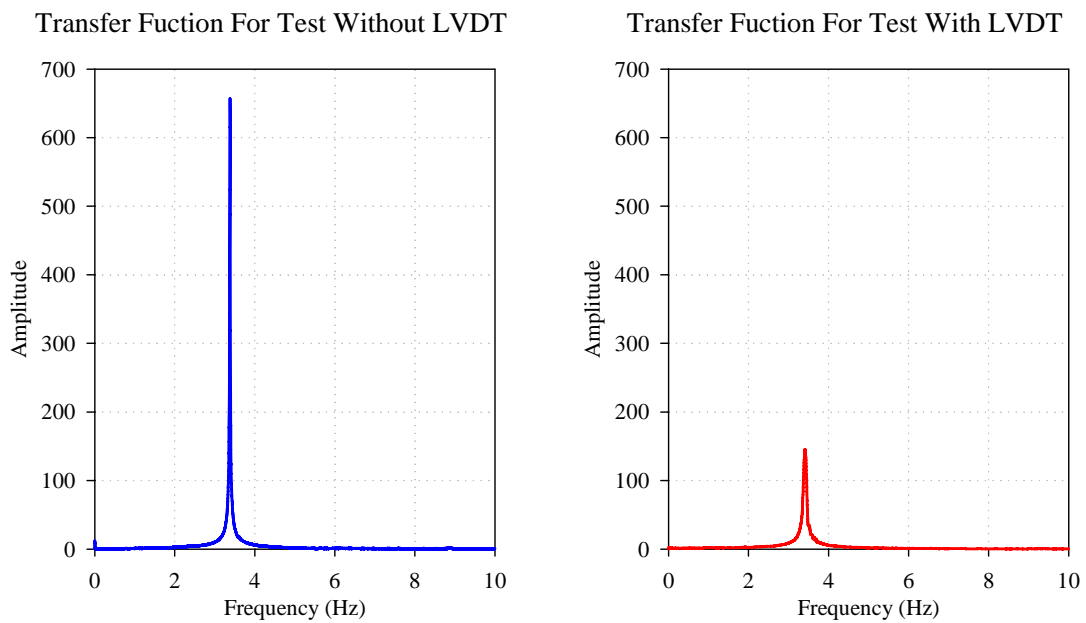


Figure 5-15 Fourier Transform of Mass M Acceleration for SDOF System

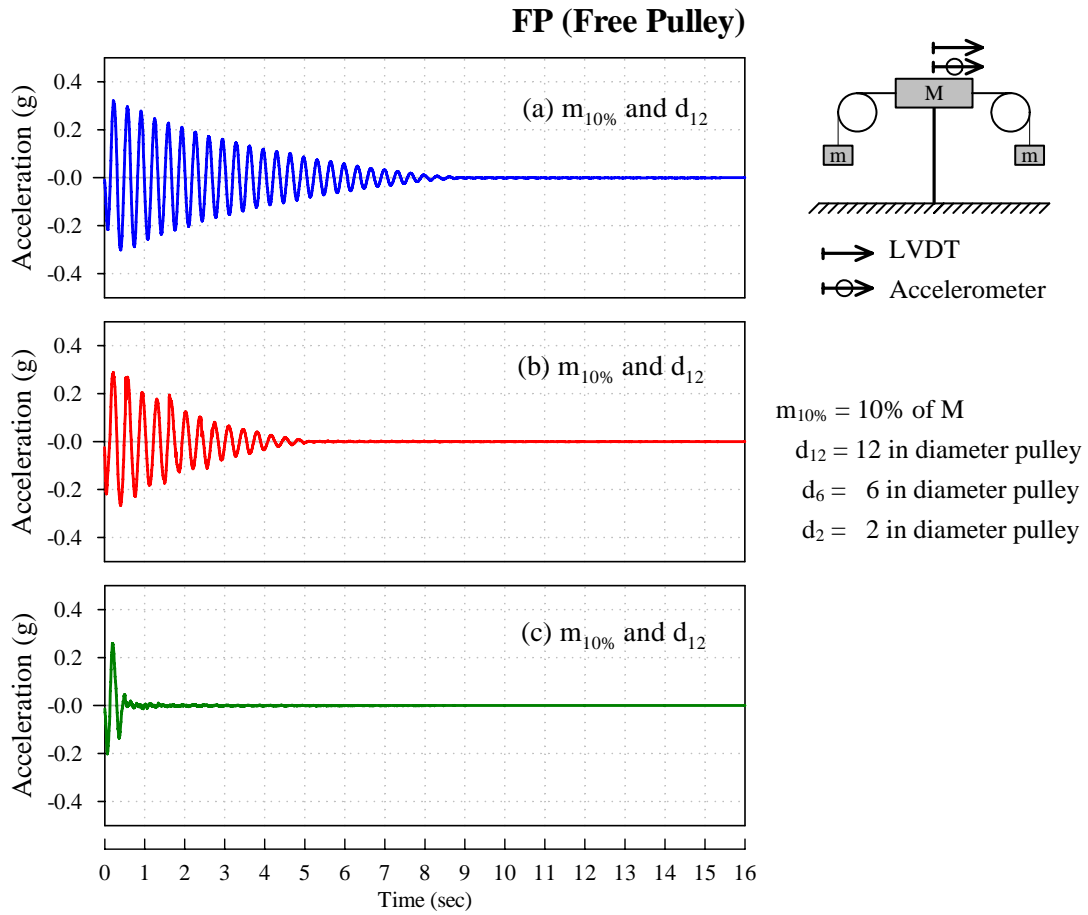


Figure 5-16: Mass M Acceleration Response from Snap-Back Tests for FP

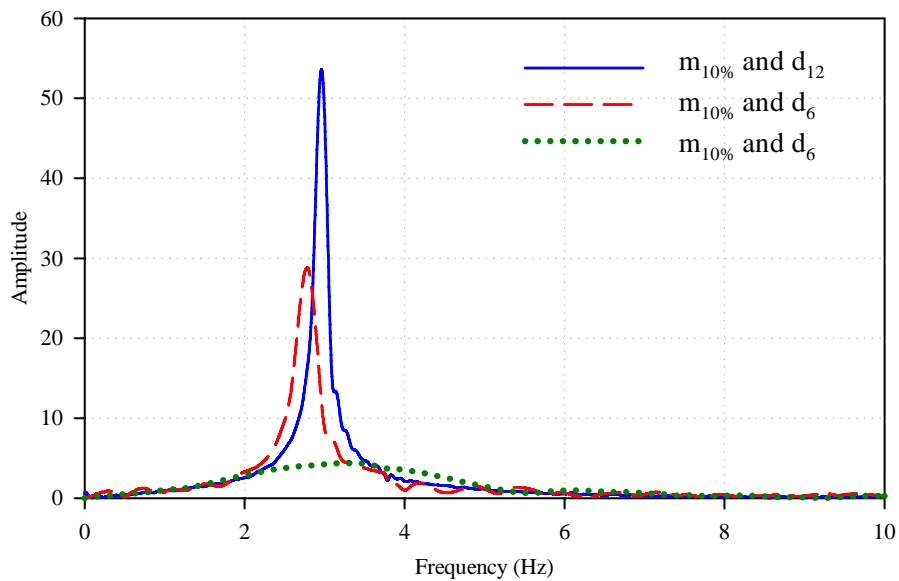


Figure 5-17: Fourier Transforms of Mass M Acceleration Tests for FP

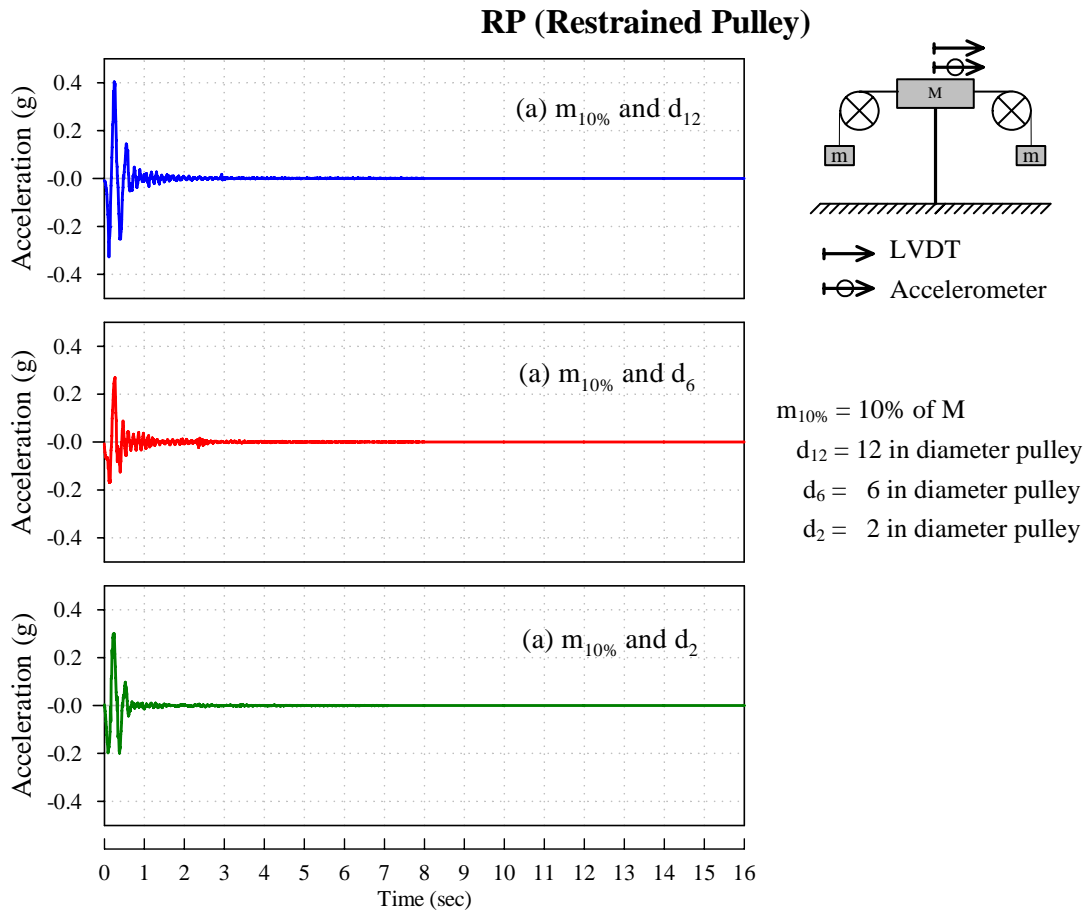


Figure 5-18: Mass M Acceleration Response from Snap-Back Tests for RP

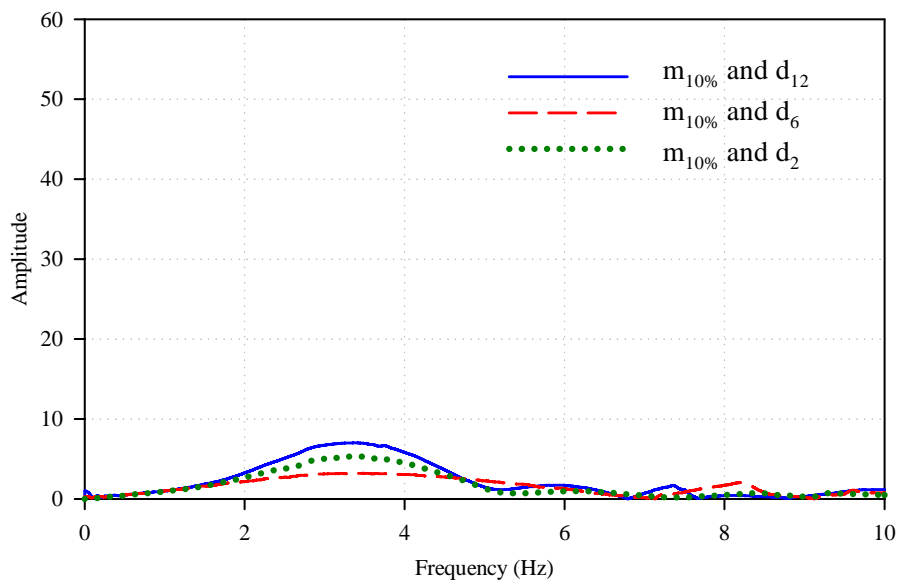


Figure 5-19: Fourier Transforms of Mass M Acceleration Tests for RP

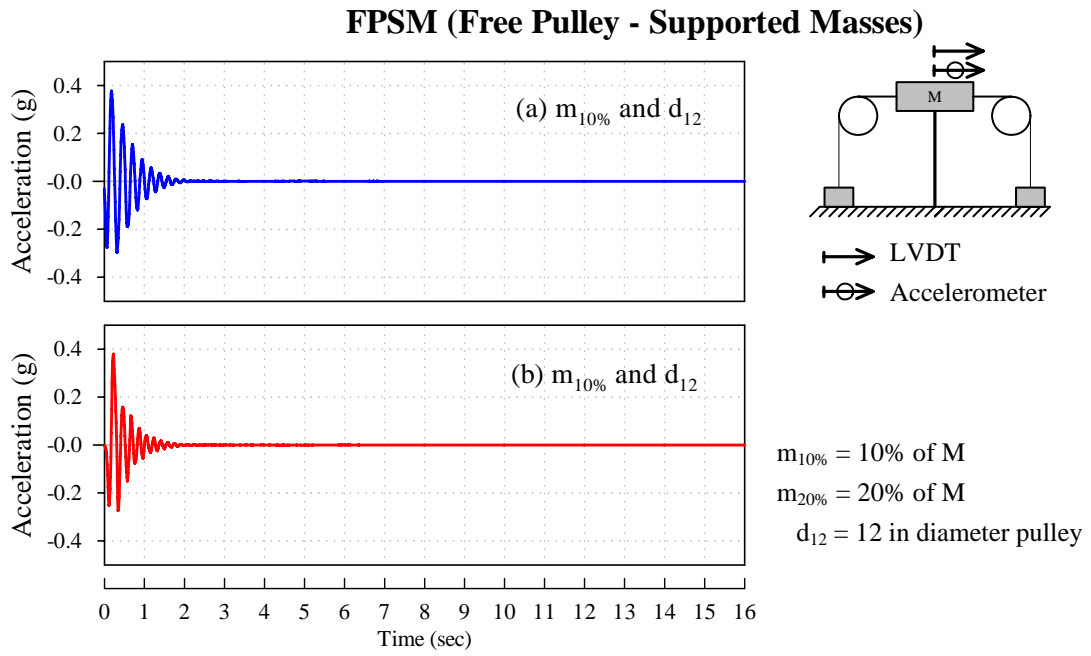


Figure 5-20: Mass M Acceleration Response from Snap-Back Tests for FPSM

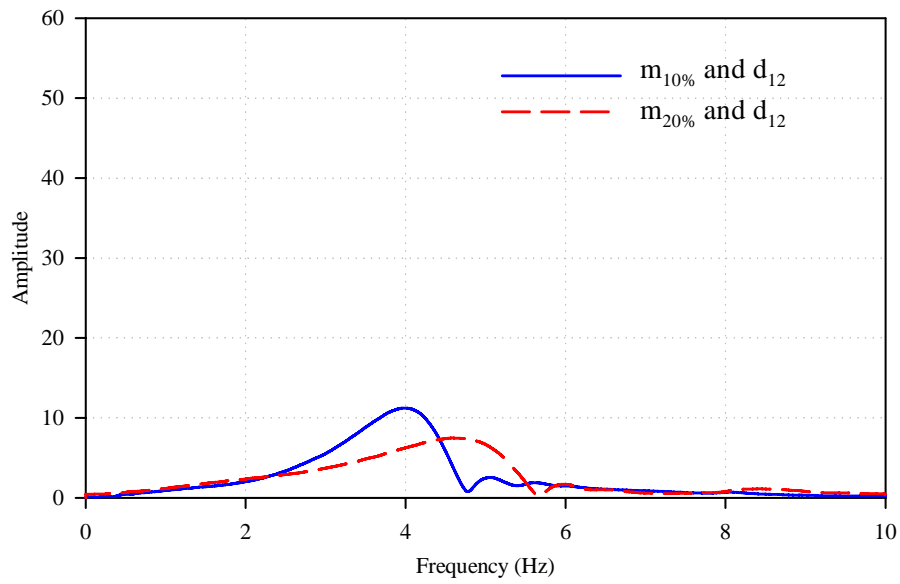


Figure 5-21: Fourier Transforms of Mass M Acceleration Tests for FPSM

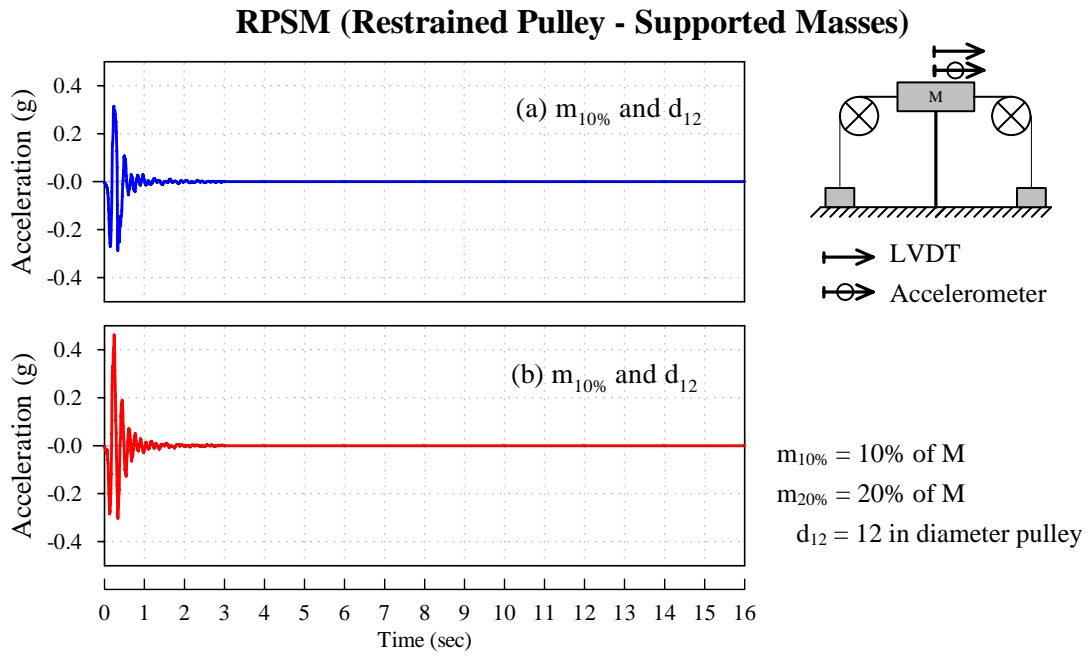


Figure 5-22: Mass M Acceleration Response from Snap-Back Tests for RPSM

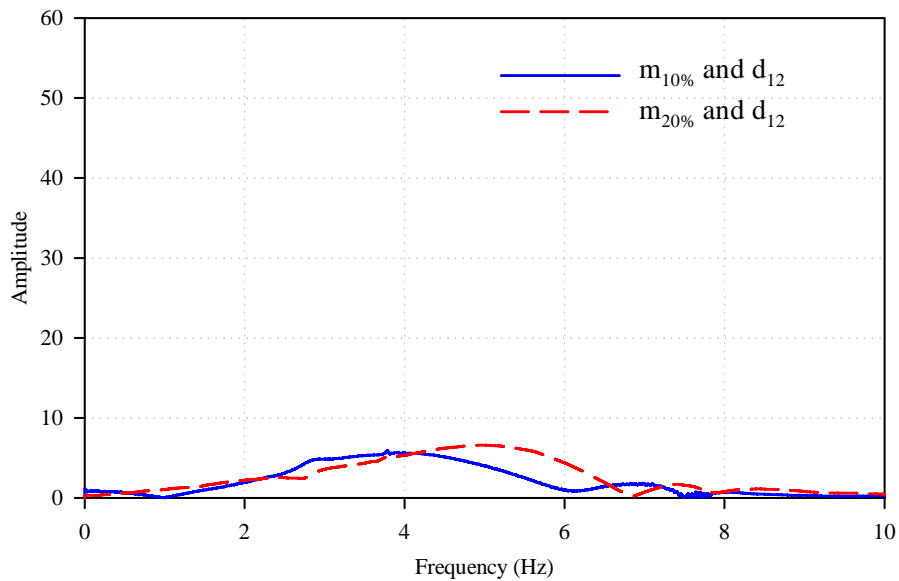
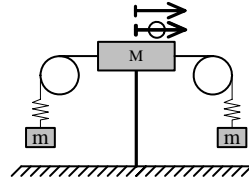


Figure 5-23: Fourier Transforms of Mass M Acceleration Tests for RPSM

FC (Flexible Cable)



↔ LVDT

⊗ Accelerometer

$m_{10\%} = 10\%$ of M

$d_{12} = 12$ in diameter pulley

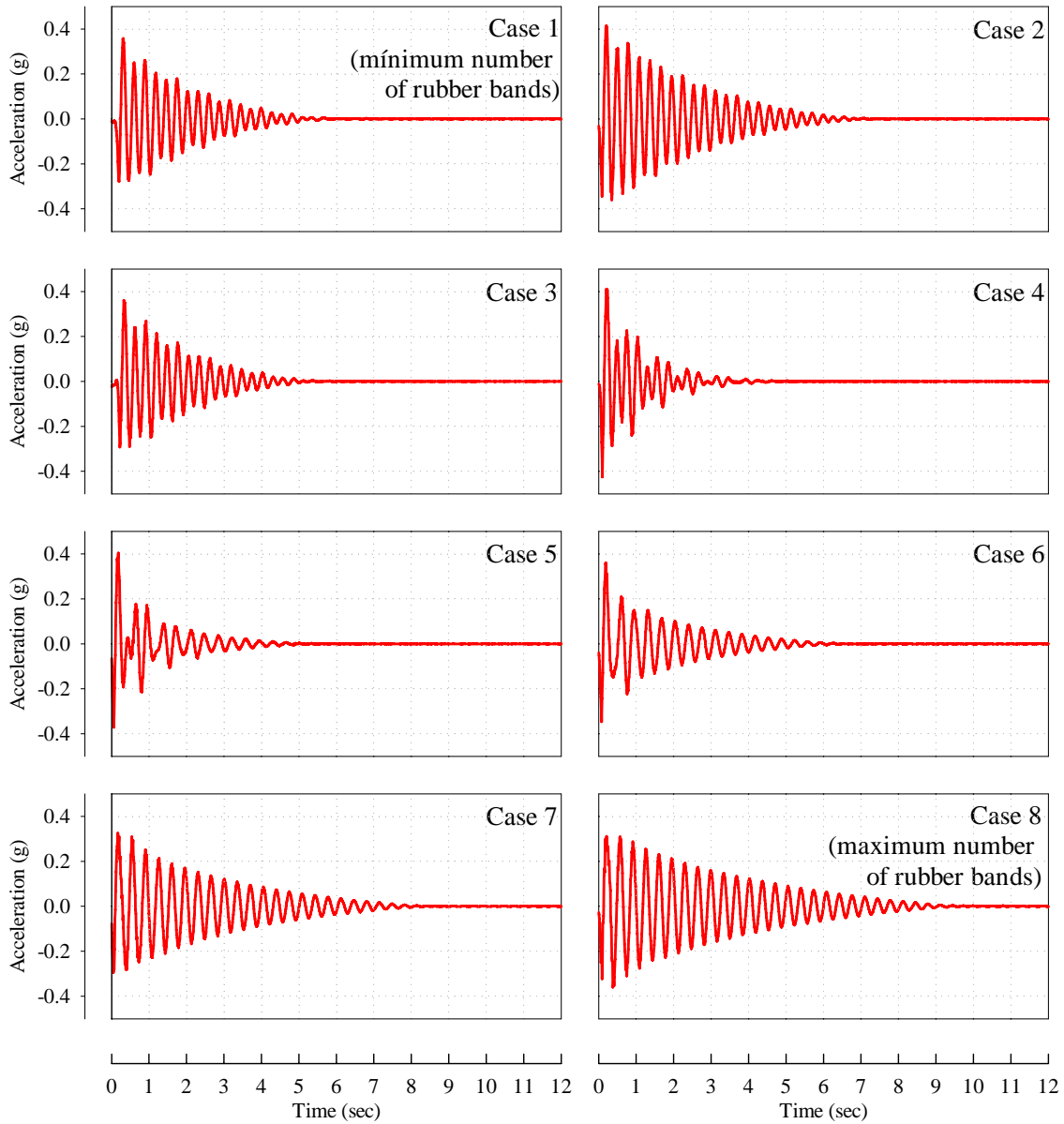


Figure 5-24: Mass M Acceleration Response from Snap-Back Tests for FC Cases

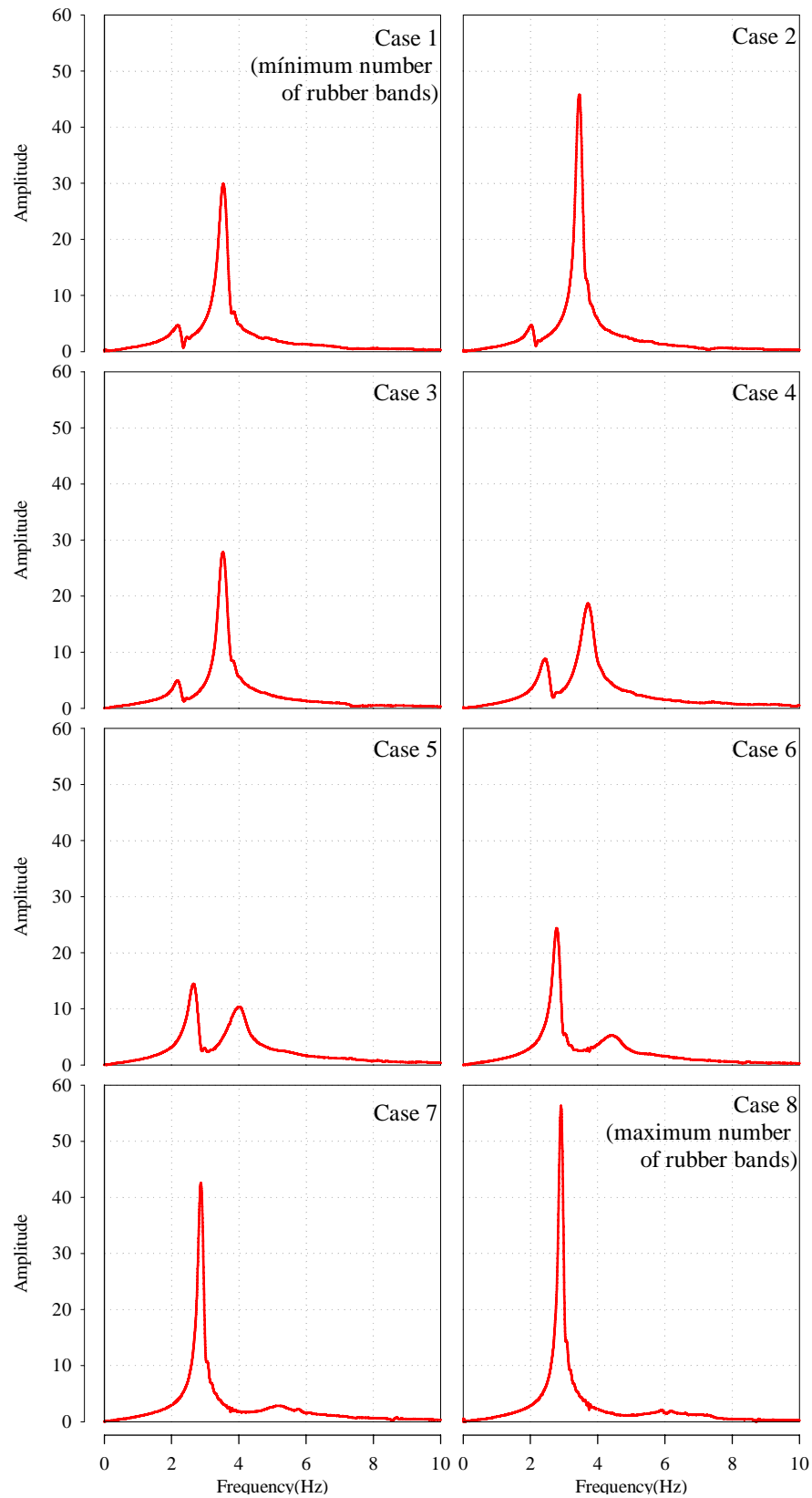


Figure 5-25: Fourier Transform of Mass M Acceleration for FC cases

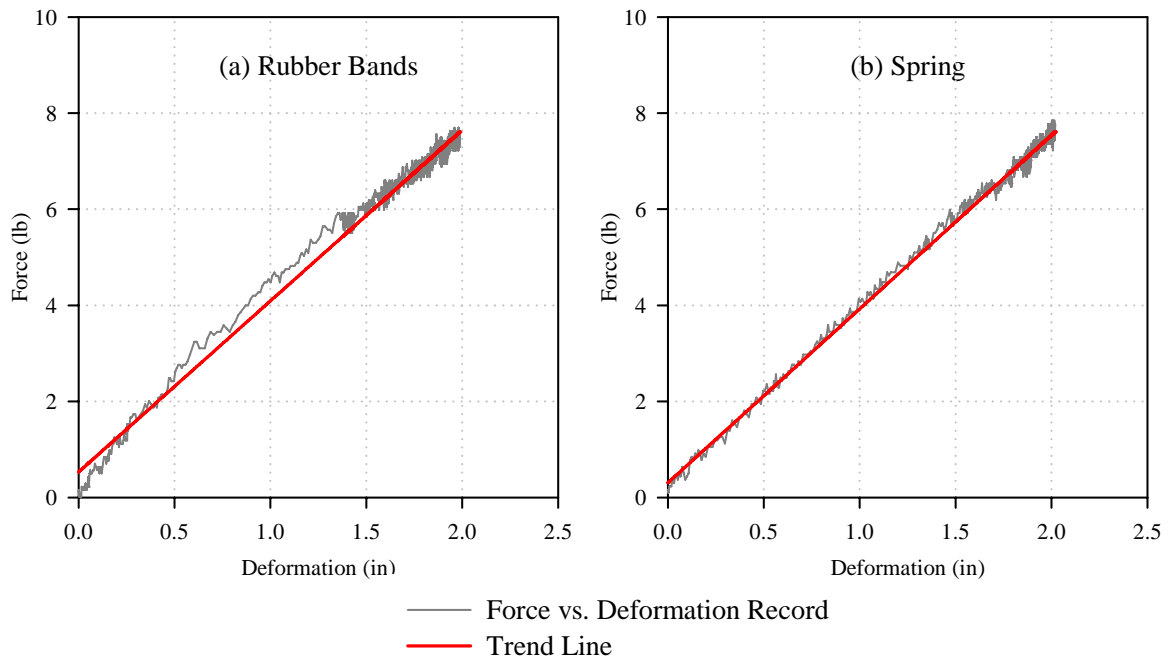


Figure 5-26: Force vs. Deformation for Rubber Bands and Spring

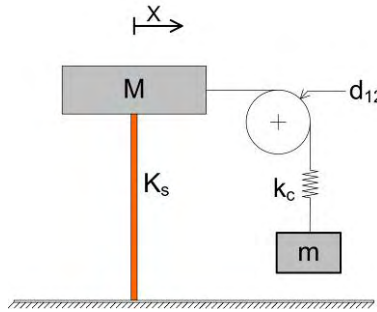


Figure 5-27: Set-Up for the Comparison of the System using Rubber Bands and Spring

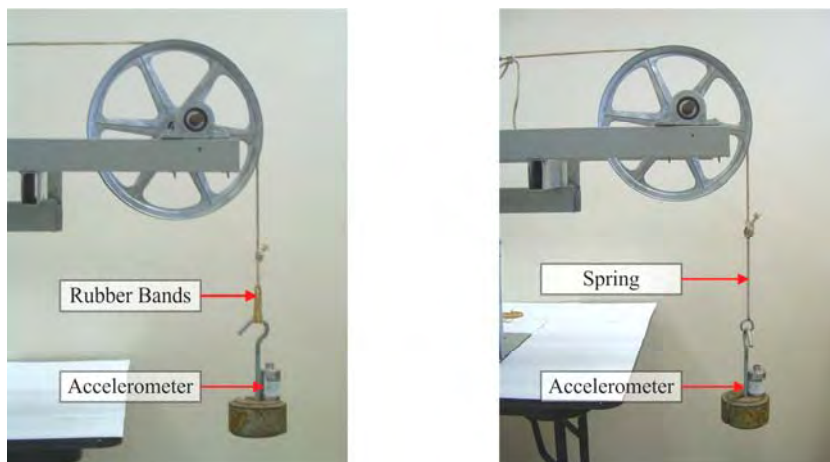


Figure 5-28: View of the Set-Up for the Comparison of the System using Rubber Bands and Spring

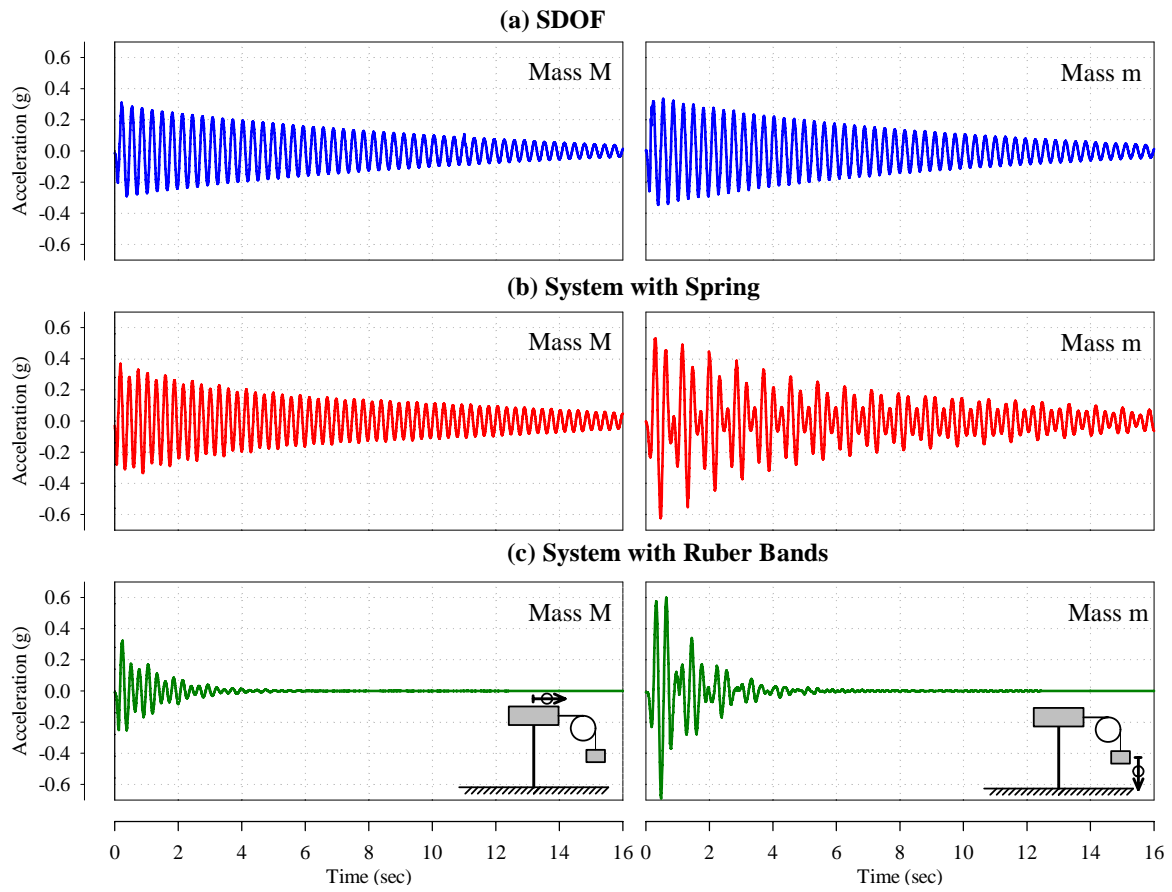


Figure 5-29: Accelerations for FC System with spring and rubber bands

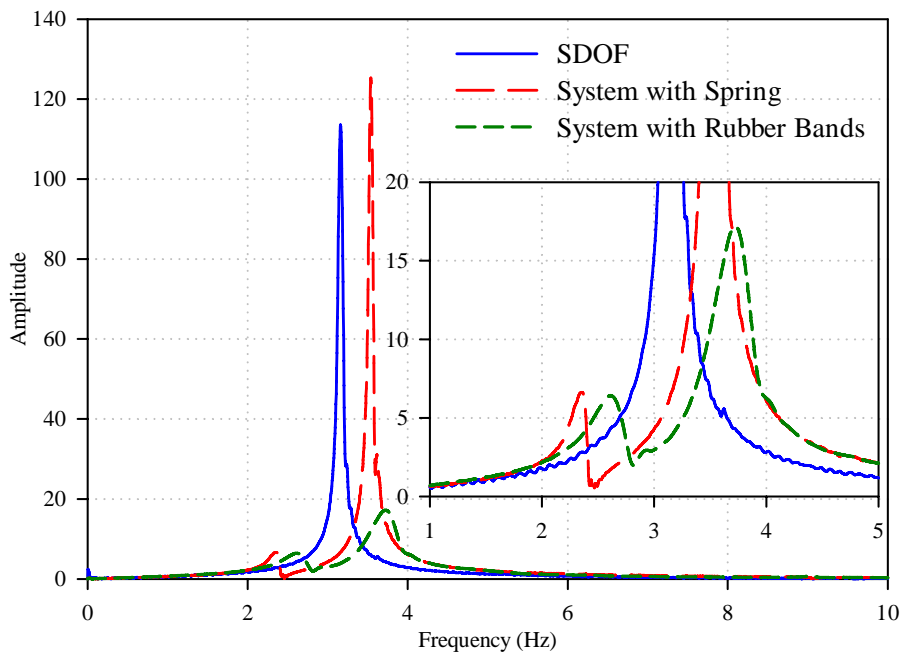


Figure 5-30: Fourier Transform of Mass *M* Acceleration for FC

5.7 RESULTS FROM SIMULATED EARTHQUAKES TESTS

The SDOF retrofitted with the different alternatives was subjected to scaled acceleration time histories of the El Centro, Taft, Northridge and San Salvador earthquakes. Table 5-5 summarizes the maximum acceleration for the mass M measured in each test, along with the measured peak ground accelerations of the input signals. Table 5-6 presents the maximum drift measured. The acceleration and displacement records of the mass M recorded when the different alternatives were subjected to El Centro Earthquake are presented in Figure 5-31 and Figure 5-32 respectively.

Table 5-5: Peak Accelerations (fraction of g) from Simulated Earthquake Tests

Alternative	El Centro (PGA=0.19g)	Taft (PGA=0.13g)	Northridge (PGA=0.16g)	San Salvador (PGA=0.18g)
SDOF	0.48	0.96	0.68	0.46
FP	0.58	0.49	0.59	0.36
RP	0.16	0.17	0.16	0.21
FPSM	0.35	0.25	0.27	0.33
RPSM	0.20	0.19	0.19	0.32
FC	0.32	0.27	0.25	0.34

Table 5-6: Maximum Drift (inches) from Simulated Earthquake Tests

Alternative	El Centro	Taft	Northridge	San Salvador
SDOF	0.40	0.81	0.58	0.28
FP	0.59	0.50	0.60	0.35
RP	0.09	0.09	0.09	0.14
FPSM	0.18	0.14	0.15	0.21
RPSM	0.07	0.08	0.09	0.15
FC	0.23	0.24	0.19	0.23

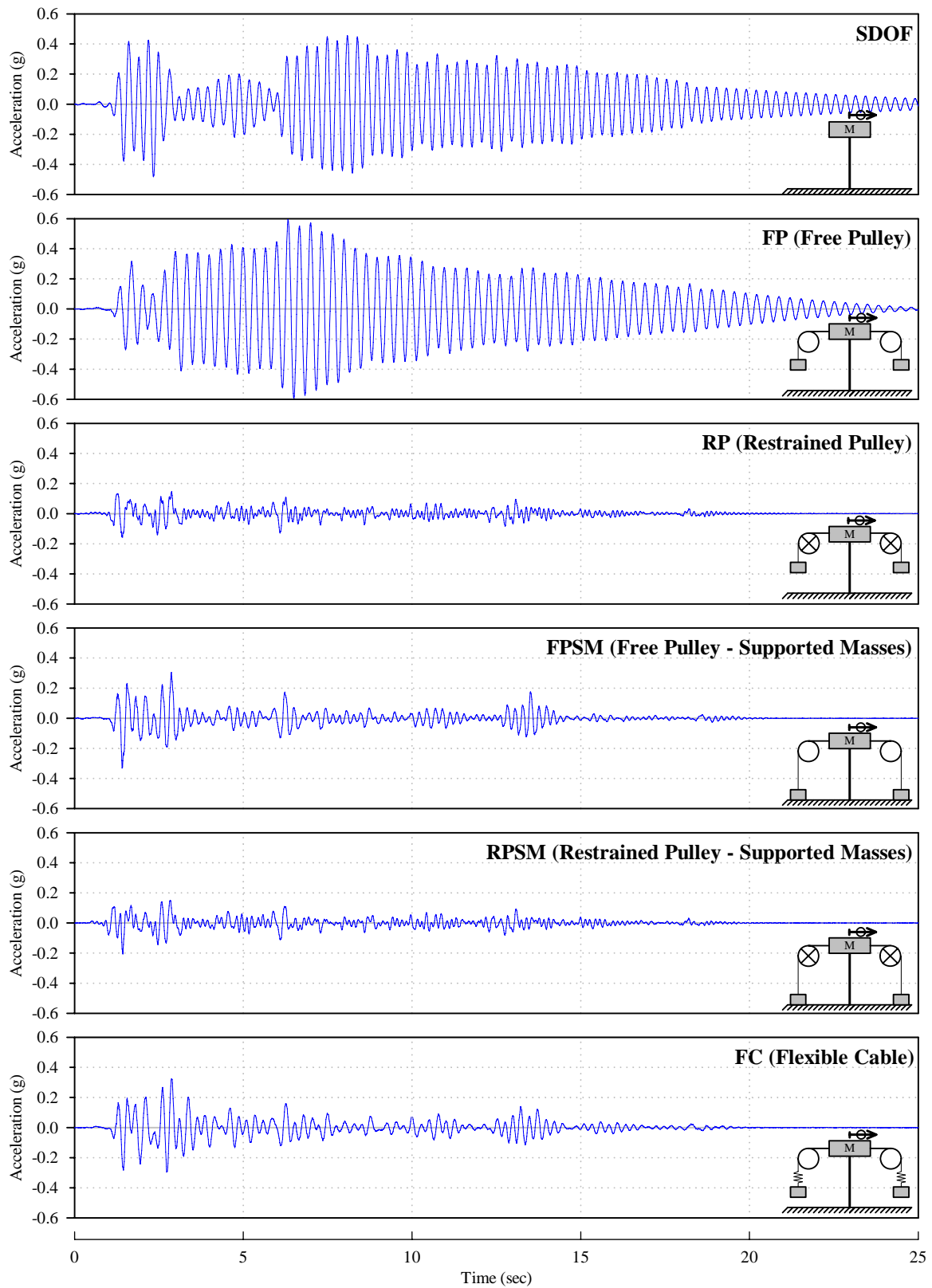


Figure 5-31: Comparison of Mass M Acceleration Response for El Centro Test

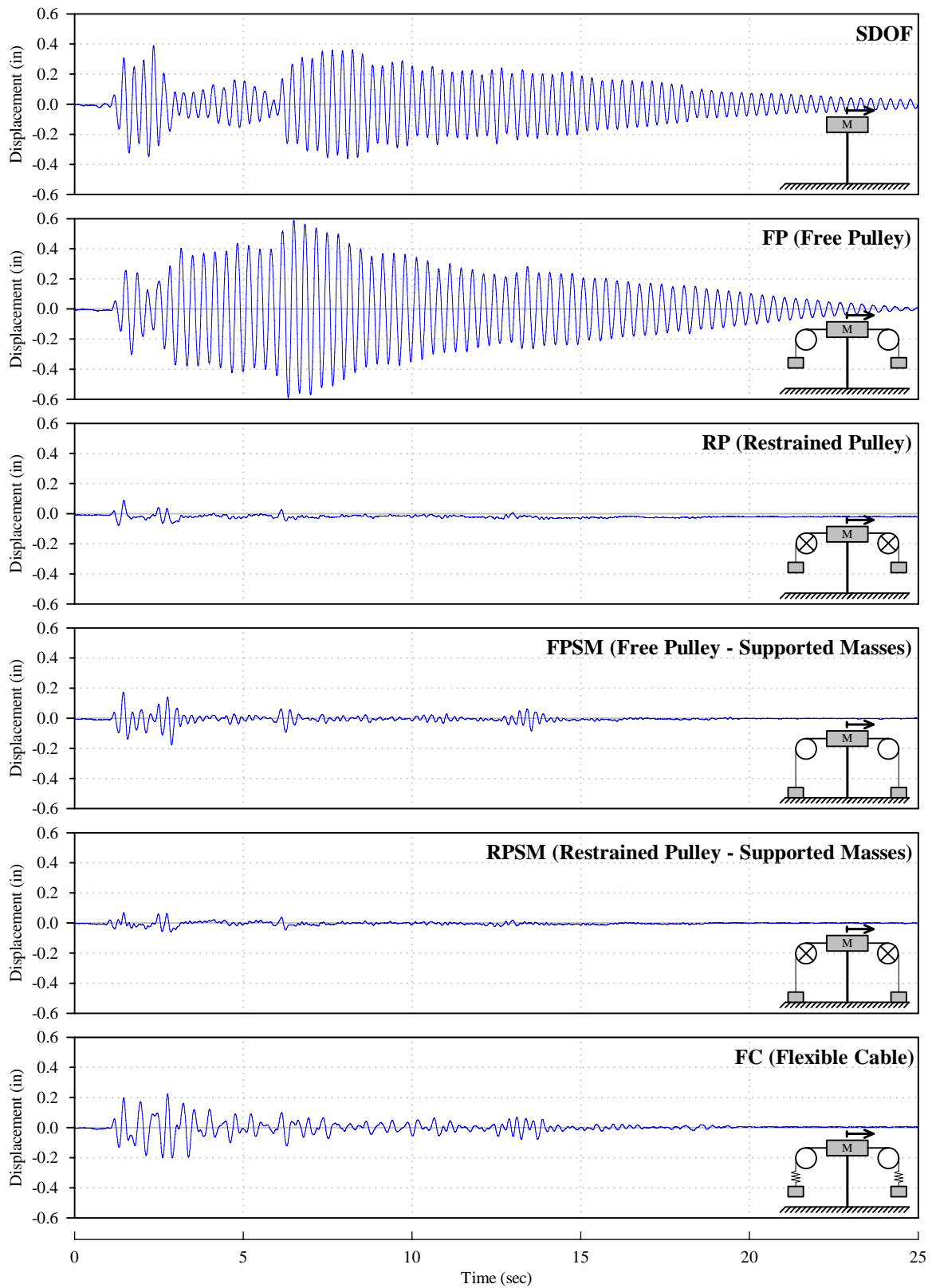


Figure 5-32: Comparison of Mass M Relative Displacements for El Centro Test

5.8 CONCLUSIONS FROM SIMULATED EARTHQUAKES TESTS

The amount of input energy introduced to the system for a given earthquake is the same, and therefore, the tests carried out permit a direct comparison among the retrofitting alternatives. The results summarized in Table 5-5 and Table 5-6 are presented again in Figure 5-33 and Figure 5-34, but now as a percentage of the SDOF response. Examining the results obtained from these tests the following conclusions can be drawn:

- The best reduction in peak accelerations was obtained using the RP alternative. A drop of the peak acceleration between 18% and 46% was achieved. In second place were the results obtained using RPSM.
- The best reductions in peak drift values were obtained using RP and RPSM. A reduction of the drift between 10% and 54% was obtained.
- The best results were achieved by using systems in which friction between the cable and the pulley occurred.
- Some tests conducted on FP showed peaks in acceleration and displacements higher than those for the SDOF. Therefore it was concluded that in some cases this retrofitting scheme can produce a detrimental effect on the system performance.

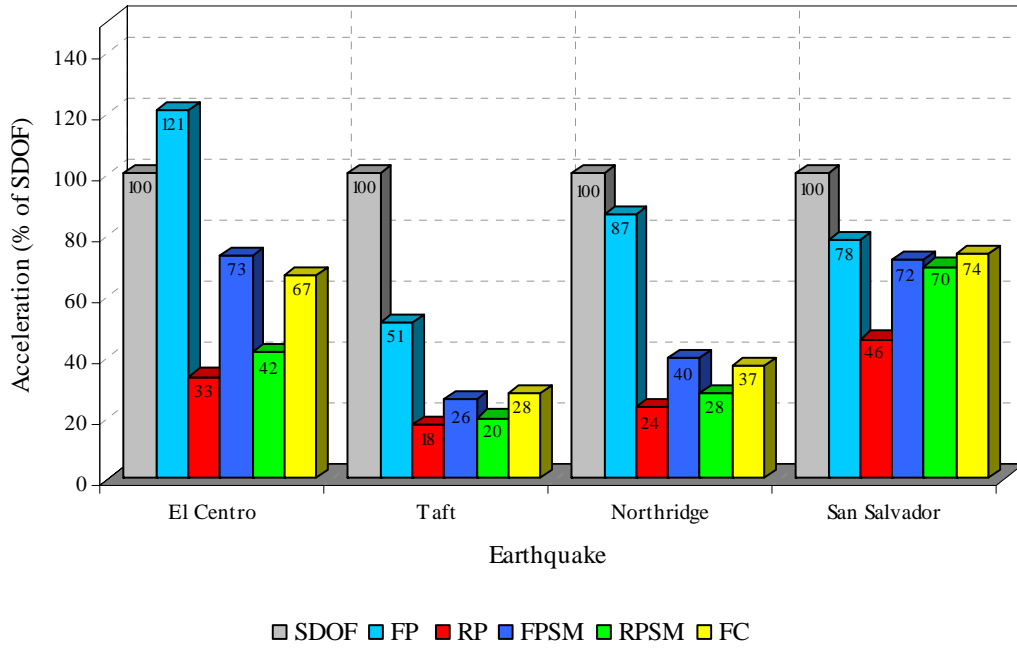


Figure 5-33: Peak Accelerations on % of the SDOF Peak Acceleration from Simulated Earthquake Tests

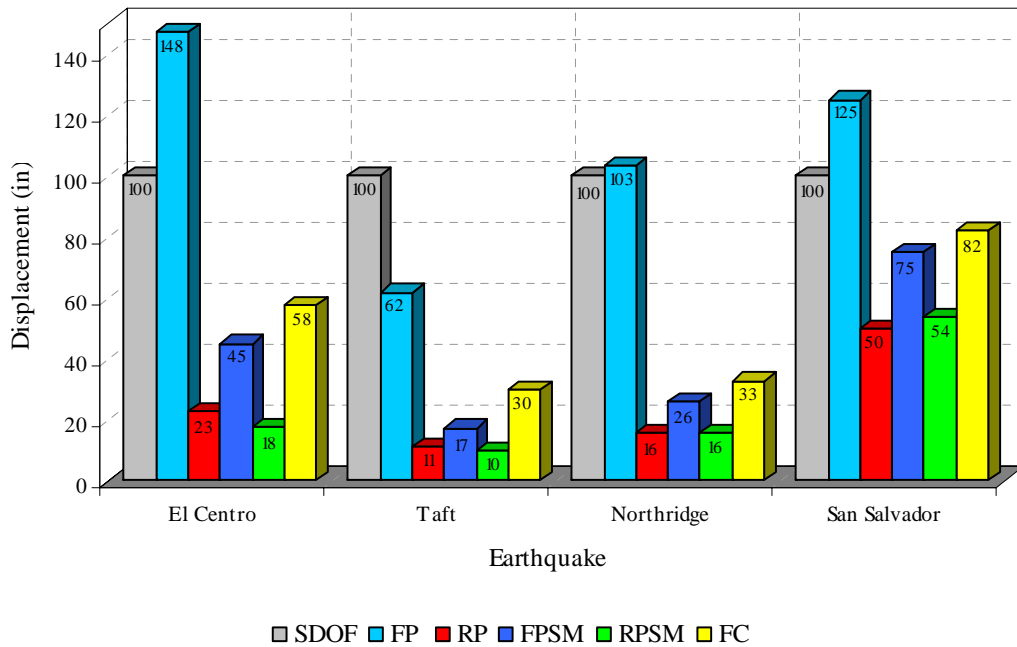


Figure 5-34: Maximum Drifts on % of the SDOF Maximum Drift from Simulated Earthquake Tests

CHAPTER VI:

SCALE MODEL TESTS

6.1 INTRODUCTION

Shaking table tests were performed to analyze the effectiveness of the retrofitting alternatives applied on a scale structure. The results of these tests are presented and discussed in the following sections.

The identification of the dynamic characteristics of the scale model using white noise tests is presented first. Simulated earthquakes tests performed on the scale model retrofitted with different alternatives, are presented next. The nodes acceleration, relative displacements of the second level nodes, and internal forces at the first level measured in these tests were used as parameters to evaluate the effectiveness of each alternative.

6.2 TESTING PROGRAM

The testing program was divided in two parts: identification of the dynamics properties of the scale model and evaluation of the retrofitted scale model response to simulated earthquakes tests. Table 6-1 summarizes the tests performed.

Natural frequencies, modal shapes, and the equivalent viscous damping ratios were found by means of White Noise tests. Bracci et al. (1992) presents the derivations which lead to the use of the transfer functions to determine the dynamic characteristics desired. The transfer function can be defined as an output structural response normalized by a input base motion in the frequency domain. The transfer function of the nodes acceleration was used in this work. It was defined as the Fourier Transform of a node acceleration time history normalized by the Fourier Transform of the base acceleration time history.

A white noise excitation with a frequency content between 0 to 20 Hz was used. The shaking table acceleration record from a white noise test is presented in Figure 6-1, and the respective Fourier Transform is shown in Figure 6-2. After filtering the signal, the peak base acceleration measure was 0.17 g.

Simulated earthquake tests were performed on the scale model to evaluate the effectiveness the proposed retrofitting alternatives. Secondary structures were constructed to support the secondary masses, as shown in Figure 6-3 and Figure 6-4. Two load cells, shown in Figure 6-5, were used to measure the cable forces. These forces were considered as two concentrated loads acting on the second level of the frame 2 as shown in Figure 6-6.

In tests where the pulleys were allowed to rotate (FP, FPSM and FC), pulleys with diameter d_{12} were used to minimize the pillow block internal friction. Secondary masses $m_{10\%}$ (10% of the model mass M) were used for FP, RP, FPSM and RPSM tests. For tests involving FC, secondary masses $m_{5\%}$ were used to prevent excessive deformation of the rubber bands used. Figure 6-7 presents a view of the rubber bands used. Finally, a test on the RP system using secondary masses $m_{5\%}$ was conducted

Table 6-1: Summary of the Testing Program

Alternative	d	m (%M)	WN	El Centro	Taft	Northridge	San Salvador
MDOF	-	-	✓	✓	✓	✓	✓
FP	12	10	-	✓	✓	✓	✓
RP	2	10	-	✓	✓	✓	✓
FPSM	12	10	-	✓	✓	✓	✓
RPSM	2	10	-	✓	✓	✓	✓
FC	12	5	-	✓	✓	✓	✓
RP*	2	5	-	✓	✓	✓	✓

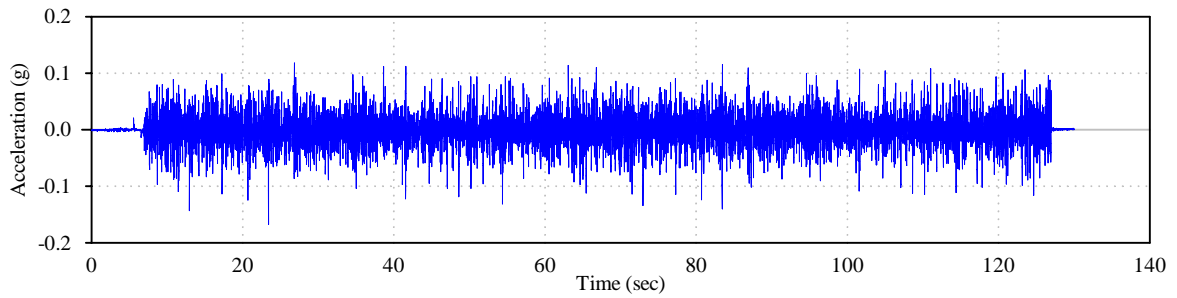


Figure 6-1: Shaking Table Acceleration Record from White Noise Test

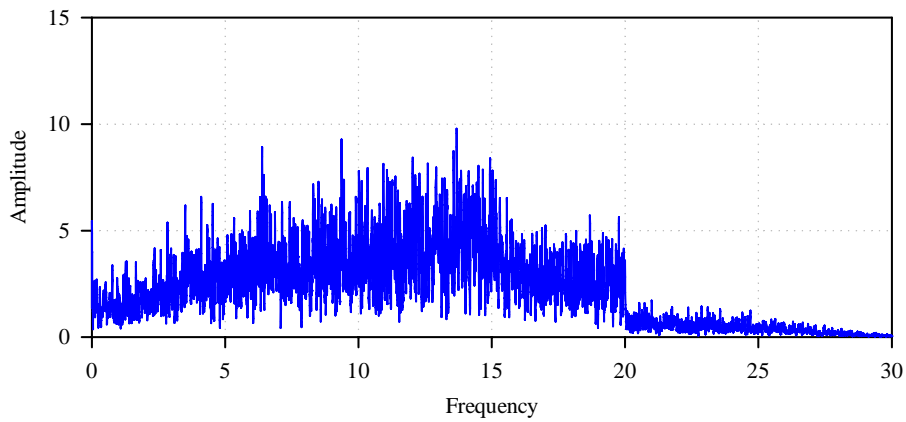


Figure 6-2: Fourier Transform of the Table Acceleration from White Noise Test

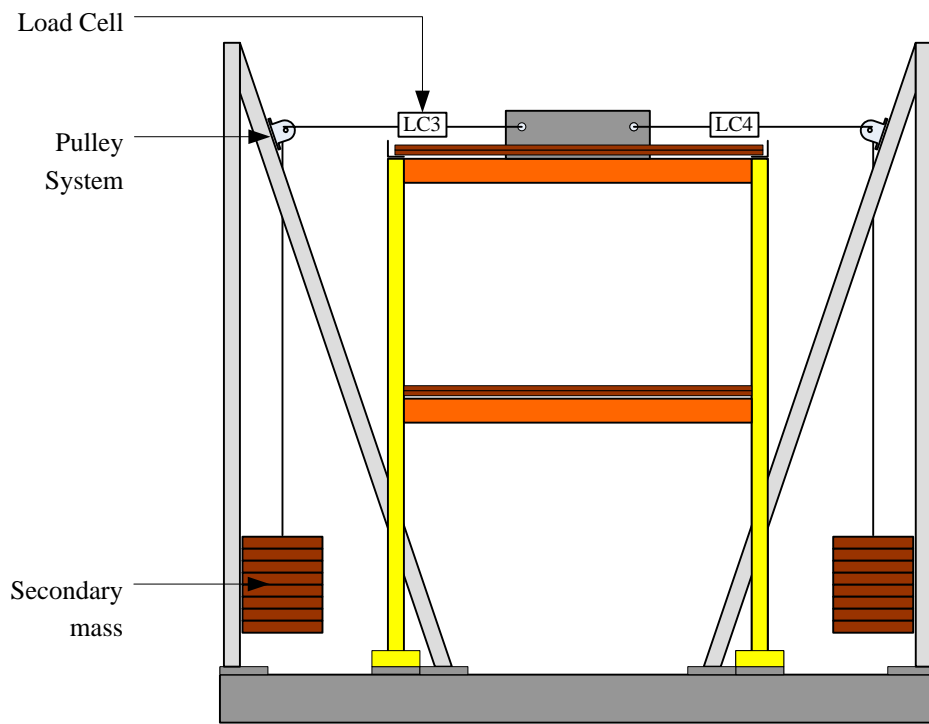


Figure 6-3: General Set Up



Figure 6-4: West and East Side View of the Model with Secondary Structures

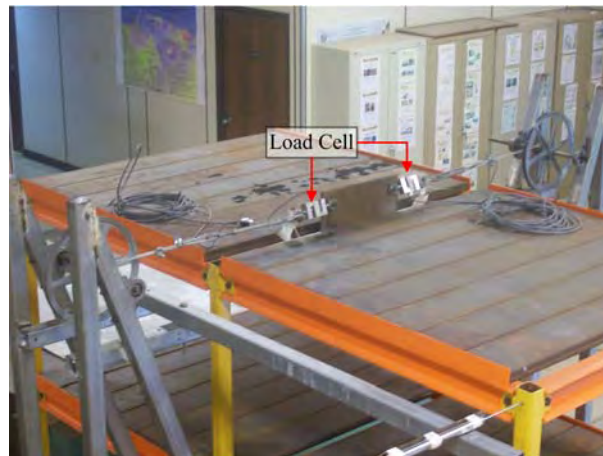


Figure 6-5: View of the Load Cells

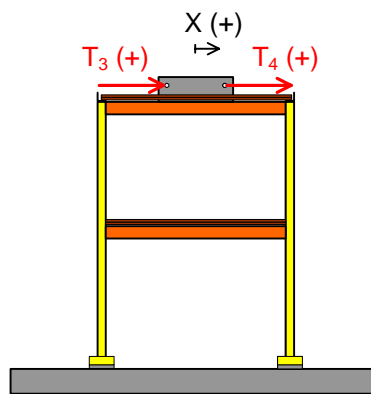


Figure 6-6: Sign Convention for Cable Forces



Figure 6-7: View of the Rubber Bands

6.3 IDENTIFICATION OF STRUCTURAL DYNAMIC PROPERTIES

The transfer functions of the nodes accelerations obtained from the white noise test are presented in Figure 6-8.

When a structure is lightly damped and its modes are well separated, the magnitude of the k-th peak magnitude of the j-th node transfer function occurs very close to the k-th natural frequency (Bracci et al. 1992). Then, the first and second natural frequencies were identified from the peaks of the transfer functions at 4.47 Hz and 15.51 Hz. as shown in Figure 6-8.

The ratios of the peaks of the Transfer Functions for different nodes at the k-th natural frequency are equal to the ratio of the mode shapes for the k-th mode. Since the mode shapes have relative magnitudes, the largest Transfer Function value was used as the base for normalization. The mode shape phases were determined by comparing the phase angles of the Fourier Transform for each node at each natural frequency. The modes obtained from the scale model tests are shown in Figure 6-9.

The first mode damping ratio from each transfer function was calculated using the half-power bandwidth method. The first mode damping ratio of the model, obtained as an average of these values, is equal to 0.26 %. Since the transfer function have many peaks near the second natural frequency, the damping ratio calculated with the half-power bandwidth method was deemed in accurate and it is not reported here.

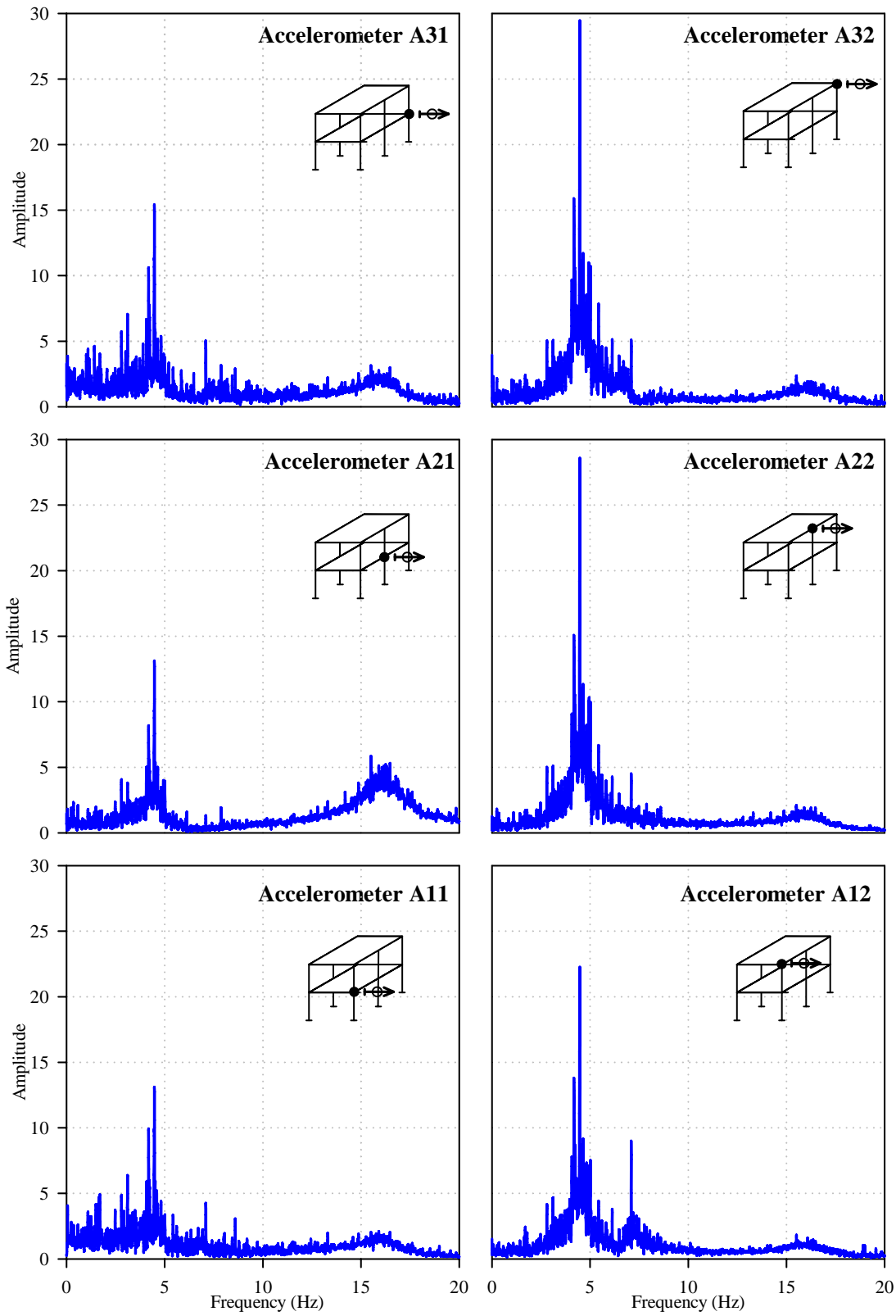


Figure 6-8: Transfer Functions of the Nodes Accelerations from White Noise Test

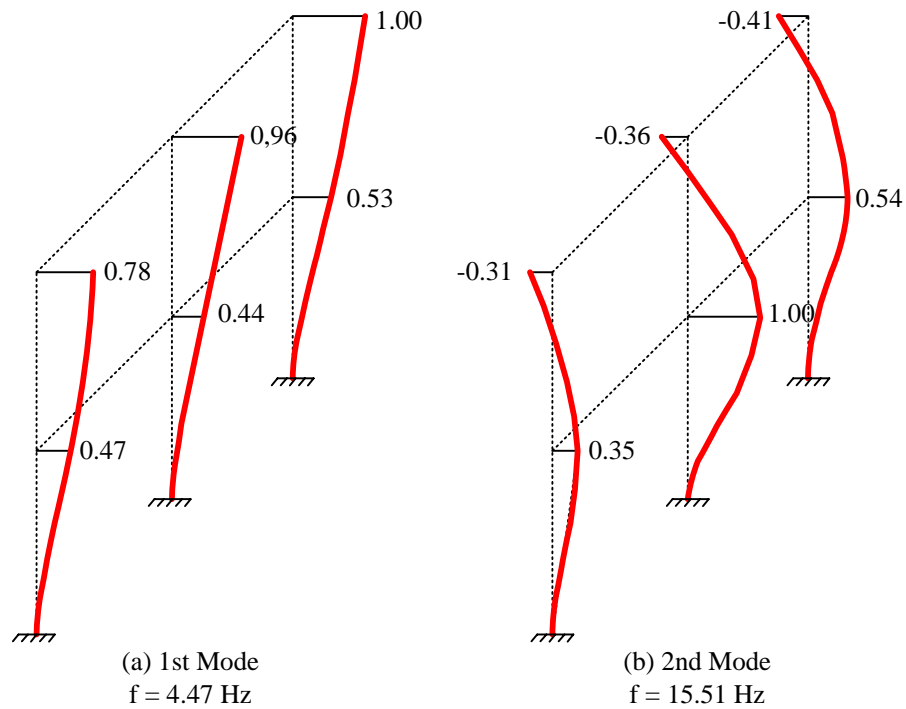


Figure 6-9: Natural Modes of Vibration

6.4 RESULTS FROM SIMULATED EARTHQUAKES TESTS

Results from the Simulated Earthquake Tests considered to be of importance are presented in this section. Peak accelerations measured in each node are presented in Table 6-2, and the maximum relative displacements of the frames measured at the second level are presented in Table 6-3. Table 6-4 summarizes the internal forces in the structure.

Because of the model characteristic, the bending moment in columns 1 and 2 (Figure 3-2) are equal through time; the same with columns 3 and 4. For that reason only values obtained from columns 2 and 4 are presented. The shear forces at the bottom of these columns were calculated from the bending load cells readings, as:

$$V_i = \frac{M_{bottom} + M_{top}}{h} = \frac{LCBB_i + LCBT_i}{1.875} \quad (6.1)$$

Total base bending moment and base shear were estimated as:

$$M = 2M_4 + 4M_2 \quad (6.2)$$

$$V = 2V_4 + 4V_2 \quad (6.3)$$

were M_2 and M_4 are the bottom bending moment in columns 2 and 4, and V_2 and V_4 are the shear forces calculated for the same columns.

The acceleration and displacement measured in the second level of frame 2 were considered to be the most relevant, since a larger mass was lumped in this frame and the larger peaks acceleration and displacement of the bare model were measured in this node for every test. Figure 6-10 and Figure 6-11 show the acceleration and relative displacement response time history for the alternatives FP, RP, FPSM, RPSM and FC subjected to EL Centro record, measured with the accelerometer A₂₂ and LVDT2 respectively.

Given that in the different tests column 3 and 4, from frame 2, were the most loaded columns of the bare model, the decrease in its internal forces were considered to be the most significant parameter to evaluate the effectiveness of the retrofitting alternatives. Figure 6-12 presents the time history of the bending moment at the bottom of column 4, measured with LCBB4 during the EL Centro tests.

Figure 6-13 shows the variation of the cable tensions along with frame 2 second level velocity in RP, from the first seconds of the San Salvador test. The velocity sign indicates the direction of displacements. It can be noticed that the forces applied on the structure by the cables were opposite to the direction of motion during velocity peaks. This behavior was observed in all RP tests.

Figure 6-14 compares results from RP San Salvador tests conducted with secondary masses $m_{10\%}$ (RP) and secondary masses $m_{5\%}$ (RP*). Almost the same accelerations were measured by accelerometer A22, but some difference were noticed in displacements and loads measured by LVDT2 and LC3 respectively: the RP test presented larger loads, while the RP* tests showed larger displacements.

6.5 CONCLUSIONS

This section summarizes the conclusions obtained from the performed tests. Some results from the simulated earthquake tests considered to be of importance are presented as a percentage of the Bare Model response in Figure 5-33.

- The best results in terms of response reduction were achieved using systems in which friction between the cable and the pulley occurred.
- The best reduction in acceleration measured with accelerometer A22 was obtained using the RP system, as shown in Figure 5-33(a). The measured acceleration peaks were between 53% and 62% of the values for the bare model. Table 6-2 shows, in some cases, an increase on the peak acceleration measured in other nodes.
- Figure 6-11 shows that the best reductions on relative displacement measured at the second level of frame 2 were achieved when using the RP and RPSM alternatives. Figure 5-33(b) shows that the maximum displacements measured for the RP scheme were between 23% and 34% of the respected values for the bare

model, and for the RPSM the reductions were between 28% and 38%. As shown in Table 6-3, the other frame displacements were also reduced by these alternatives.

- The best reductions on the bending moment at the base of column 4 were produced by the RP and RPSM alternatives, as shown in Figure 5-33(c). The maximum values measured were between the 39% and 45% of the moments for the bare model the RP, and between 42% and 52% for the RPSM system. The reductions on the calculated total base shear were not so significant.
- Results from the RP and RP* tests are summarized in Figure 6-16 as a percentage of the bare model response. It can be noticed that the results obtained by using this alternative with secondary masses $m_{5\%}$ were very similar to those obtained with the secondary masses $m_{10\%}$.

Table 6-2: Peak Acceleration from the Simulated Earthquake Tests

Earthquake	Alternative	Peak Acceleration (% g)						
		A ₁₁	A ₁₂	A ₂₁	A ₂₂	A ₃₁	A ₃₂	A _{b2}
EL Centro	MRF	0.22	0.34	0.18	0.47	0.19	0.30	0.23
	FP	0.24	0.38	0.15	0.34	0.20	0.38	0.18
	RP	0.26	0.34	0.19	0.25	0.20	0.39	0.24
	FPSM	0.17	0.30	0.15	0.28	0.17	0.37	0.18
	RPSM	0.27	0.40	0.23	0.34	0.22	0.48	0.21
	FC	0.17	0.24	0.19	0.33	0.20	0.38	0.18
	RP*	0.22	0.36	0.18	0.24	0.17	0.32	0.25
Taft	MRF	0.18	0.27	0.16	0.37	0.16	0.34	0.16
	FP	0.20	0.28	0.16	0.35	0.16	0.35	0.18
	RP	0.23	0.33	0.15	0.23	0.16	0.33	0.18
	FPSM	0.18	0.29	0.15	0.32	0.15	0.37	0.16
	RPSM	0.33	0.33	0.17	0.25	0.16	0.40	0.16
	FC	0.17	0.26	0.15	0.32	0.15	0.32	0.16
	RP*	0.18	0.28	0.14	0.24	0.14	0.30	0.18
Northridge	MRF	0.16	0.25	0.16	0.34	0.17	0.30	0.18
	FP	0.18	0.31	0.13	0.30	0.14	0.28	0.20
	RP	0.19	0.34	0.15	0.20	0.19	0.36	0.16
	FPSM	0.18	0.32	0.16	0.31	0.17	0.41	0.18
	RPSM	0.18	0.33	0.17	0.25	0.19	0.44	0.18
	FC	0.16	0.25	0.15	0.30	0.17	0.30	0.20
	RP*	0.17	0.27	0.15	0.22	0.16	0.31	0.28
San Salvador	MRF	0.22	0.31	0.16	0.46	0.15	0.42	0.19
	FP	0.21	0.30	0.14	0.44	0.32	0.16	0.22
	RP	0.29	0.43	0.19	0.28	0.23	0.50	0.19
	FPSM	0.28	0.44	0.18	0.38	0.22	0.46	0.23
	RPSM	0.27	0.44	0.22	0.33	0.29	0.63	0.22
	FC	0.22	0.34	0.17	0.45	0.17	0.42	0.23
	RP*	0.23	0.36	0.18	0.29	0.21	0.43	0.25

Table 6-3: Peak Relative Displacement from the Simulated Earthquake Tests

Earthquake	Alternative	Peak Relative Displ. (% g)		
		LVDT1	LVDT2	LVDT3
EL Centro	MRF	0.18	0.30	0.28
	FP	0.16	0.28	0.23
	RP	0.10	0.08	0.15
	FPSM	0.10	0.18	0.20
	RPSM	0.12	0.10	0.21
	FC	0.14	0.20	0.15
	RP*	0.11	0.11	0.15
Taft	MRF	0.16	0.25	0.25
	FP	0.14	0.25	0.21
	RP	0.09	0.07	0.13
	FPSM	0.09	0.12	0.15
	RPSM	0.10	0.07	0.14
	FC	0.12	0.18	0.19
	RP*	0.09	0.10	0.14
Northridge	MRF	0.14	0.22	0.20
	FP	0.11	0.17	0.15
	RP	0.08	0.05	0.13
	FPSM	0.11	0.11	0.16
	RPSM	0.07	0.07	0.17
	FC	0.12	0.18	0.18
	RP*	0.08	0.08	0.13
San Salvador	MRF	0.18	0.32	0.29
	FP	0.11	0.24	0.21
	RP	0.12	0.11	0.21
	FPSM	0.14	0.23	0.25
	RPSM	0.14	0.12	0.24
	FC	0.18	0.26	0.28
	RP*	0.13	0.16	0.21

Table 6-4: Maximum Internal Forces from the Simulated Earthquake Tests

Earthquake	Alternative	Mcol2	Mcol4	Vcol2	Vcol4	Mt	Vt
EL Centro	MRF	0.26	0.44	0.12	0.17	1.81	0.74
	FP	0.23	0.35	0.12	0.14	1.48	0.71
	RP	0.18	0.17	0.10	0.12	1.03	0.64
	FPSM	0.17	0.29	0.09	0.14	1.20	0.62
	RPSM	0.20	0.20	0.11	0.13	1.19	0.69
	FC	0.21	0.35	0.11	0.18	1.49	0.77
	RP*	0.17	0.20	0.10	0.12	1.05	0.59
Taft	MRF	0.24	0.38	0.11	0.17	1.65	0.74
	FP	0.20	0.35	0.10	0.13	1.35	0.63
	RP	0.16	0.16	0.09	0.10	0.92	0.54
	FPSM	0.16	0.18	0.08	0.10	0.96	0.52
	RPSM	0.17	0.16	0.09	0.11	0.99	0.56
	FC	0.19	0.27	0.10	0.13	1.27	0.63
	RP*	0.15	0.19	0.08	0.10	0.96	0.52
Northridge	MRF	0.20	0.31	0.09	0.15	1.35	0.64
	FP	0.17	0.24	0.09	0.11	1.08	0.52
	RP	0.14	0.13	0.07	0.09	1.02	0.54
	FPSM	0.17	0.20	0.09	0.12	1.06	0.60
	RPSM	0.14	0.15	0.07	0.11	0.83	0.49
	FC	0.19	0.28	0.10	0.14	1.28	0.63
	RP*	0.13	0.17	0.07	0.10	0.84	0.48
San Salvador	MRF	0.25	0.44	0.12	0.20	1.81	0.83
	FP	0.18	0.35	0.09	0.13	1.36	0.56
	RP	0.19	0.20	0.10	0.12	1.11	0.61
	FPSM	0.24	0.34	0.12	0.15	1.53	0.73
	RPSM	0.21	0.23	0.11	0.14	1.27	0.68
	FC	0.25	0.40	0.12	0.18	1.74	0.82
	RP*	0.20	0.27	0.10	0.14	1.27	0.65

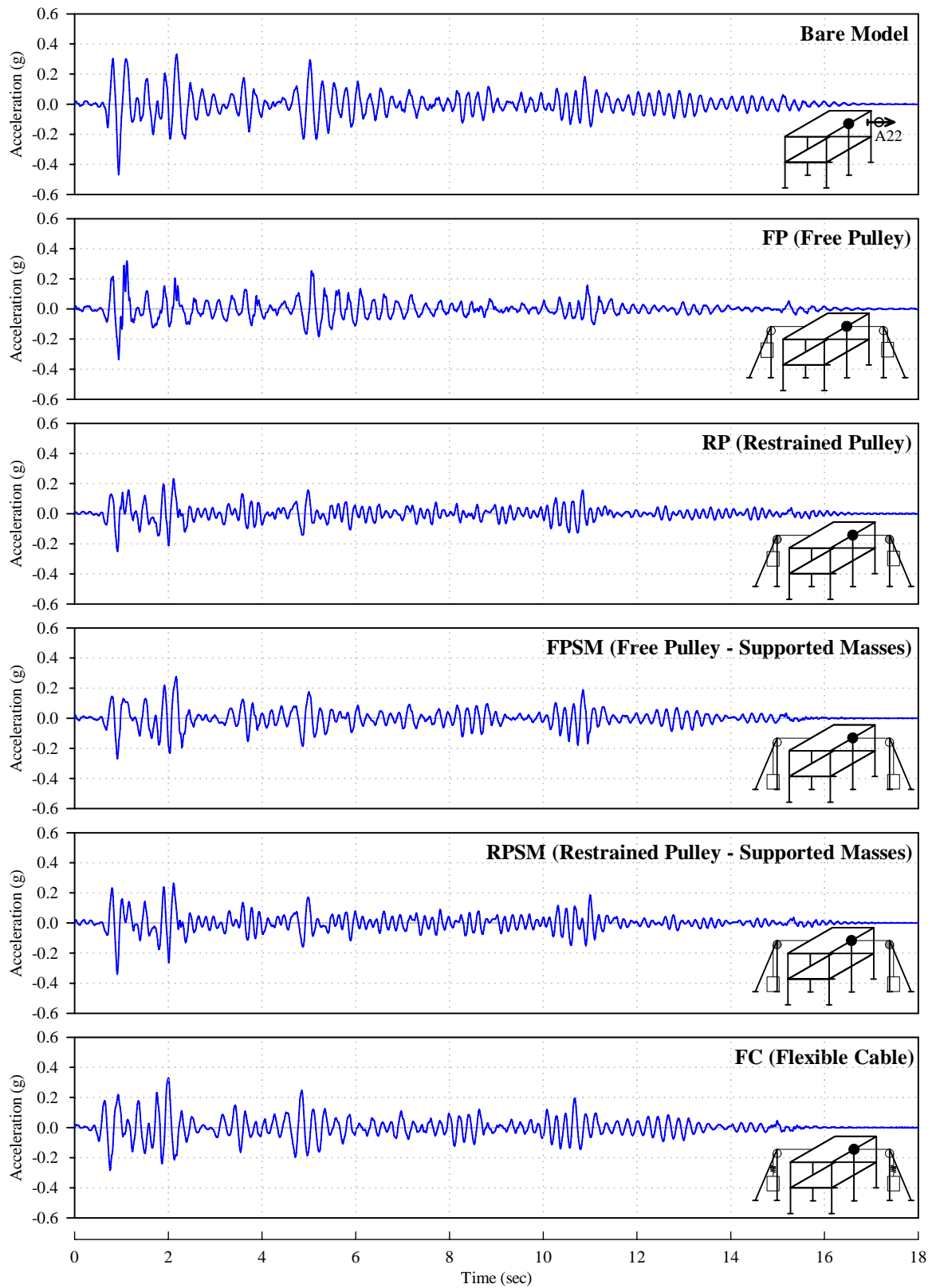


Figure 6-10: Comparison of El Centro Tests Accelerations from Accelerometer A22

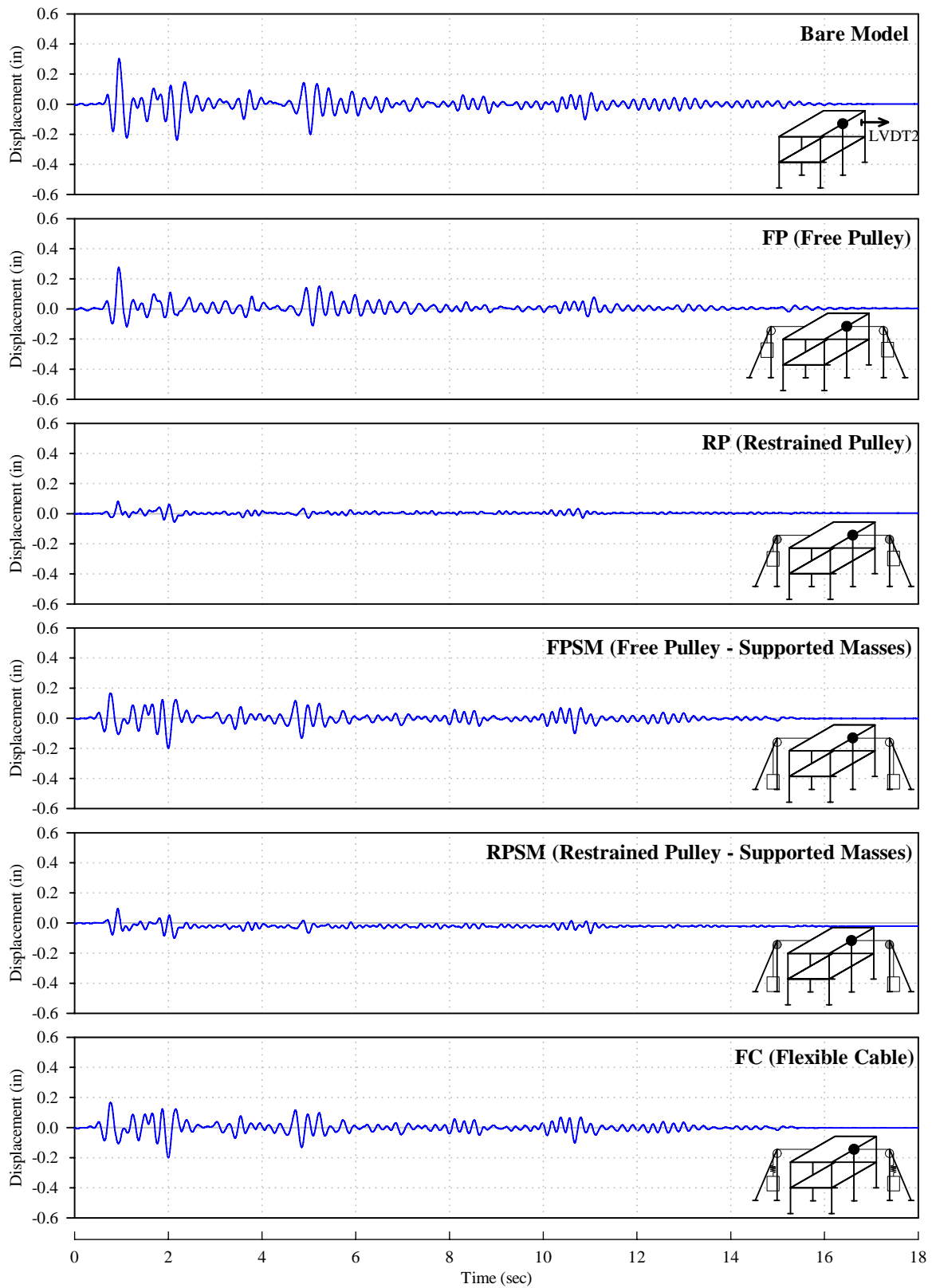


Figure 6-11: Comparison of El Centro Relative Displacement from LVDT 2

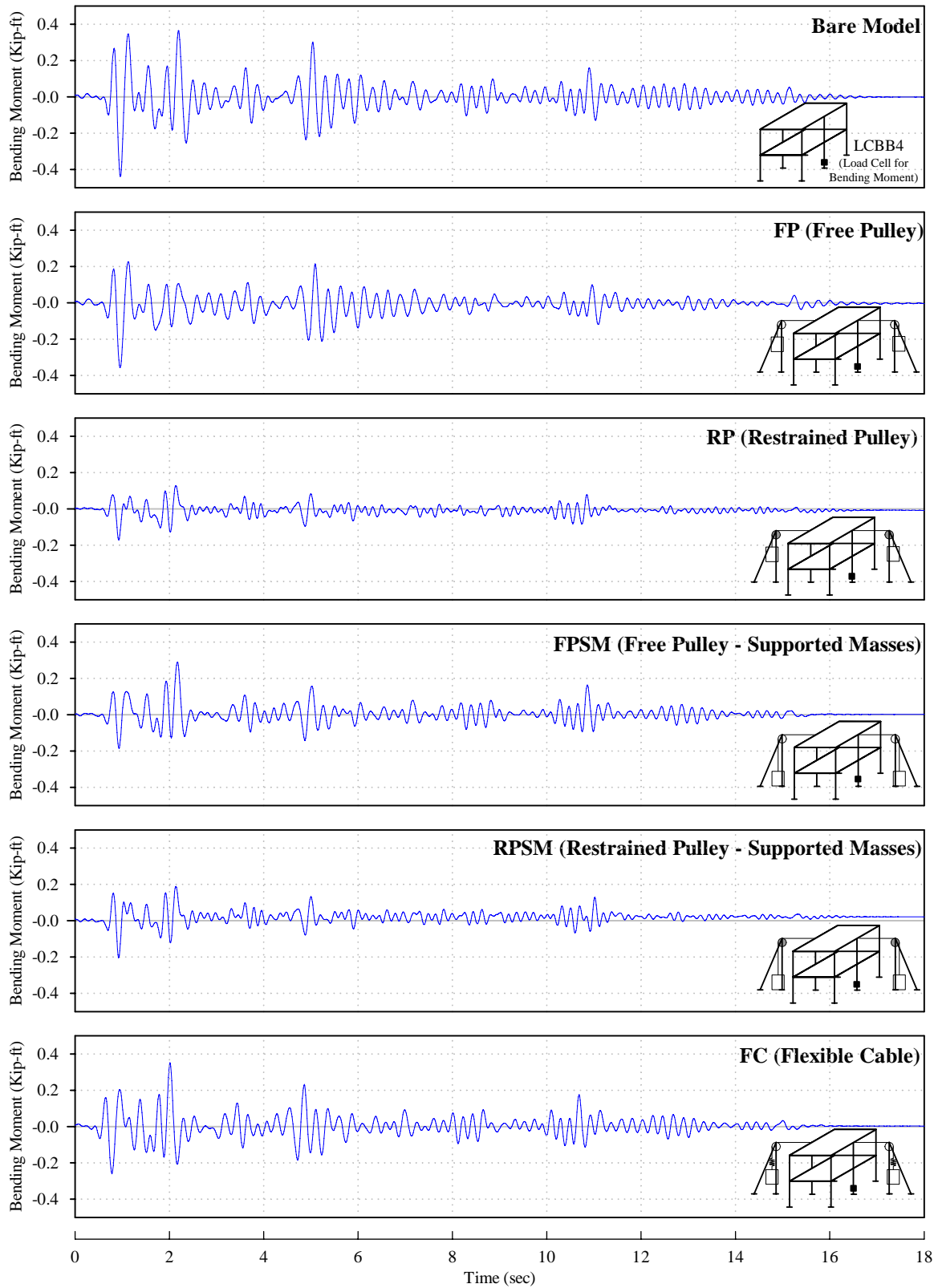


Figure 6-12: Comparison of El Centro Bending Moments at Bottom of Column 4

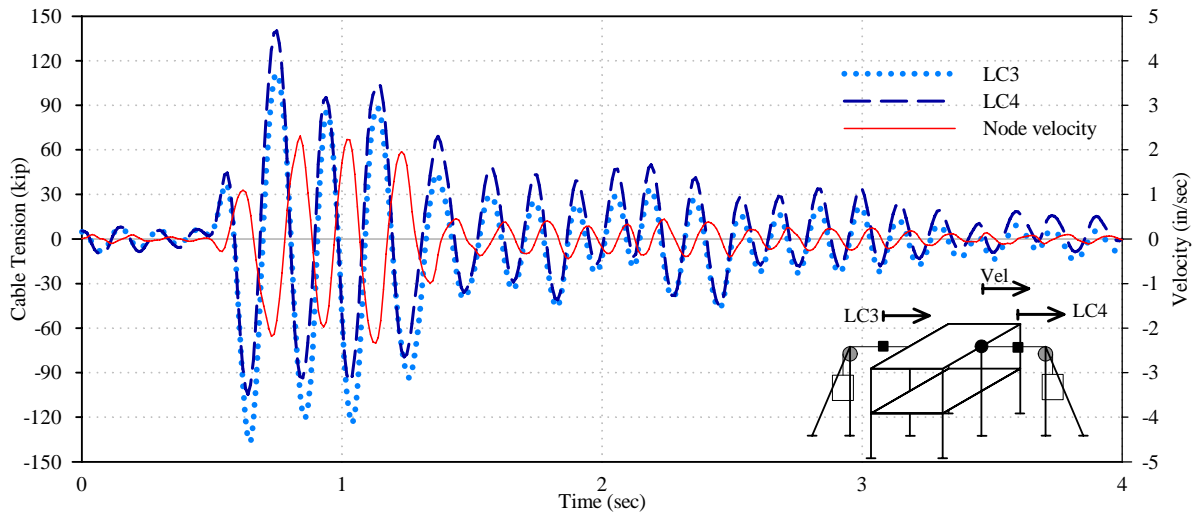


Figure 6-13: Comparison of Cable Tension and Frame 2 Second Level Velocity

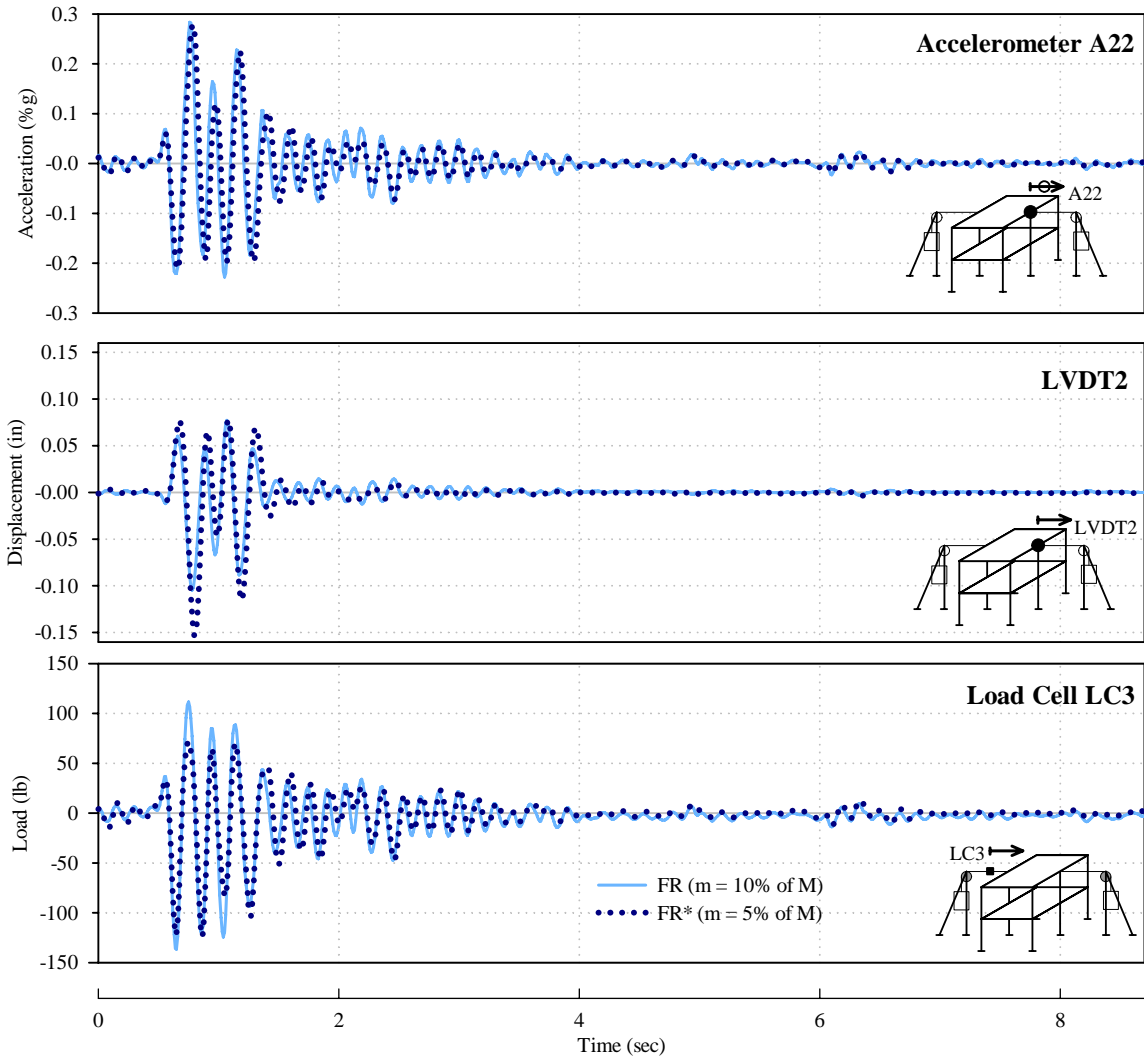


Figure 6-14: Comparison of RP and RP* Responses from the San Salvador Test

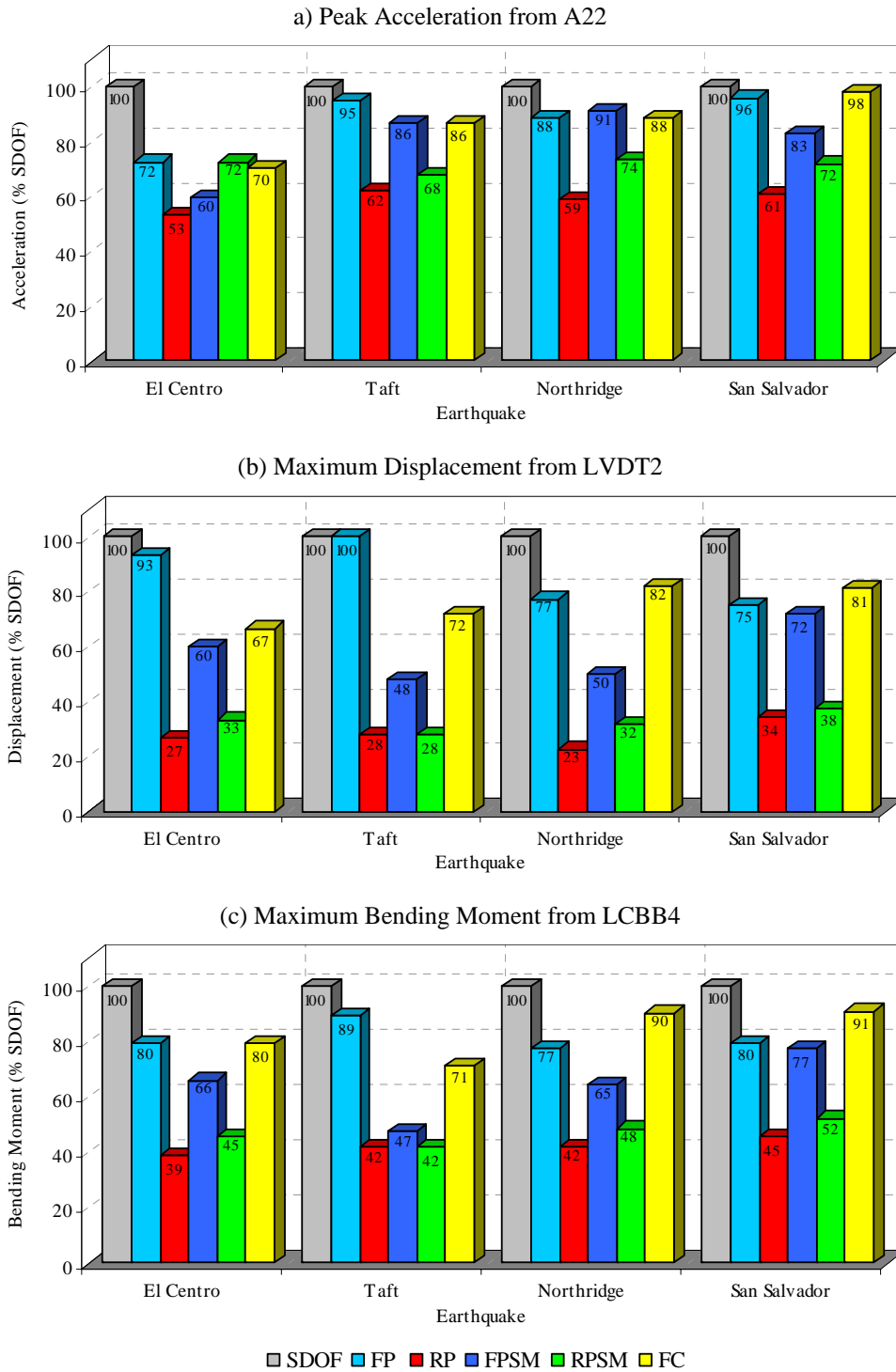


Figure 6-15: Results from Simulated Earthquake Tests as a percentage of Bare Model Response

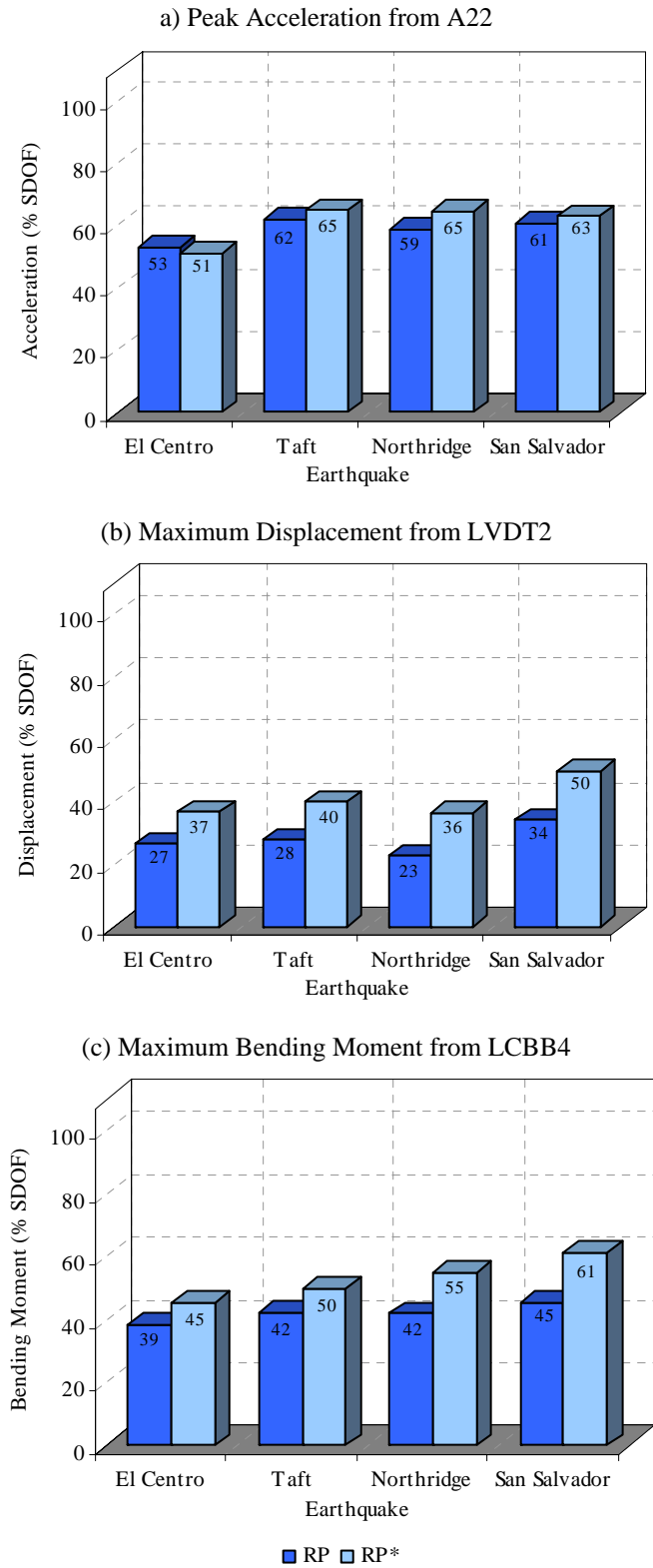


Figure 6-16: Comparison between RF and RF* Response

CHAPTER VII:

CONCLUSIONS

7.1 PROJECT SUMMARY

This thesis was divided in three parts. The first one described the design, construction and instrumentation of a 1/6 scale model of a steel structure. The similitude requirements used for this purpose were based in the Artificial Mass Simulation Method.

In the second part, five retrofitting alternatives were proposed to improve the performance of the scale model subjected to earthquakes motions. Snap-Back Tests and Simulated Earthquake Tests were performed first on a single degree of freedom system retrofitted with the different alternatives. These tests allowed to understand the operation of each mechanism, to identify which variables affected the results, and to compare the systems effectiveness.

In the third part Simulated Earthquake Tests were conducted on the scale model to study the benefits of the retrofitting alternatives. The results from all these tests were summarized and discussed.

In the following sections overall conclusions and proposed future works are

presented.

7.2 CONCLUSIONS

- A scale model of a steel structure typically used in commercial buildings in Puerto Rico was constructed following the Artificial Mass Simulation Method similitude requirements. The studies conducted on the scale model provided an adequate methodology to evaluate the alternatives of retrofitting proposed.
- An instrumentation system that provided an adequate evaluation of the model response behavior was successfully implemented. Special attention was placed in the assembly of the internal force transducer. From calibration tests performed it was concluded that this instruments provided accurate measures.
- Dynamic characteristics of the proposed model were identified through results form white noise test. Natural frequencies and modal shapes of the first and second mode of vibration were well identified. The model behavior indicated the presence of an accidental torsional component. Natural damping was intended to be identified through this test, but since the white noise used was highly irregular the transfer function obtained from the nodes acceleration records were also irregular. Thus, the application of half-power method did not produce accurate results.
- Five alternatives of retrofitting were proposed. From the Snap-Back Tests and Simulated Earthquake Tests conducted on the single degree of freedom system, it

was concluded that the best upgrades on the response were produced by RP and RPSM alternatives. Both were based on the dissipation of energy through friction forces between the cable and the pulleys. The best reduction in peak accelerations and maximum displacement obtained in the simulated earthquake tests were produced by the RP system. A drop of the peak acceleration between the 18% and the 46% and a drop of maximum drift between 10% and 54% were achieved.

- From the Simulated Earthquake Tests performed on the scale model it was concluded that the best upgrade on the behavior of the model were produced by RP and RPSM alternative. The peaks acceleration measured in the second level of the central frame produced by the RP system were between the 53% and the 63% of the bare system. The reductions on the relative displacement measured in the same node were between the 23% and the 34%. Finally, the reductions on the bending moment measured on the bottom of the central columns were between the 39% and the 45% of the bare model.
- The reductions on peak accelerations, relative displacements and bending moments obtained using RP system are similar to the reductions obtained by others energy dissipation systems presented in Filiatrault and Cherry (1987), Aiken et al.(1993) and Filiatrault et al.(2000).
- Tests were conducted on RP system with secondary masses $m_{5\%}$ and $m_{10\%}$. It was noticed that even tough the secondary masse were reduced to the half, the response obtained was similar.

7.3 RECOMMENDATIONS FOR FUTURE RESEARCH

- The aim of this research was to explore alternatives to improve the behavior of the scale model structure subjected to earthquake motions. Each proposed mechanism was intended to have a simple operation and low cost. Even though this was achieved, more research must be done to improve the system, either by improving the mechanism or by using other materials that provide larger frictional effects and lower costs.
- The previously stated research conclusions were based on the observations from experimental results. An analytical model must be developed to allow for the numerical simulation of the dynamic response of the alternatives schemes.
- A methodology to define the optimum load to be used in the RP alternative must be developed. Once the friction coefficient between the cable and the pulley is defined, the optimum load depends on the magnitude of the secondary masses used. Since in a full scale structure a large secondary mass could result in large auxiliary structures, it would be convenient to reduce these masses as much as possible.
- A cost study should be performed to compare the cost associated with this retrofitting alternative and their benefits with other methodologies, such as friction dampers.
- Finally, it was found in this research that the use of some types of rubber bands instead of inextensible cables can increase the damping ratio. The results depend on the properties of the rubber used. Further investigation on the

characterization of the rubber material should be undertaken.

REFERENCES

- Aiken, I. D., Nims, D. K., Whittaker, A. S., and Kelly, J. M. (1993). "Testing of Passive Energy Dissipation Systems." *Earthquake Spectra*, 9(3), 335-370.
- AISC. (2001). *Manual of Steel Construction*, American Institute of Steel Construction, 3th ed., Chicago.
- Barreras, F. E. (1999). "Determinación de Características Dinámicas de Estructuras," Memoria de la Tesis Doctoral, Universidad Politécnica de Cataluña, Barcelona, España.
- Bertero, R. D. (1998). "Conceptos Energéticos en la Selección de Sistemas Innovadores de Diseño Sismorresistente." *Ingeniería Estructural*, Año 4(14), 46-57.
- Bertero, V. V., Anderson, J. C., and Krawinkler, H. (1994). "Performance of Steel Building Structures During the Northridge Earthquake." *Report N° UBS/EERC-94/09*, Earthquake Engineering Research Center, University of California, Berkeley, California.
- Bracci, J. M., Reinhorn, A. M., and Mander, J. B. (1992). "Seismic Resistance of Reinforced Concrete Frame Structures Designed only for Gravity Loads. Part I : Design and Properties of a One-third Scale Model Structure." *Technical Report NCEER-92-0027*, National Center for Earthquake Engineering Research, Buffalo, New York.
- Chang, K. C., Yao, G. C., Lee, G. C., Hao, D. S., and Yeh, Y. C. (1991). "Dynamic Characteristic of a Full-size Five-story Steel Structure and a 2/5 Scale Model." *Technical Report NCEER-91-0011*, National Center for Earthquake Engineering Research, Buffalo, New York.
- Cherry, S., and Filiatrault, A. (1993). "Seismic Response Control of Buildings Using Friction Dampers." *Earthquake Spectra*, 9(3), 447-466.
- Cortés Delgado, M. D. (2005). "Development of the UPRM Earthquake Simulator Facility for Dynamic Model Analysis," M.S.C.E Thesis, University of Puerto Rico, Mayagüez.

- El-Attar, A.-G., White, R. N., and Gergely, P. (1991). "Shake Table Test of a 1/6 Scale Two-Story Lightly Reinforced Concrete Building." *Technical Report NCEER-91-0017*, National Center for Earthquake Engineering Research, Buffalo, New York.
- FEMA-355E. "State of the Art Report on Past Performance of Steel-Moment Buildings in Earthquakes." Federal Emergency Management Agency, Washington, DC.
- Filiatrault, A., and Cherry, S. (1987). "Performance Evaluation of Friction Damped Braced Steel Frames Under Simulated Earthquake Loads." *Earthquake Spectra*, 3(1), 57-78.
- Filiatrault, A., Tremblay, R., and Kar, R. (2000). "Performance Evaluation of Friction Spring Seismic Damper." *Journal of Structural Engineering*, 126(4), 491-499.
- Harris, H. G., and Sabnis, G. M. (1999). *Structural Modeling And Experimental Techniques*, CRC Press, Boca Raton, Florida.
- Krawinkler, H. (1988). "State of the Art Report: Scale Effects in Static and Dynamic Model Testing of Structures." Proceedings of the Ninth World Conference on Earthquake Engineering, August 2-9, 1988, Tokyo-Kyoto, Japan (Vol.III).
- Krawinkler, H. (1995). "Earthquake Design and Performance of Steel Structures." Proceedings of the Pacific Conference on Earthquake Engineering PCEE 95, Melbourne, Australia.
- Krawinkler, H., Anderson, J., and Bertero, V. (1996). "Steel Buildings." *Earthquake Spectra*, 12(S1), 25-47.
- López-Rojas, H. D. (2005). "Estimación de Daños Ocasionados por Vientos Huracanados sobre Estructuras en Puerto Rico," M.S.C.E Thesis, Universidad de Puerto Rico, Mayagüez.
- Martinez-Rueda, J. E. (2002). "On the Evolution of Energy Dissipation Devices for Seismic Design." *Earthquake Spectra*, 18(2), 309-346.
- Martínez Cruzado, J. A., Irizarry Padilla, J., and Portela Gautier, G. (2001). "Espectros de Diseño para las Ciudades Principales de Puerto Rico Basado en Registros de Aceleraciones Mundiales." *Revista Internacional de Desastres Naturales, Accidentes e Infraestructura Civil*, 1(1), 21-31.
- Mills, R. S., Krawinkler, H., and Gere, J. M. (1979). "Model Tests on Earthquake Simulators; Development and Implementation of Experimental Procedures." *Report N° 39*, The John A. Blume Earthquake Engineering Center, Dept. of Civil Engineering, Stanford University, Stanford, California,.
- Moncarz, P. D., and Krawinkler, H. (1981). "Theory and Application of Experimental Model Analysis in Earthquake Engineering." *Report N° 50*, The John A. Blume Earthquake Engineering Center, Dept. of Civil Engineering, Stanford University, Stanford,

- California.
- Nader, M. N., and Astaneh-Asl, A. (1989). "Experimental Studies of a Single Story Steel Structure with Fixed, Semi-rigid and Flexible Connections." *Report N° UBS/EERC-89/15*, Earthquake Engineering Research Center, University of California, Berkeley, California.
- Naeim, F. (2001). *The Seismic Design Handbook*, Kluwer Academic Publishers, Boston, Massachusetts.
- Nakashima, M., and Chusilp, P. (2002). "A Partial View of Japanese Post-Kobe Seismic Design and Construction Practices." *Earthquake Engineering and Engineering Seismology*, 4 (1), pp. 3 - 14.
- Rodriguez, M. E., Restrepo, J. I., and Blandon, J. J. (2006). "Shaking Table Tests of a Four-Story Miniature Steel Building--- Model Validation." *Earthquake Spectra*, 22(3), 755-780.
- Sause, R., and Bertero, V. V. (1983). "A Transducer for Measuring the Internal Forces in the Columns of a Frame-Wall Reinforced Concrete Structure." *Report N° UBS/EERC-83/05*, Earthquake Engineering Research Center, University of California, Berkeley, California.
- Soong, T. T., and Spencer, B. F. (2002). "Supplemental Energy Dissipation: State-of-the-art and State-of-the-practice." *Engineering Structures*, 24(3), pp. 243-259.
- Uang, C. M., and Bertero, V. V. (1986). "Earthquake Simulation Tests and Associated Studies of a 0.3-Scale Model of a Six-Story Concentrically Braced Steel Structure." *Report N° UBS/EERC-86/10*, Earthquake Engineering Research Center, University of California, Berkeley, California.
- Uang, C. M., and Bertero, V. V. (1988). "Use Of Energy as a Design Criterion in Earthquake-Resistant Design." *Report N° UBS/EERC-88/18*, Earthquake Engineering Research Center, University of California, Berkeley, California.
- Vishay Measurements Group. (2001a). "Force and Torque Measurement." Technical Article, <http://www.measurementsgroup.com/guide/ta/ftm/ftm.htm>.
- Vishay Measurements Group. (2001b). "Measurement of Force, Torque, and Other Mechanical Variables With Strain Gages." Technical Article, <http://www.measurementsgroup.com/guide/ta/msg/msg.htm>.
- Vishay Measurements Group. (2001c). "Strain Gage Based Transducers, Their Design and Construction." Technical Article, <http://www.measurementsgroup.com/guide/ta/sGBT/sGBTindex.htm>.
- Vishay Measurements Group. (2001d). "Strain Gage Measurement Systems, Design and

- Construction." Technical Article,
<http://www.measurementsgroup.com/guide/ta/sgms/sgmsindex.htm>.
- Wallace, B. J., and Krawinkler, H. (1985). "Small-scale Model Experimentation on Steel Assemblies : U.S.-Japan Research Program." *Report N° 75*, The John A. Blume Earthquake Engineering Center, Dept. of Civil Engineering, Stanford University, Stanford, California.
- Youssef, N. F. G., Bonowitz, D., and Gross, J. L. (1995). "A Survey of Steel Moment-Resisting Frame Buildings Affected by the 1994 Northridge Earthquake." *NISTIR 5625*, National Institute of Standards and Technology, Gaithersburg, Maryland.

APENDIX A

TYPICAL DIMENSIONS OF COMMERCIAL BUILDINGS IN PUERTO RICO

Building	Column	Beam	Story Height (ft)	Span (ft)
1	HSS8x8	W21x44	18	30
2	W14x99	-	18	40
3	W8x24	-	15	30
4	W14x90	W18x35	9	25

Table A- 1: Survey conducted on Mayagüez Area

Building	No. of Stories	First Story Height (ft)	Span (ft)
1	2	16	22
2	3	18	20
3	2	13	20
4	1	32	20
5	2	16	30
6	2	10	30
7	4	20	35
8	1	27	30
9	1	16	-
10	2	11	30
11	2	13	40
12	2	19.5	20
13	2	12	25
14	1	14	14
15	2	13	40
16	2	21	20
17	1	13.75	-
18	1	13.75	-
19	1	32	20
20	1	16	24

Table A- 2: Information Obtained from López-Rojas (2005)

APENDIX B

LOAD CELLS CALIBRATION PLOTS

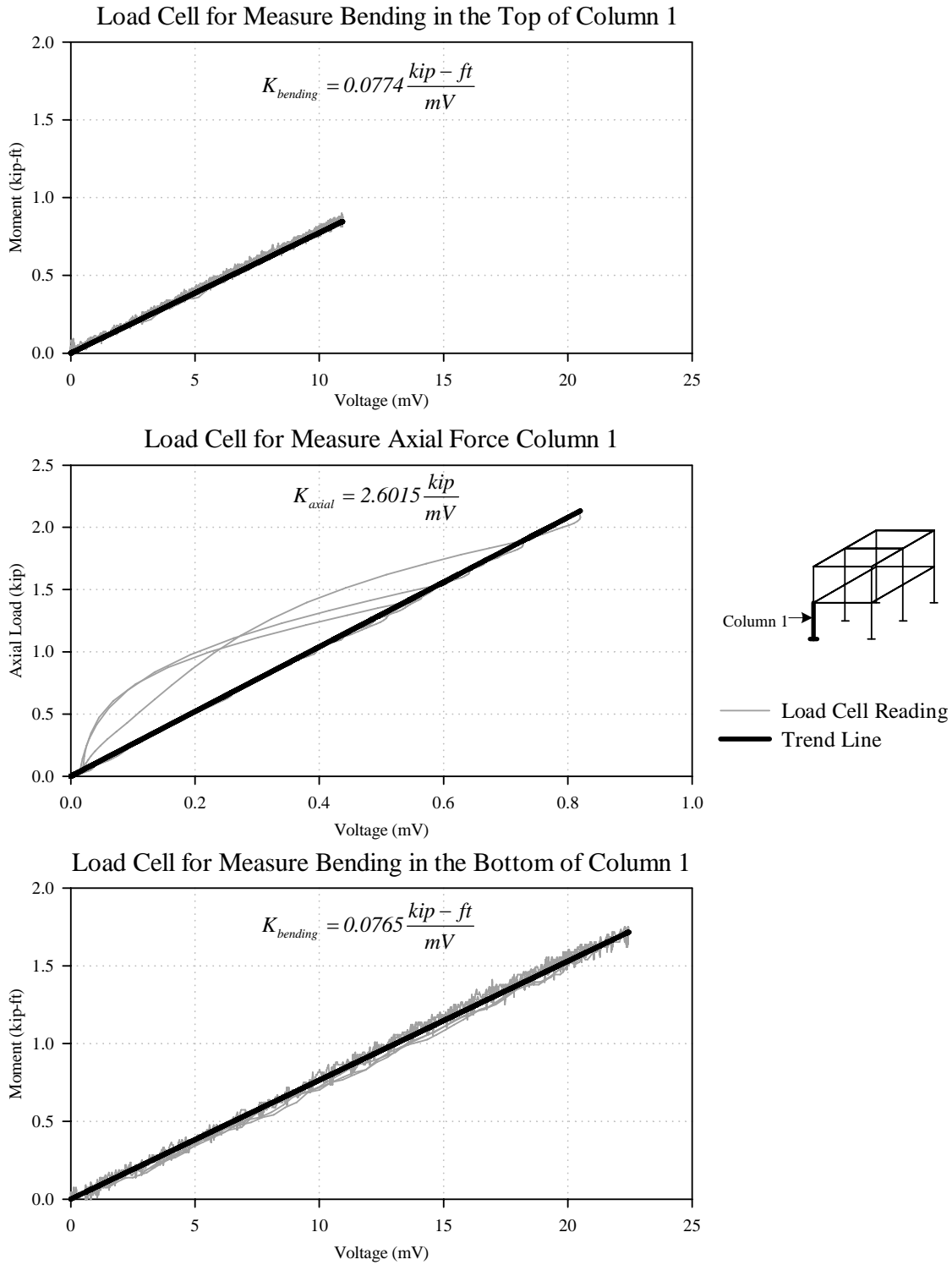


Figure B-1: Calibration Plots for Load Cells in Column 1

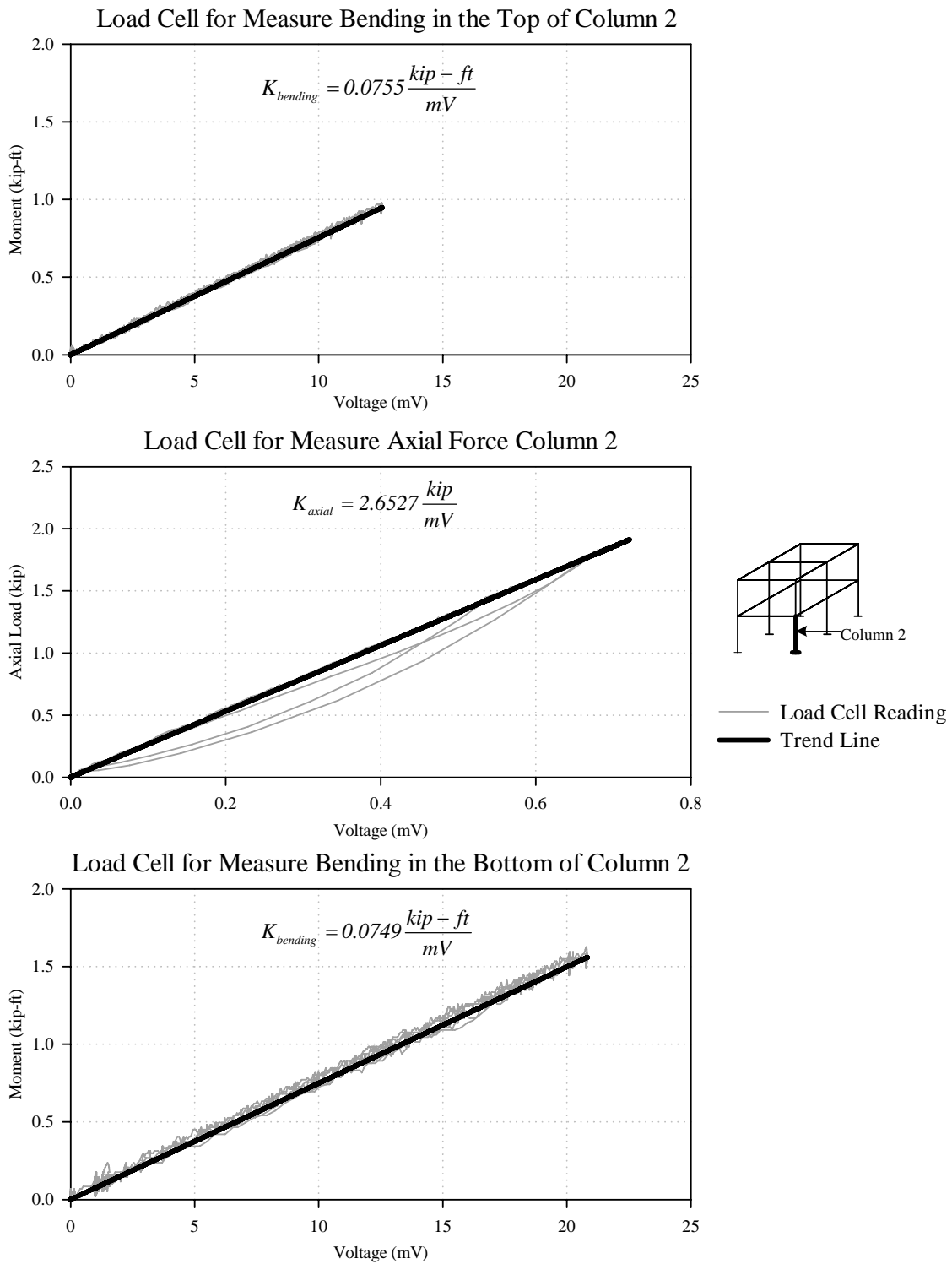


Figure B-2: Calibration Plots for Load Cells in Column 2

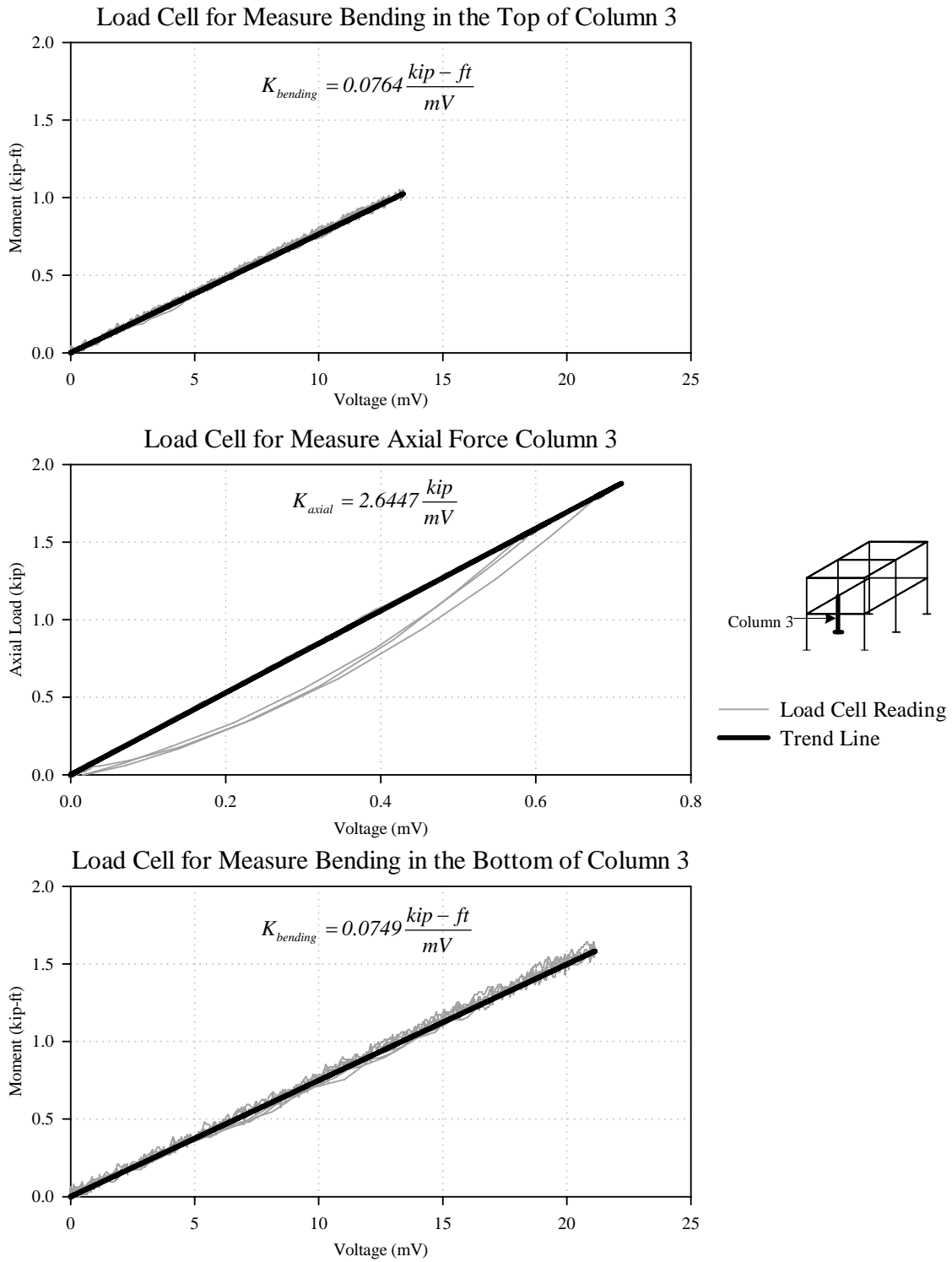


Figure B-3: Calibration Plots for Load Cells in Column 3

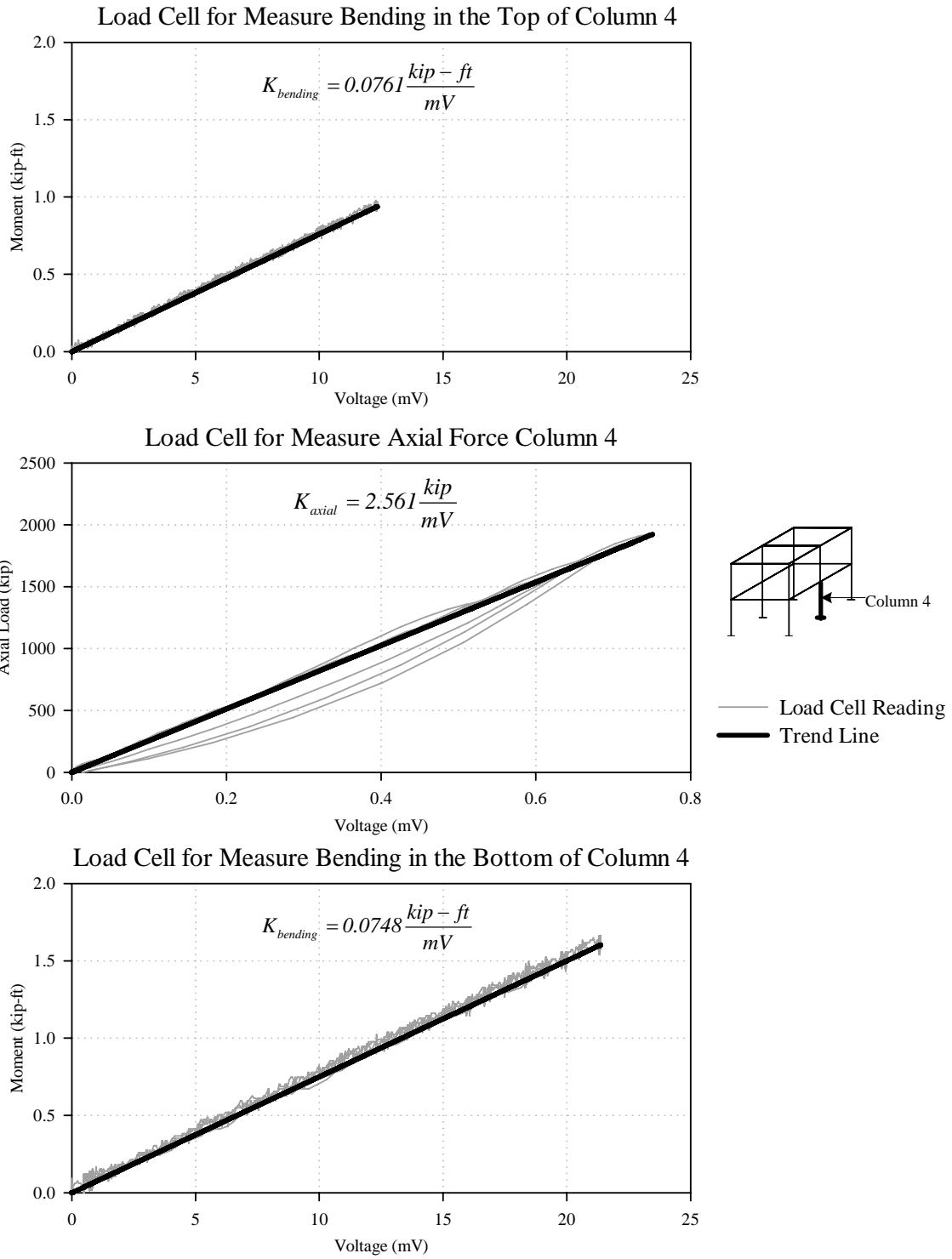


Figure B-4: Calibration Plots for Load Cells in Column 4

APENDIX C

**INTERNAL FORCES OF THE PROTOTYPE CALCULATED
FROM THE SCALE MODEL RESPONSE FROM THE
SIMULATED EARTHQUAKE TESTS**

The moment versus axial load interaction histories for the column 4 of the prototype and the different earthquakes are shown in Figure C-2 and Figure C-3. In the same graphs the limits set by equations H1-1a, and H1-1b from the AISC (2001) were plot. These equations are summarized as follows:

for $\frac{P_u}{\phi P_n} \geq 0.2$,

$$\frac{P_u}{\phi P_n} + \frac{8}{9} \frac{P_u}{\phi P_n} \leq 1$$

and for $\frac{P_u}{\phi P_n} < 0.2$,

$$\frac{P_u}{2\phi P_n} + \frac{P_u}{\phi P_n} \leq 1$$

The internal forces of the prototype were calculated using the similitude requirements and the measured internal forces of the model. The bending moment of the prototype can be determined from the bending moment measured in the model as follows:

$$M_m = \frac{M_p}{\lambda_L \lambda_F} \quad \therefore \quad M_p = M_m \lambda_L \lambda_F = M_m \lambda_L^3$$

where M_m is the bending moment in the model, M_p is the bending moment in the prototype, and λ_L and λ_F are the scaling laws for length and force respectively.

Also, the axial forces in the prototype were can be determined from the axial forces measured in the model considering that:

$$P_m = \frac{P_p}{\lambda_F} \quad \therefore \quad P_p = P_m \lambda_F = P_m \lambda_L^2$$

Since the columns at the central frame are the most loaded columns of the model, and therefore are the most loaded columns of the prototype, only plots for column 4 are presented. Also should be consider that the bending moment in the plots corresponds to the bottom bending moment in the column, and that the axial load correspond to measures at the center of the column as shown in Figure C- 1.

It can be noticed from these graphs that the predicted forces are bellow the limits provided by the AISC, therefore no damage is expected.

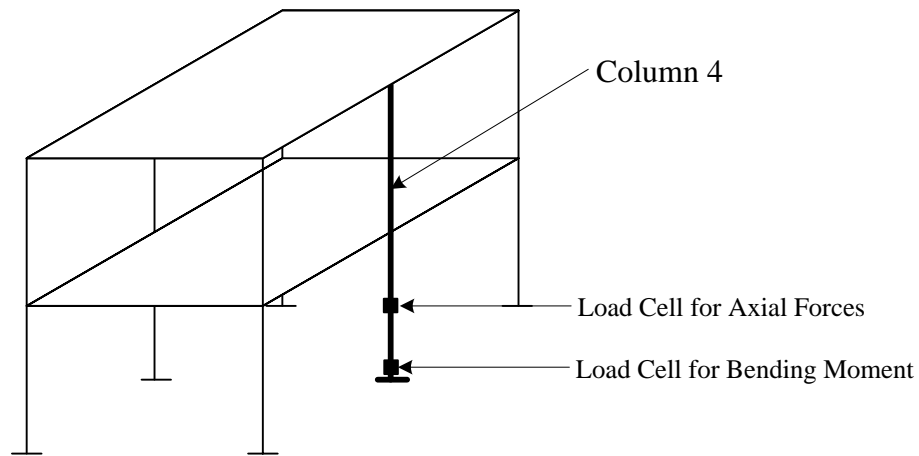
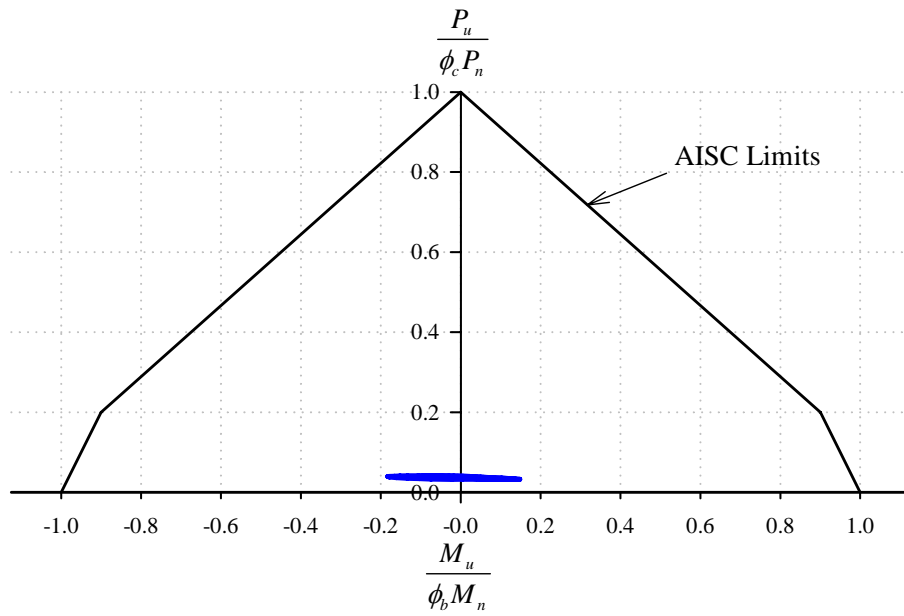


Figure C- 1: Location of the Column 4

Interaction Histories from El Centro Test



Interaction Histories from Taft Test

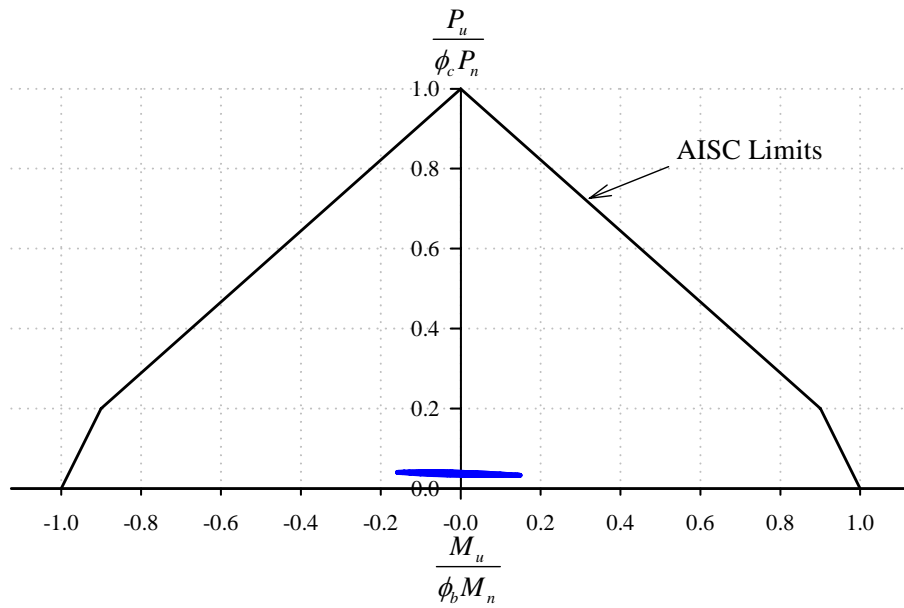
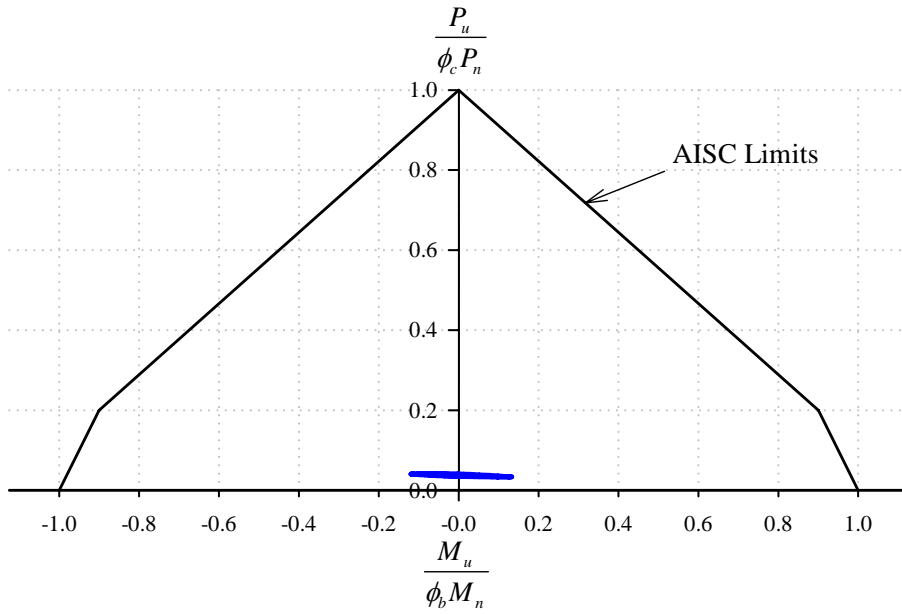


Figure C-2: Interaction Histories at the Bottom of Column 4 of the Prototype from El Centro and Taft Tests

Interaction Histories from Northridge Test



Interaction Histories from San Salvador Test

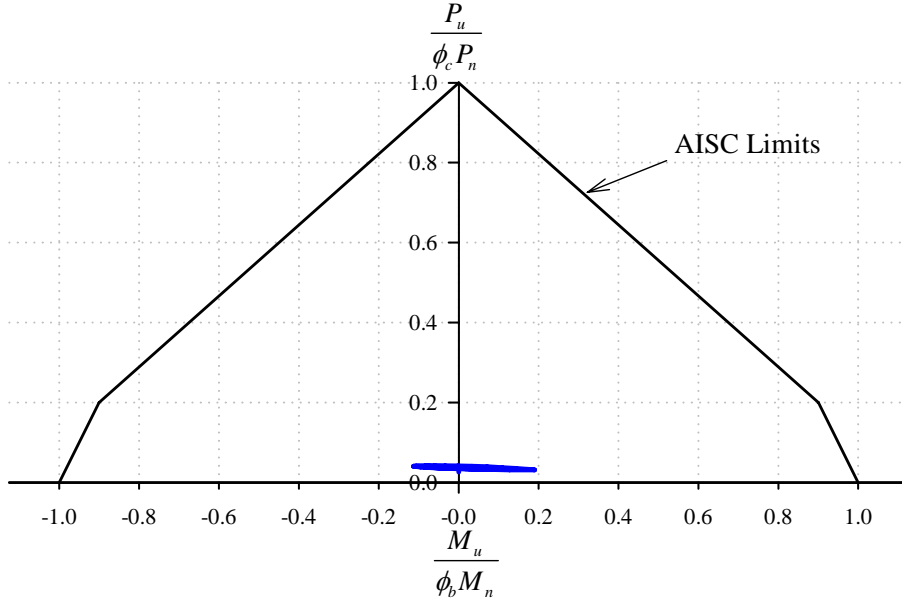


Figure C-3: Interaction Histories at the Bottom of Column 4 of the Prototype from Northridge and San Salvador Tests

APENDIX D

ADDITIONAL PLOTS FROM SIMULATED EARTHQUAKE TESTS

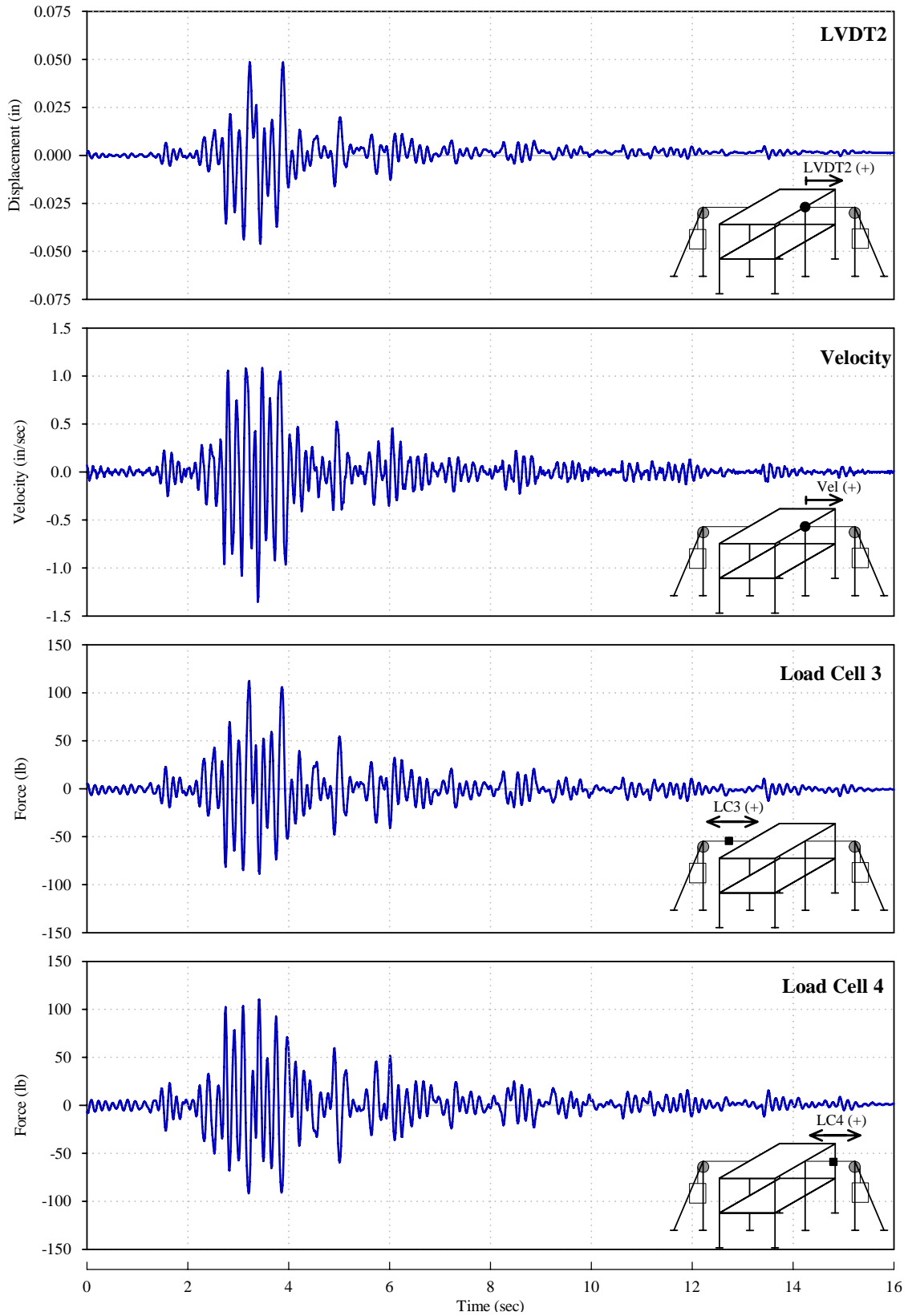


Figure C- 4: Results from Northridge Test for RP system

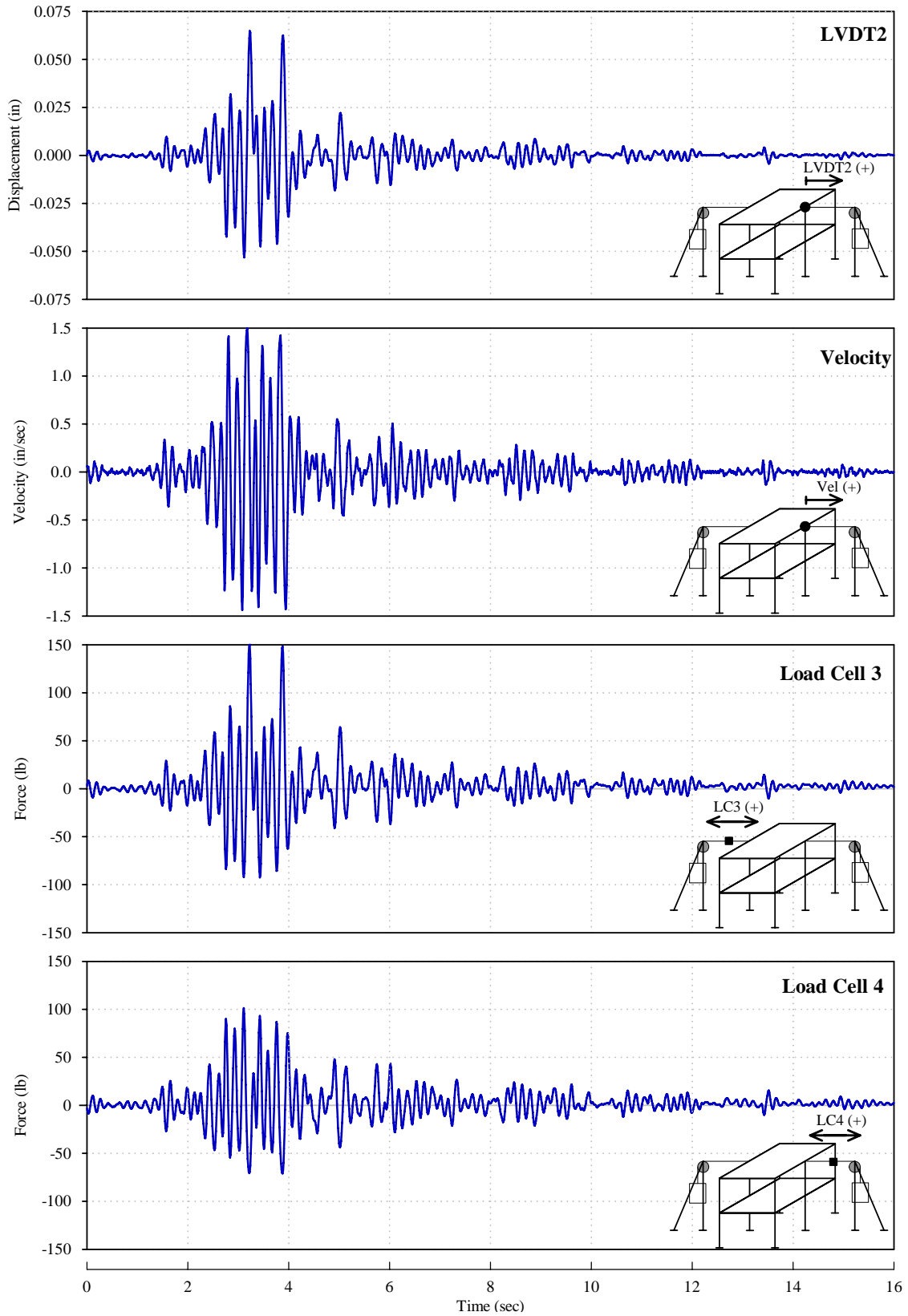


Figure C- 5: Results from Northridge Test for RPSM system